Doctoral Thesis

Detection of forest disturbance and recovery after a serious fire in the Greater Hinggan Mountain area of China based on remote sensing and field survey data

Wei CHEN

Department of Social Informatics
Graduate School of Informatics
Kyoto University

August 2014

A thesis submitted in partial fulfillment of the requirements for the degree of
Doctor of Philosophy in Informatics

Graduate School of Informatics
Kyoto University
Japan

Abstract

Forest disturbance and recovery has been regarded as a primary mechanism for transferring carbon between land surface and the atmosphere, and thus plays a key role in the terrestrial carbon balance. Identification and monitoring of forest disturbances is an important global and regional application, where updated information about where and when disturbances have occurred, and the area affected and recovered, is crucial.

Traditional forest investigation appears comparatively time-consuming, costly, but inefficient, and difficult to achieve full-cover and real-time monitoring. It is believed that, at regional and greater scales, the only feasible and effective means to monitor forest disturbance and recovery continuously and regularly is remote sensing.

Fire is a common disturbance regime, especially in boreal forests. It is a complex issue, both ecologically and socially, affecting the forest ecological process either as a positive agent of renewal or a highly destructive force. Fire effects and post-fire forest dynamics have been widely studied. A wide range of such studies are based on field forest investigation alone, while many researchers and managers are combining field survey data with remote sensing imagery to monitor post-fire forest patterns relying on their long temporal coverage, sufficient spatial and spectral resolutions which permit capture of most forest features.

The Greater Hinggan Mountain area, located in the northeast China, is rich in forest resources while suffers from a high incidence of forest fires simultaneously. Among all the fires in this area, the most noteworthy one is the “5.6 Fire” that occurred on May 6 1987 and developed to be the most serious forest fire for P. R. China. Aiming at this fire, this thesis proposes to detect the burned forest area, and monitor the post-fire forest recovery using field survey records and multi-source optical and SAR data. Particular emphasis has been laid on the effects of different restoration strategies for post-fire forest regeneration and vegetation recovery.

First of all, the fire scar and burned forest area was extracted and mapped using Landsat TM imagery by multiple methods. During the mapping, the fire perimeter, as well as rivers, roads and building areas were first delineated and masked, and then four indices were calculated. For comparison, threshold segmentation using the reflectance of original six multispectral bands was performed, in addition to a MLC-based supervised classification of all features and forest area alone. Their accuracies were also evaluated and analyzed. Compared to the traditional methods used to report official statistics on burned areas, the remote sensing-based extraction is less labour- and time-consuming, and more objective and efficient.

Following this fire, the local forestry bureaus have taken a series of measures for the forest recovery. Typically three different restoration treatments, namely natural regeneration (NR), artificial regeneration (AR), and artificial promotion (AP), are adopted for the forest regeneration in the burned area. In order to elucidate the effects of the three treatments, a field survey was conducted to collect the attribute data, specifically species composition, structural parameters, and LAI, which were

analyzed through ANOVA and a post-hoc test. Results suggest AR to be adopted in post-fire recovery if the goal is timber production, while NR should be selected when focusing on canopy vertical density and species richness. These findings can be used for reference in local forest management.

Considering the limitations of field forest survey, multi-source remote sensing data were also employed to monitor the forest recovery trajectories after the “5.6 Fire”. These data include the Landsat TM/ETM+ imagery, MODIS Land Cover Type and Vegetation Indices products, and ALOS PALSAR FBD data.

With Landsat TM/ETM+ records, totally 12 scenes covering the period of 1987-2011 were used for the post-fire forest recovery monitoring. In addition to the commonly used vegetation indices, a more effective index of DI was examined and evaluated. Combining with the field survey data analysis, the availability of different remote sensing indices and applicability of the three restoration treatments were evaluated and compared. Results indicated that the forest under NR achieved a totally different recovery process with those under the other two treatments.

Due to the unique characteristics of MODIS sensor, the well-developed MODIS Land Cover Type products were exploited to monitor the temporal and spatial dynamics of forest coverage. It centered on the hypothesis that the annual variability in coverage of different types of forest during 2001-2012 can be detected. Results suggested that the area of “Mixed forest” gradually increased from 46.34% in 2001 to 80.50% in 2012, while that of “Cropland/Natural vegetation mosaic” decreased from 30.46% to 5.94% in this period.

In addition to the optical images, ALOS PALSAR data covering the period 2007-2010 were also applied to detect the post-fire dynamics. The backscattering intensity in HH and HV polarization and the derived radar indices of RRVI and RNDVI were examined and evaluated. Results showed that, compared to the other two treatments, forests under NR presented a different recovery trajectory. They were consistent with those achieved by LAI and DI which together demonstrated the reliability of the forest recovery trajectory monitoring.

For more direct and targeted evaluation and comparison among the performances of different sensors, the linear statistical modeling was applied using field measured LAI and remote sensing indices from ALOS AVNIR-2, Landsat-5 TM and MODIS NBAR, ALOS PALSAR data. The gap between the spatial resolution of Landsat-5 TM and MODIS NBAR data with the field plot size can account for the reduced accuracy. Nonetheless, the data with higher spatial resolution and retrieval accuracy usually have lower efficiency in spatial and temporal coverage, and require higher acquisition costs. Thus in specific applications, the actual accuracy needs should be carefully considered to achieve a cost-efficient result.

Finally, the knowledge gained throughout this thesis is summarized, and limitations and deficiencies existed within this exercise has also been identified and commented, based on which, the improvements with regard to future studies are discussed and recommended.

Contents

List of Figures

List of Tables

1 Introduction

1.1 Background

1.1.1 Forest and forest disturbance

Forests are multi-functional and multi-value ecosystems, which are widely distributed across land surfaces and have a complex composition. Although occupying less than 14% of the Earth's surface, forests and savannahs together account for more than 40% of the total solar energy captured by green plants, as well as containing the largest concentrations of organic material compared to all other global ecosystems (Perry *et al.*, 2008; Chen *et al.*, 2010). "Forest" is a comprehensive description that has the greatest biodiversity among all terrestrial ecosystems. For example, tropical rainforests, which cover only 7% of the total land area, contain 50%–70% of all global terrestrial species (Perry *et al.*, 2008; Krishnaswamy *et al.*, 2009). Forests contain the most abundant biological resources and thus play an irreplaceable role in maintaining ecological balance on Earth. Additionally, forest ecosystems provide a wide range of products and services to humans, directly and indirectly, including climatic regulation, water purification, provisioning of wood, fibre and fuel, food, clear air, natural medicines, supporting of soil formation, nutrient cycling etc (MA, 2005).

The forests worldwide are unevenly distributed. For example, the five most forest-rich countries (the Russian Federation, Brazil, Canada, the United States and China) account for about 53% of total forest area, however, 64 countries with a combined population of 2.0 billion have less than 0.1 ha of forest per capita (FAO, 2006). What is more, forests are suffering a variety of unwanted disturbances, mainly in the form of wildfires, deforestation, insect and disease infestation, and other disturbance factors including extreme weather conditions (wind, snow, ice, floods and drought), pollutants, and invasive species and so on. These disturbances result in a decline in forest coverage and changes in forest structure and composition, which in turn affect its functional mechanisms as a whole (Bacles, 2014). It was concluded by Millennium Ecosystem Assessment that "Forests have essentially disappeared from 25 countries, with 9.4 million hectares being lost annually" (Mooney *et al.*, 2005; Perry *et al.*, 2008). In the United States, a few species of forest pests routinely have significant impacts on up to 20 million hectares of forest with economic costs that probably exceed 1 billion USD per year (Ayres and Lombardero, 2000).

The detection of forest disturbances is a key process in terrestrial ecosystem research, especially in fields related with global carbon cycles and climate change (Cao *et al.*, 2011; Schroeder *et al.*, 2006, 2012). Forest disturbance and recovery have been proposed as primary mechanisms for transferring carbon between land surface and the atmosphere, and thus plays an important role in both regional and global carbon budgets, as well as in long-term forest monitoring processes (Masek *et al.*, 2008; Sönmez *et al.*, 2011). However, the timing and geography of these disturbance

events are still in need of being more quantitatively described and studied. Moreover, the magnitude and duration of the impacts of various disturbances on forest health and vitality vary greatly in time and space, which may translate to significant variability in ecosystem state and climate change (FAO, 2006; Townshend *et al.*, 2012).

1.1.2 Forest fire and its effects

On a global basis, forest fire is one of the most widespread and common disturbance regimes, with significant implications for both carbon cycles and forest health. It has been regarded as a dominant disturbance, especially in boreal forests (Díaz-Delgado and Pons, 2001; Forkel *et al.*, 2012). It is a primary process responsible for organizing the physical and biological attributes of a boreal biome, as well as shaping forest age structure, landscape diversity and influencing energy flows and biogeochemical cycles (Weber and Flannigan, 1997; Wotton *et al.*, 2010; Stroppiana *et al.*, 2012).

Forest fire is a complex issue, both ecologically and socially, being of beneficial and detrimental effects on forest ecosystems, depending on the specific circumstances. With respect to detrimental impacts, it can be easily understood that the fire disturbance will cause the loss of lives and property, greenhouse gas emissions, soil erosion and degradation, haze pollution as well as the destruction of biomass and biodiversity (Flannigan *et al.*, 2005; Shvidenko and Schepaschenko, 2013). On the other hand, it can also positively facilitate the early and abundant seed dispersal and germination, especially in the initial stages of forest regeneration, thus bring about the rapid recruitment of natural seedlings (Babintseva and Titova, 1996; Chu and Guo, 2014). In conclusion, fire influences the forest ecological process either as an essential agent of renewal or a highly destructive force.

A Large Fire Database (LFDB) has been developed for all fires larger than 200 ha in Canada for the period of 1959-1997, which includes information about fire location, start date, final size, cause, and suppression action. The LFDB represents only 3.1% of the total number of Canadian fires during this period, yet accounts for nearly 97% of the total burned area, allowing a spatial and temporal analysis of recent Canadian landscape-scale fire effects and their relationship to other factors (Stocks *et al.*, 2002; Skinner *et al.*, 2006). Gillett *et al.* (2004) have demonstrated that the observed increase in area burned in Canada during the last four decades mainly result from the human-induced climate change. A study using various remote sensing instruments have shown that the average vegetation area by wildfire in Russia for 1998-2010 accounted for $(8.2 \pm 0.8) \times 10^6$ ha, with an average annual fire carbon balance during the same period being (121 ± 28) Tg C/yr. However, it still should be noticed that, according to the statistics by Food and Agriculture Organization, only 78 countries responding to fire effect surveys, representing 63% of the global forest area, reported that 60 million hectares of land, including forests and other wooded land, were burned per year throughout 2003-2007 (FAO, 2010). The forest fire disturbance and its effects are generally underreported because of various reasons.

Both traditional acquisition of forest products and the increased use of forests for recreational, educational and tourism purposes increase the risk of forest fires. Fires occurred with varied location, range, intensity and duration will result in different

effects. Therefore, it is crucial to quantify the distribution and frequency of forest fire disturbances in an ecologically sound way, which helps to understand the environmental and climate change. It is also enormously useful for identifying spatial and temporal trends in forest utilization and management (Schroeder *et al.*, 2012; Pflugmacher *et al.*, 2012). Due to the specific characteristics of forest fires in frequency, intensity and spreading ability, additional information are in great need regarding their direct and underlying causes, temporal and spatial dynamics, as well as the ecological impacts of fire and desired long-term conditions of post-fire ecosystems.

1.1.3 Remote sensing

1.1.3.1 Concept and history

In forest-related studies, many researches rely on the field survey data, which are costly, labor- and time-consuming, but inefficient, and difficult to achieve real-time monitoring and change capturing. Furthermore, ground measurements are not always standardized, lacking for many remote areas that are dangerous or difficult to access. Thus there is great need for remotely sensed estimates of forest attributes over landscapes in order to obtain information for forest monitoring, assessment and management (White, 1998; Perry *et al.*, 2008; Bergen *et al.*, 2009).

Actually, at regional and global scales, the only feasible and effective means of monitoring land surface, atmosphere and oceans continuously and regularly is remote sensing. Especially airborne and spaceborne remote sensing offers an affordable and effective tool for monitoring forest state and its change over large areas and long periods (Carlson and Ripley, 1997; Cohen and Goward, 2004; Cao *et al.*, 2011).

Remote sensing is the science of acquiring data and information about objects, areas or phenomena without touching it by detecting the signals reflected from the Earth through a sensor typically aboard aircraft or satellites. The remote sensors can be either passive or active. Passive sensors merely record radiation that is emitted or reflected by the objects on Earth, usually from the sun and thus can only be used to collect data during daylight hours (Fig. 1.1(a)). They generally include aerial photography, infrared, charge-coupled devices, thermal cameras, and radiometers. In contrast, active sensors receive the signals emitted by their own and reflected or backscattered from the targets on Earth’s surface (Fig. 1.1(b)). Therefore, active sensors can achieve day-and-night observations under all weather conditions. Light Detection and Ranging (LiDAR) and radar are typical examples of active sensors.

The term of “Remote Sensing” was first introduced by the division of scientific research of U.S. navy and officially adopted in the early 1960s. The launch of the Earth Resources Technology Satellite "ERTS-1" (i.e. Landsat-1) in the early 1970s is considered as a milestone in the history of the development of satellite remote sensing. SEASAT launched in 1978 was the first civilian satellite designed for remote sensing of the Earth's oceans with the first spaceborne synthetic aperture radar (SAR). In 1999 the first commercial satellite (IKONOS) collecting very high resolution imagery was launched. Thus far there are more than 6000 satellites have been launched, over 60% of which serve military purposes (Cao, 2013). Those for civilian and scientific use

mainly include the series of Landsat, meteorological, ocean, geodetic, astronomical observation and communications satellites (Zhao, 2003).

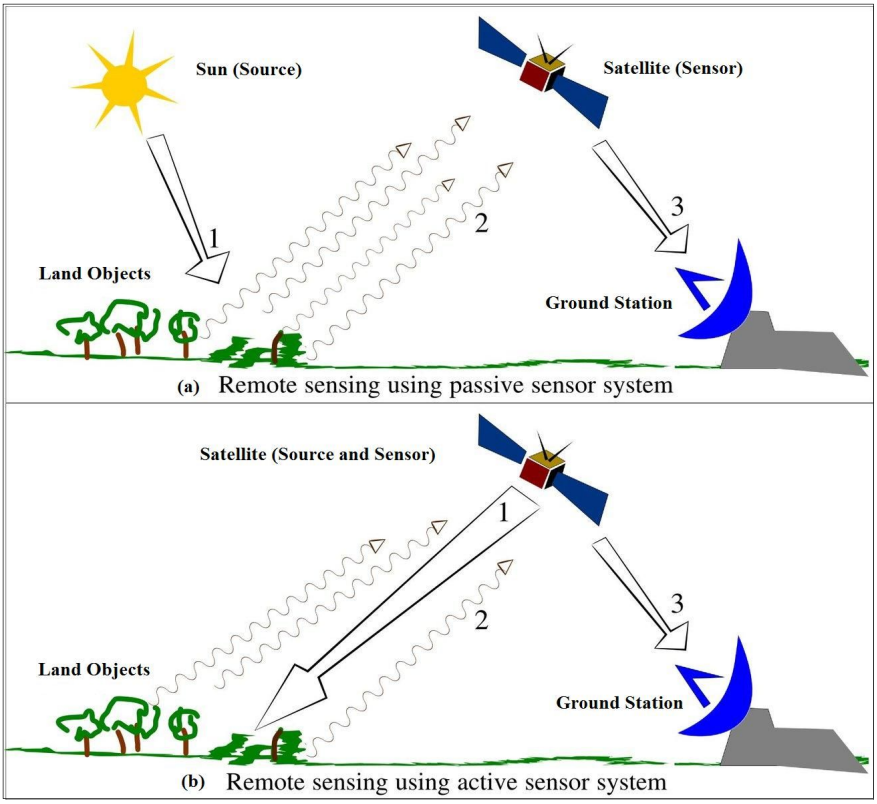

Figure 1.1 Illustration of remote sensing system using (a) passive sensor; (b) active sensor. The number of 1 denotes the source of reflected signals, 2 means the energy emission of land features, 3 indicates signal transfer from sensor to ground station. (Courtesy of Arkarjun, published on Wikipedia).

1.1.3.2 Optical sensors

Optical remote sensing refers to wavelengths ranging from the visible spectrum to the thermal infrared (TIR) spectrum (0.4-14 μm) (Liang, 2004). From the wavelength range, it can be divided into visible, reflected infrared, and emitted (thermal) infrared, while the forest disturbance monitoring mainly requires the utilization of the former two. Without considering TIR, the passive optical sensors can be briefly grouped into two categories of multispectral (a limited number of spectral bands) and hyperspectral (about two hundred channels) sensors from the aspect of spectral characteristics (Table 1.1). There are abundant multispectral sensors, mainly including Landsat TM/ETM+ (Thematic Mapper/Enhanced Thematic Mapper plus), SPOT (Satellite Pour l'Observation de la Terre) VEGETATION, IKONOS, QuickBird, WorldView, GeoEye, Pleiades-1A/B, ALOS/AVNIR-2 (Advanced Land Observing Satellite/Advanced Visible and Near Infrared Radiometer-2), ASTER (Advanced Spaceborne Thermal Emission and Reflection Radiometer), CBERS (China-Brazil Earth Resources Satellite), HJ-1A/B (Huan Jing-"Environment" in Chinese), SeaWiFS (Sea-viewing Wide Field-of-view Sensor), AVHRR (Advanced Very High

Resolution Radiometer) and so on. The typical examples of hyperspectral sensors include AVIRIS (Airborne Visible/Infrared Imaging Spectrometer), HYDICE (Hyperspectral Digital Imagery Collection Experiment), HyMap, Hyperion etc. Besides, MODIS (Moderate-resolution Imaging Spectroradiometer) which has 36 spectral bands is either thought to be a medium-spectral resolution sensor or incorporated into the multispectral category.

When viewed from spatial resolution, the optical sensors can be simply summarized into three types: low, medium, high resolution ones (Table 1.1). Currently there is no common consensus about the definition of low, medium and high spatial resolution. From the perspective of forest-related research, here we define that low resolution means pixels being ≥ 100 m; high resolution represents ≤ 10 m and hence medium resolution is 10-100 m (usually 30 m). According to this definition, sensors with low resolution mainly include AVHRR, MODIS and SPOT VEGETATION; that of medium resolution is a collection of Landsat TM/ETM+, ASTER, HJ-1A/B, CBERS, AVIRIS (by ER-2), Hyperion etc.; the high resolution sensors consist of IKONOS, QuickBird, WorldView, GeoEye, Pleiades-1A/B, ALOS/AVNIR-2, AVIRIS (by Twin Otter), HYDICE, HyMap and so on.

Table 1.1 Classification of remote sensing sensors from the perspectives of spectral characteristics and spatial resolution.

Spatial resolution	Multispectral sensor	Hyperspectral sensor
Low (≥ 100 m)	AVHRR, MODIS, SPOT VEGETATION	
Medium (10-100 m)	Landsat TM/ETM+, ASTER, HJ-1A/B, CBERS	AVIRIS (by ER-2), Hyperion
High (≤ 10 m)	IKONOS, QuickBird, WorldView, GeoEye, Pleiades-1A/B, ALOS/AVNIR-2	AVIRIS (by Twin Otter), HYDICE, HyMap

In addition, there is a relatively new active optical sensor of LiDAR, which transmits a laser onto the surface of Earth and measures the time delay between emission to and return from the targets, is gradually being widely used in the field of forest measurements and disturbance investigation by remote sensing.

1.1.3.3 SAR technique

SAR is an airborne or spaceborne side-looking radar system which records the backscattering signals emitted by its own, and generates high-resolution remote sensing imagery at wavelengths from millimeters up to 1 meter. SAR has some unique properties which are not known from optical sensors. Firstly, it is an active imaging technology. Typical microwave bands that SAR uses are X-band (2.4-3.8 cm), C-band (3.9-7.5 cm), and L-band (15.0-30.0 cm). As these microwaves can penetrate clouds, canopy, soil and snow partially, it allows the volumetric detection into these objects. Additionally, SAR employs polarized radiation and, therefore, can exploit polarization

signatures to obtain more abundant information about the target's structure (e.g., forests). Finally, SAR is also a coherent imaging technique which serves as the prerequisite for interferometric SAR (InSAR) and polarimetric SAR interferometry (PolInSAR) (Bamler, 2000; Gartley *et al.*, 2010).

Recently, a wide variety of SAR instruments with various bands, polarimetric and interferometric characteristics have been attached onto satellite platforms under different observation modes, which rapidly made available the acquisition of large amounts of SAR data as well as their further applications. Typical cases of SAR missions include ERS-2/SAR, Envisat/ASAR and Radarsat-1/2, TerraSAR-X, ALOS/PALSAR (Phased Array type L-band Synthetic Aperture Radar), etc. However, compared with optical data, the geometric and radiometric interpretation of SAR images seems more difficult due to the terrain distortion (e.g., foreshortening, layover, shadowing) and speckle effect (Schmullius and Evans, 1997).

1.1.4 Fire disturbance and forest recovery investigation

Passive and active remote sensing have a wide range of applications in many fields including resource management, environment monitoring, urban planning and ocean exploration, as well as climate change related studies. As this research focuses on the fire disturbance detection and post-fire forest recovery monitoring based on remote sensing data, here an overall review on this specific field would be made.

Previous studies have demonstrated that there is a significant difference between the spectral characteristics of vegetation and other land surface features. Especially for healthy vegetation, spectral curve characteristics (Fig. 1.2) are particularly notable: a low peak of reflectivity of 10%-20% high at the green band with central wavelength of 0.55 μm; two absorption valleys at the blue-purple band of 0.45 μm and red band of 0.65 μm, respectively; a sharp increase shown as a steep on the curve at about 0.7-0.8 μm followed by a significant reflectivity peak of 40% or greater in the near-infrared band of 0.8-1.3 μm. Besides, there are another three absorption valleys at the bands of 1.45 μm, 1.95 μm and 2.6-2.7 μm, respectively. However, when the vegetation suffers a fire disturbance, there is a sharp decrease in the reflectance of visible-to-near-infrared channels, accompanied by an increase in the surface reflectance of short and middle infrared bands. Thus the spectral signatures of forest vegetation are a comprehensive reflection of its own structural characteristics and environmental conditions, which can be used to identify various disturbances and monitor vegetation recovery in a wide variety of studies (Kennedy *et al.*, 2012).

Therefore optical remote sensing technology is particularly the most common and traditional approach used to extract forest attributes, including vegetation fractional cover (VFC), leaf area index (LAI), biomass and other structural parameters, benefiting from their abundant spectral signatures, sufficient spatial resolution and temporal coverage. Thus it is always available to perform forest disturbance monitoring based on optical data in large scales for long time series. SAR, which is one type of active sensors, serves as another attractive tool for forest disturbance detection due to its ability to penetrate cloud cover and characterize forest geometry volumetrically (Miles *et al.*, 2003).

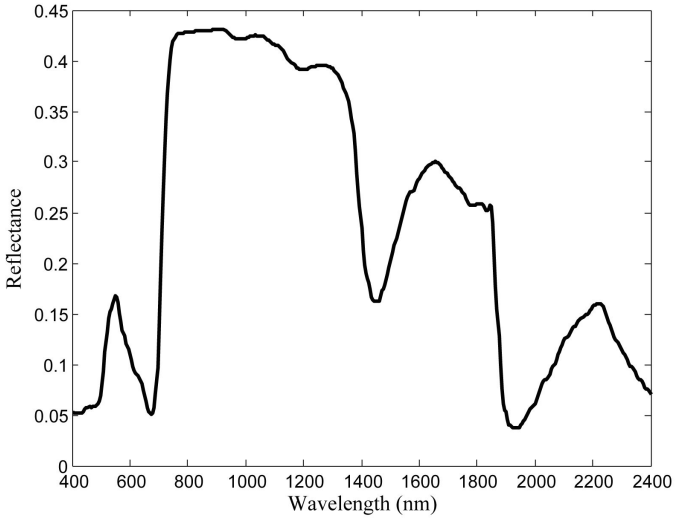

Figure 1.2 The spectral curve of healthy vegetation within visible and infrared wavelength range.

1.1.4.1 Based on medium resolution data

Among all optical remote sensing imagery, especially with medium spatial resolution, the Landsat records, are particularly suitable to detect forest disturbances and monitor forest dynamics as they have unprecedented historical coverage (40 years), as well as a necessary spatial (30 m) and spectral resolutions (7 bands) which permit capturing of most forest disturbance events (Wilson and Sader, 2002; Tucker *et al.*, 2004; Schroeder *et al.*, 2012). The Landsat TM/ETM+ images are mainly used for the burned area mapping, burn severity assessment and post-fire forest recovery monitoring when regarding fire disturbance studies (Chen *et al.*, 2013; Chu and Guo, 2014). Most previous studies were performed using the methods of regression models, image classification, and other non-parametric approaches.

Statistical regression models are among the most commonly used methods, through the establishment of linear and non-linear relationships between spectral bands or derived spectral indices and the field measured parameters. For example, Hoy *et al.* (2008) assessed the differenced Normalized Burn Ratio (dNBR) and other spectral indices and image transforms derived from Landsat TM/ETM+ data for mapping fire severity in Alaskan black spruce forests using ground measurements of severity and obtained low correlations overall, with the highest linear correlation (R^2 = 0.52) between dNBR and field-measured Composite Burn Index (CBI). Epting *et al.* (2005) evaluated 13 remotely sensed indices, including single bands, band ratios, vegetation indices, and multivariate components, across four wildfire burn sites in interior Alaska by examining the linear correlation between each index and field-based CBI values. Similar studies were also conducted with various forest ecosystems in different regions by building the linear regression relationships between NBR/dNBR/RdNBR and CBI (De Santis and Chuvieco, 2007; Allen and Sorbel, 2008; Murphy *et al.*, 2008; Cansler and McKenzie, 2012) or post-fire organic soil depth (Verbyla and Lord, 2008). Additionally, Song *et al.* (2007) found that the successional trajectories, from young

to old-growth stages, can be identified by a linear regression model between the Landsat Tasseled Cap indices and forest stand ages.

In addition to linear regression models, non-linear regression was also conducted in many forest environments. For example, Soverel *et al.* (2011) examined the non-linear correlation between Landsat-derived dNBR and filed-measured CBI, and obtained an overall model with R^2 of 0.69. Hall *et al.* (2008) assessed both the linear and non-linear relationships of the CBI-dNBR and found non-linear model performed better than linear model. More specifically, for the different types of temperate forest and boreal forest in North America, the exponential and second-order polynomial relationships between CBI and dNBR/RdNBR achieved better results respectively.

As stated in many above studies, the statistical regression models are usually limited to specific study regions with specific forest types, and need to be examined whether they can be extended to other forest sites with different tree characteristics and environmental conditions (De Santis and Chuvieco, 2007). Thus an alternative method to regression models is image classification, in terms of supervised or unsupervised classification etc (Castellana *et al.*, 2007). For example, Michalek *et al.* (2000) used supervised classification (maximum likelihood decision rule) to classify burn severity classes, which was later used to estimate carbon efflux for the burned black spruce in an Alaskan forest. Epting and Verbyla (2005) performed an unsupervised classification (ISODATA algorithm) on both pre-fire and post-fire Landsat scenes to identify six vegetation types. Some other studies based on classification of spectral indices were also conducted aiming at the boreal forest in Northeast China (Cai *et al.*, 2013; Wu *et al.*, 2013).

Except the image classification, there are other alternatives of non-parametric approaches, including spectral unmixing, neural network, genetic algorithm, random forest etc. Sunderman and Weisberg (2011) tested and compared the performance of two methods of dNBR classification and differenced linear spectral unmixing for delineating fire perimeters and burn severity mosaics using field observations of burn presence and fire severity for two recent wildfires. Liu *et al.* (2008) explored the potential of using Forest Inventory and Analysis (FIA) plot data to extract forest successional stage information from Landsat TM imagery with two other predictive models of neural networks and decision trees, which achieved better results than linear regression method.

The above summarization is obtained from the perspective of method when using medium spatial resolution data, especially Landsat imagery. As is well known, temporal resolution is another crucial characteristic of remote sensing data which will also be discussed here. A large number of previous studies have proven that the time series data usually gave better results compared with single-phase application. For example, Song *et al.* (2007) concluded that multi-temporal Landsat imagery improved identification of forest successional stages, especially for the separation of mature from old-growth stands. Bastarrika *et al.* (2011) proposed an automatic algorithm applied for burned area mapping in two Mediterranean sites based on two-phase Landsat images. Compared with one-phase method, this algorithm minimized the commission errors and omission errors by the synergic using the two phases and thus

improved the accuracy of burned patches delimitation.

1.1.4.2 Based on low resolution data

The optical data with low or coarse spatial resolution, such as AVHRR, MODIS, SPOT VEGETATION, are particularly suited for the forest disturbance detection and monitoring in regional and global scales, and in long time series when with high temporal resolution. The validation and verification are usually conducted through either the official statistics of field records or the results from higher spatial resolution datasets (such as Landsat).

AVHRR is a key data source for detecting fire disturbances and their effects as it has quite a long temporal coverage since 1978 over most regions. Thus it has been mainly used for the forest fires occurred in the 1990s and early 2000s. However, due to its relatively low spectral and spatial resolution, the accuracy and efficiency of the applications based on AVHRR data vary among different regions with different climatic and environmental conditions. For example, Kasischke *et al.* (1993) used AVHRR NDVI images to map forest fire boundaries. Comparison with those mapped by field observers indicated that 89.5% of all fires with sizes greater than 2000 ha were detected while only 61% of the total area was mapped. Similarly, French *et al.* (1995) used the AVHRR NDVI data composite from two seasons and finally detected more than 80% of fires greater than 2000 ha and mapped 78% of the burned area of all boreal forest fires in Alaska. Some other studies of fire scar and burned area mapping using AVHRR NDVI data were also conducted and varied results depending upon forest types and fire years were obtained (Kasischke and French, 1995; Remmel and Perera, 2001; Jiang *et al.*, 2008).

Besides, AVHRR data have also been used for the mapping of fire frequency, distribution and area burned (Soja *et al.*, 2004), operational detection of boreal forest fire (Kelhä *et al.*, 2003), and assessment of the impact of fire on net primary productivity (NPP) (Hicke *et al.*, 2003), as well as estimation of gaseous emissions to the atmosphere (Kajii *et al.*, 2002). Finally, long time series AVHRR products on fire disturbance are given particular emphasis during recent years. For example, a 12-year (1989-2000) daily 1-km forest fire dataset across the entire North America from AVHRR records was developed (Pu *et al.*, 2007). A time series of burned land areas was also generated for a 23-year period (1984-2006) using 10-day composites of AVHRR data in western Canada (Chuvieco *et al.*, 2008). By a new algorithm, an extensive product of burned areas in boreal forest in Canada was acquired using AVHRR Long Term Data Record (LTDR) data from burn records for the 16-year period (1984-1999). This product was subsequently evaluated against AVHRR 1 km and AVHRR-PAL 8 km burned area map products (Ruiz *et al.*, 2012).

MODIS data which has a relatively higher spectral resolution (36 bands covering 0.4-14.4 μm) and temporal resolution (1-2 days) and temporal coverage since 2000, as well as its free availability policy, has been mostly widely used in a wide variety of fields among coarse spatial resolution datasets. It can be used to detect active fires and map burned areas as well as assess their influences in long time series and large scales. George *et al.* (2006) combined the normalized difference SWIR from MODIS with

thermal anomaly data to detect and date burned areas. Loboda and Csiszar (2007) introduced an approach of fire spread reconstruction to reconstruct the occurrence and development of fire events based on active fire detections from MODIS. Another dNBR-based algorithm was proposed by Loboda *et al.* in the same year (2007) through inputting MOD09A1 and MOD14 data to output yearly maps of burned area of forests in Central Siberia. This algorithm was enhanced through a data limitations-driven modification for the forests in Alaska (Loboda *et al.*, 2011).

Additionally, Jin *et al.* (2012) used the MODIS dNBR and albedo changes in spring as measures of burn severity. Besides, MODIS Enhanced Vegetation Index (EVI) was observed for monitoring the recovery process. Chen *et al.* (2005) used MODIS LAI and VI products to study the forest recovery in four post-fire sites. Results indicated that MODIS LAI overestimated values in the low LAI deciduous forests (LAI < 5) and underestimated values in the high LAI conifer forests (LAI > 6). Some other studies were conducted concerning post-fire forest recovery using MODIS-derived indices (Cuevas-Gonzalez *et al.*, 2008, 2009; Urban *et al.*, 2010).

SPOT VEGETATION has also been widely used to study fire disturbance although it has only four multispectral bands (Blue, Red, NIR and SWIR) with a spatial resolution of 1.15 km. Fraser and Li (2002) investigated the utility of the SPOT VEGETATION (VGT) sensor for estimating three crucial parameters related to forest fire: burned area, post-fire regeneration age, and aboveground biomass based on a sample of fires across Canada. Zhang *et al.* (2003) provided estimates of monthly burned area and forest fire carbon emission for the entire Russian Federation from SPOT VGT. Additionally, the stand age distribution of forest regeneration following fire could also be evaluated using the SPOT VGT NIR and SWIR bands in conjunction with AVHRR imagery (Zhang *et al.*, 2004).

Due to the high availability and accessibility of these data, in addition to the original reflectance data, many derived mature products, including MODIS burned area products (e.g. MCD45A1, MCD64A1 and GFED), AVHRR products (e.g. GBS), and SPOT VEGETATION products (L3JRC, GEOLAND-2, and GLOBCARBON etc.) are also available and convenient for direct utilization (Chang and Song, 2009; Giglio *et al.*, 2010; Kasischke *et al.*, 2011a; Chu and Guo, 2014). The accuracy and applicability of all these products were also evaluated and compared in previous studies. For example, Giglio *et al.* (2010) compared the GFED2, L3JRC, GLOBCARBON, and MCD45A1 global burned area products and found substantial differences in many regions. Mouillot *et al.* (2014) made a survey on a wide range of users of global fire data products, and finally summarized the current needs on available burned area products.

1.1.4.3 Based on high resolution data

Currently, the development of high and very high spatial resolution spaceborne sensors has brought new insight into the provision of information related with active fire characteristics and post-fire forest patterns. These studies are mainly based on textual information of high resolution image in addition to their spectral signatures. Thus object-based approaches are more common compared to pixel-based methods.

For example, Mitri and Gitas (2006, 2008) aimed to develop an object-oriented model to map the fire type and fire severity by employing post-fire IKONOS imagery. It was concluded that object-based classification applied to IKONOS imagery had the potential to distinguish and map areas of surface and crown fire spread, and produce accurate maps of fire severity, especially in open Mediterranean forests. The main source of inaccuracy was the inability of IKONOS to penetrate the dense canopy of unburned vegetation. In 2013, the two scholars proposed to map post-fire forest regeneration and vegetation recovery in Mediterranean vegetation using a combination of very high spatial resolution (QuickBird) and hyperspectral (EO-1 Hyperion) imagery and by employing object based image analysis (OBIA). The achieved accuracy was 8% higher when compared to the results from the employing of Hyperion image alone to map the same classes (Mitri and Gitas, 2013). Moskal and Jakubauskas (2013) applied the OBIA approach to develop a hierarchical classification with the application of second order image texture (SOIT) in image segmentation to classify high-spatial imagery to fine detail level of tree crowns, shadows and understory, while still allowing discrimination between density classes and mature forest versus burned classes.

It was concluded that, in the last decade, high and very high resolution optical remote sensing have widespread, providing affordable multi-temporal and multispectral pictures of the considered phenomena, at different scales (spatial, temporal and spectral resolutions) with regard to the monitoring needs (Corona *et al.*, 2008). However, it should be noted that, compared with medium and low spatial resolution data, the high and very high resolution imagery was limitedly applied in local scale because of the narrow swath width and high costs of data acquisition.

1.1.4.4 Based on SAR data

Compared to optical imagery, SAR data are more widely used to characterize the forest vertical attributes due to its penetration into vegetation canopy. They have also been applied for the detection of forest disturbance and monitoring of recovery in many studies. For example, the backscatter information from C-band SAR imagery of ERS-1 was used for mapping and estimating areal extent of fire scars in interior Alaska (Bourgeau-Chavez *et al.*, 1997) and globally (Bourgeau-Chavez *et al.*, 2002). In 2007, Bourgeau-Chavez *et al.* conducted another research on developing algorithms for the retrieval of spatially and temporally varying patterns of soil moisture from recently burned boreal forest ecosystems using C-band radar data. The Radarsat-1 intensity data were used to map the onset and progression of the fire, and interferometric coherence images were used to qualify burn severity and monitor post-fire recovery (Rykhus and Lu, 2011). Radarsat-2 quad-pol data were analyzed utilizing the polarimetric phase information to map historical fire scars over two main study sites (Goodenough *et al.*, 2011). Millin-Chalabi *et al.* (2014) evaluated the potential of SAR intensity and InSAR coherence from ERS-2 and Envisat/ASAR to detect a large peat moorland wildfire scar in northern England. There were a considerable number of other studies regarding burned area mapping, fire effect detection, and vegetation recovery monitoring based on C-band SAR sensors (Miles

et al., 2003; Gimeno *et al.*, 2004; Gimeno and San-Miguel-Ayanz, 2004; Menges *et al.*, 2004; Huang and Siegert, 2006; Abbott *et al.*, 2007; Minchella *et al.*, 2009).

Epting and Verbyla (2005) used L-band SAR data to monitor the recovery of backscatter at burn sites to the pre-fire level after 60 years since fire. Kasischke *et al.* (2011b) investigated the utility of L-band PALSAR for estimating aboveground biomass in sites with low levels of vegetation regrowth. Mari *et al.* (2012) applied a semi-automatic algorithm to the images of the L-band PALSAR for the estimate of the burned area and the results were compared with those from optical data and ground based information. Polychronaki *et al.* (2013) developed an object-based classification scheme to map the burned areas using the ALOS/PALSAR imagery acquired before and shortly after fire events. The investigation revealed that the pre-fire vegetation conditions and fire severity should be taken into account when mapping burned areas using PALSAR in Mediterranean regions.

Comparison between the performances of SAR with different bands (X-, C- and L-band) was also conducted (Ranson *et al.*, 2003; Tanase *et al.*, 2010a, 2010b, 2011, 2014). Ranson *et al.* (2003) evaluated the capabilities of three radars (ERS, JERS and Radarsat) to detect fire scars, logging, and insect damage in the boreal forest. Tanase *et al.* (2010a, 2010b, and 2011) examined the sensitivity of SAR data of multiple bands to post-fire forest regrowth. The results showed that TerraSAR-X X-band backscatter showed the lowest sensitivity to forest regrowth, with the average backscatter increasing by 1–2 dB between the most recent fire scar and the unburned forest. Increased sensitivity (around 3–4 dB) was observed for C-band Envisat/ASAR backscatter. The ALOS/PALSAR L-band backscatter presented the highest dynamic range from unburned to recently burned forests (approximately 8 dB). The interferometric coherence showed low sensitivity to forest regrowth at all SAR frequencies. In 2014, Tanase *et al.* evaluated the polarimetric properties of burned forest areas at C- and L-band, respectively. It was found only volume and dihedral scattering related components provided significant relationships with burn severity levels at L-band. For C-band, polarimetric components related to surface scattering mechanisms had increased sensitivity to burn severity levels for steep SAR acquisition geometries, and for datasets acquired with more grazing geometries, the result was same as at L-band.

1.1.4.5 Based on synergic using of multi-source data

As different types of remote sensors differ in their technical characteristics, and thus show advantages in different aspects, the synergic using of multi-source remote sensing data (including optical imagery, LiDAR and SAR data) was widely applied in the forest disturbance studies, especially during recent decade. For examples, Potapov *et al.* (2008) combined Landsat and MODIS imagery to estimate and map forest cover loss due to wildfires in 2002 and 2003. Morton *et al.* (2011) developed a Burn Damage and Recovery (BDR) algorithm to identify understory fires based on the reduction and recovery of live canopy cover as well as the size and shape of individual understory burn scars in Amazon forests using spatial and spectral information from time series Landsat (1997–2004) and MODIS (2000–2005) data. It

was found that Landsat resolution was significant for detection of burn scars < 50 ha, MODIS data were suitable for mapping medium (50–500 ha) and large (>500 ha) burn scars that accounted for the majority of all fire-damaged forests in this area. The MODIS and Landsat data were used to study the observed patterns of forest disturbance at different spatial scales in temperate forest and tropical rainforests (Broich *et al.*, 2011; Negron-Juarez *et al.*, 2014). Additionally, comparative study using SPOT, Landsat, MODIS, and AVHRR indices which had different spatial resolution had been conducted (Tong and He, 2013).

As LiDAR data are more appropriate for capturing vertically distributed elements of forest structure and change, it was used to characterize post-disturbance forest conditions combing with Landsat data (Wulder *et al.*, 2009), MODIS data (Goetz *et al.*, 2010) as well as QuickBird imagery (Arroyo *et al.*, 2010). Ranson *et al.* (2003) found that the combined use of the radar and optical sensors improved the results of discriminating the disturbances by fire, logging, and insect damage. Furthermore, Andersen *et al.* (2011) utilized a combination of ground plots, LiDAR strip sampling, multispectral optical imagery (Landsat TM) and SAR, as well as classified land cover information to estimate forest biomass resources in interior Alaska. The results indicated a substantial improvement in the precision when the estimate was based on the biomass map derived via nearest-neighbor imputation. More results and conclusions on forest disturbance and recovery using multi-source spaceborne sensors could be found in the review by Frolking *et al.* (2009).

1.2 Study area

1.2.1 The Greater Hinggan Mountain area

The Greater Hinggan Mountain area (Da Xing'an Mountain), which spans the northern part of Heilongjiang Province and the Inner Mongolia Autonomous Region of China, is the watershed of the Mongolian Plateau in the west and the flat Songliao Plain in the east (China DXAL). Its geographic coordinates range from 50°11′ to 53°33′ N in latitude, and from 121°12′ to 127°00′ E in longitude (Fig. 1.3). It has a northeast-southwest direction starting from Heilongjiang River in the north and extending southward to the upper valley of Xilamulun river. The region has a total length of over 1200 km, and a width of 200–300 km, as well as an average altitude of 573 m. The western slope slowly tilts toward the Mongolian Plateau while the steep eastern slope is eroded by the tributaries of the Songhua River and Nen River.

This region is an important climatic zone, having a typical continental cold-temperate monsoon climate with warm summers and cold winters. The annual average temperature is -2.6 °C, with a minimum temperature being -52.3 °C, and an annual precipitation of 428.6–526.8 mm. It has an annual frost-free period of 80–110 days and freezeup period of 180–200 days, an annual solar radiation time of 2600 hours and an annual effective accumulated temperature of 2100 °C. This region has rich mineral resources in terms of over 40 kinds of coal, non-ferrous and noble metal, around 584 mineral deposits, and among one of the 16 national key metallogenic belts

and 3 national prospecting targets. There are more than 500 rivers and streams inside with a drainage area of up to 710 km^2 and total water resources of 16.07 billion m^3, as well as the theoretical reserves of hydropower resources of 0.78 million kilowatts.

The Greater Hinggan Mountain area is also China's northernmost and largest state-owned modern forest area, with a total ground area of 8.35×10^6 ha and a forest-covered area of 6.78×10^6 ha. Thus, the forest coverage is around 81.20%, providing a total stand volume of up to 5.38×10^8 m^3, which accounts for around 7.8% of the total national stand volume. This region contains more than 400 species of wild animals and 1000 varieties of wild plants, and is therefore a significant collection of biological resources. It is a mixed forest area dominated by the coniferous species, Mongolian pine (*Pinus sylvestris*) and Larch (*Larix gmelini*), and the broad-leaved species, Birch (*Betula platyphylla*) and Aspen (*Populus davidiana*). Administratively, this area consists of three counties (Mohe, Tahe and Huma) and four districts (Jiagedaqi, Songling, Xinlin and Huzhong), including 10 forestry bureaus and 52 forest farms.

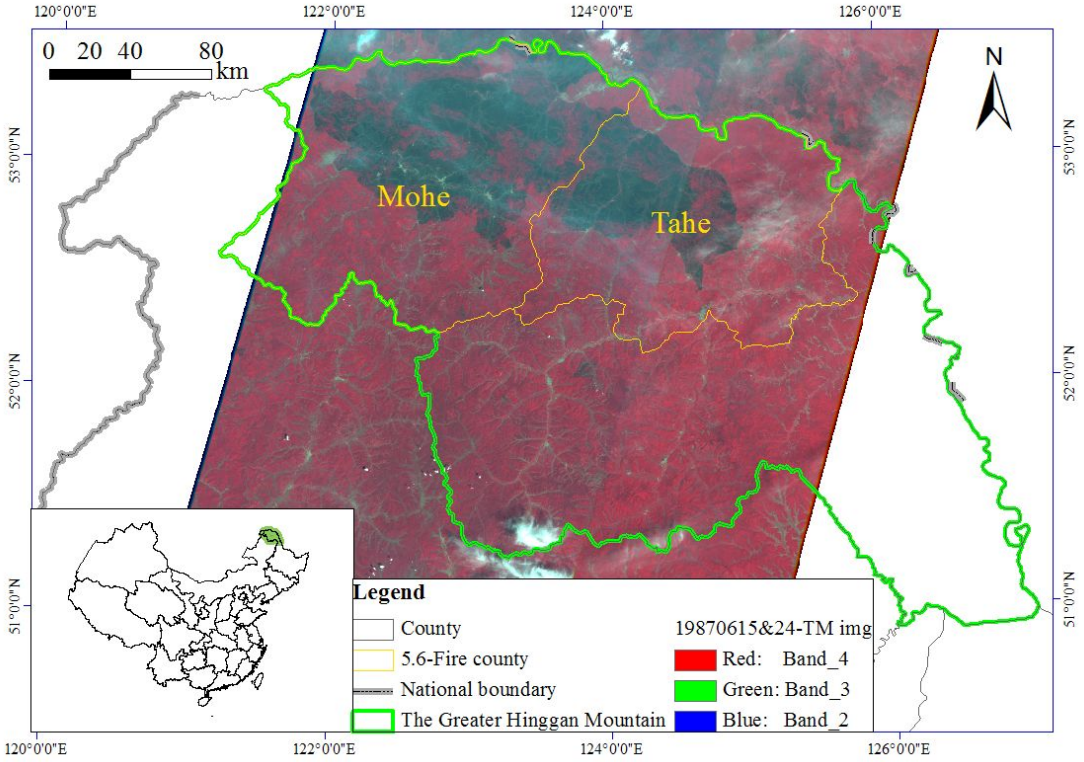

Figure 1.3 Location of the study area of the Greater Hinggan Mountain area. Background is the mosaic of two Landsat TM scenes acquired on June 15 and 24, 1987 (R: band 4; G: band 3; B: band 2).

1.2.2 The "5.6 Fire"

This region is rich in forest resources, but also suffers a high incidence of forest fires (Chang *et al.*, 2007; Chen *et al.*, 2011). The annual burned forest area of this region ranks first in People's Republic of China, making it to be the most serious forest fire hazard areas. The Greater Hinggan Mountain area has been regarded as a key focus

for the studies of forest fire prevention and post-fire vegetation recovery due to the forest and fire conditions in this region (Cahoon *et al.*, 1991; Sun *et al.*, 2011).

According to the records of fire in a period of 20 years from 1987 to 2006 (Tian *et al.*, 2010, 2011; Chen *et al.*, 2011), 1059 fires occurred, with a burned area of 2.81×10^6 ha, including 1.36×10^6 ha of forest area. It means that there is an averaged burned area of 2653 ha and burned forest area of 1284 ha for each fire. For each year, there are average 53 fires resulting in a 1.40×10^5 ha burned area, including a 6.80×10^4 ha forest-covered area.

From the perspective of vegetation type which has the occurrence of forest fires, it can be found that 61.3% of all fires occurred in needle-leaved forest followed by 23.9% in grassland, and 8.0% in broad-leaved forest, 4.7% in swamp, and the remaining are mostly in farmland. Aiming at the fire season, it is concluded that forest fires mainly occurred in spring (March-June) and autumn (October). The percentages of number of fires (27.1%) and the burned area (69.1%) as well as the burned forest area (86.8%) in May are all the highest. Although the frequency of fires in March seem not high (1.2%), it has a high percentage of burned areas (11.3%). From the aspect of the fire causes, lightning is the dominant cause for this region as it accounts for 57.1% of the total, followed by smoking (11.7%) and self-ignition (4.3%).

Among all the fires occurred in this region, the most noteworthy one is that broke out on May 6 1987. On this date, there were four forestry bureaus of Xilinji, Tuqiang, Amuer (located in Mohe) and Tahe (located in Tahe) on fire, which subsequently caused the most serious forest fire in the history of P. R. China (abbreviated to be "5.6 Fire" hereinafter). Due to the specific climatic and environmental (especially the dry forest fuels and strong winds) and topographic conditions, this fire continued to burn for as long as 28 days and brought great loss of both life and property (Cahoon *et al.*, 1991, 1994; Zhao *et al.*, 1994). Some direct losses are listed in Table 1.2. The Landsat TM scenes in Fig. 1.3 illustrate the burn scar of this fire in dark blue color.

Table 1.2 Direct loss caused by the serious forest fire on May 6 1987 ("5.6 Fire").

Item (a)	Figure	Item (b)	Figure
Burned land	1.70×10^4 km^2	Destroyed equipments	2488 sets
Burned forest area	1.01×10^4 km^2	Bridges and culverts	67
Burned houses	6.36×10^5 m^2	Railway lines	9.2 km
Burned residential houses	4.0×10^5 m^2	Power transmission lines	284.2 km
Log yards	4.5	Communication lines	483 km
Forest farms	9	Affected people	About 50,000
Stored woods	8.55×10^5 m^3	The deaths	211
Grain	3.25×10^6 kg	The injured	226

1.2.3 Post-fire research

The catastrophic forest fire ("5.6 Fire") caused tremendous damage to the ecological environments. After this fire, the local forestry bureaus had taken a series of favorable measures and conditions for local forest recovery. Also there were a considerable number of studies with respect to the local forest ecosystems from a wide variety of points of view. Most studies were performed only using the data and materials collected from the field survey and measurements of local environments within the fire scar. For example, Zhao *et al.* (1994) predicted that the swamp area would expand after that fire; however, different landscape conditions would complicate the trends of evolution. Cai *et al.* (1995) conducted lots of observations and found that river runoff increased at the initial stage after this fire, however, as the recovery of vegetation, the river runoff decreased firstly and then increased gradually until restored to the pre-fire level. Luo (2002) investigated the changes of the forest ecosystems and analyzed the impact of this fire on local ecosystems through comprehensive field survey. Xie *et al.* (2006) selected the forest farms of Yuying and Fendou in the forestry bureau of Tuqiang to reveal the change of wetland pattern and regulating capacity of forest hydrology as well as the permafrost active layer.

Recently, more emphasis has been put on the fire risk assessment and post-fire effect monitoring (forest landscape change, carbon emission etc.) based on ecological index or models. For example, Tian *et al.* (2011) analyzed the changes in the risk of forest fires at this area during the recent 20 years based on the Canadian forest fire weather index system and finally evaluated its applicability for this area. Chen *et al.* (2011) used a spatially explicit landscape model, LANDIS, to simulate the changes of fire regime and forest landscape under scenarios of four larch caterpillar disturbance intensity levels in Huzhong forest area. Sun *et al.* (2011) examined the spatio-temporal patterns of forest fires from 1980 to 1999 in this mountain area and estimated the carbon emissions from forest fires based on both field survey and laboratory experiments. Zhang *et al.* (2011) computed the amount of carbon released by forest fires in Great Xing'an Mountains from 1980 to 2005. Based on the field survey data and allometric equations, biomass of 32 separate carbon pools in 8 forest types was estimated and an improved estimation method was used.

Remotely sensed data, especially the optical imagery with medium and low spatial resolution were incorporated in some studies concerning this fire. In the context of the review from space on the severe "5.6 Fire" in 1987 (Cahoon *et al.*, 1991), Cahoon *et al.* (1994) used National Oceanic and Atmospheric Administration (NOAA) 9 AVHRR Global Area Coverage (GAC) and Defense Meteorological Satellite Program (DMSP) satellite imagery to examine fire occurrence and development and to estimate the areal extent of burning in "5.6 Fire". Based on the examination of general climatology of this region, the overall trace gas emissions to the atmosphere were derived by combining burned area estimate with fuel consumption figures and carbon emission ratios for boreal forest fires. Yi *et al.* (2013) described the long-term effects on vegetation following the severe "5.6 Fire" in 1987 on the northern Great Xing'an Mountain by analyzing the AVHRR Global Inventory Monitoring and Modeling Studies (GIMMS) 15-day composite NDVI dataset for 1984-2006. The spatial pattern

and temporal trend analyses were done using the pixel-based annual stands regrowth index (SRI) with a nonparametric Mann-Kendall (MK) statistics method. The results revealed that October was a better period compared to other months for distinguishing the vegetation conditions using the NDVI in this area.

Thus, from above review on research involving with this forest fire, it can be found that, among all previous studies, those addressing post-fire ecological issues mainly focused on one specific region (e.g. forestry bureau) or a limited period using the data from field observations. The research in time series generally aimed at the fire itself, including the fire risk, fire occurrence surveillance and fire-caused carbon emissions based on historical fire statistics, terrain and climate data as well as remote sensing imagery with low resolution (e.g. AVHRR). Little has been done aiming the entire burned area of this severe fire in large scales over the long post-fire period of 1987-2012. Many issues associated with this fire need to be addressed from the perspective of forest ecology using both the multi-scale remote sensing imagery and data collected from field survey. Especially, the effects of different forest restoration strategies on post-fire forest regeneration and vegetation recovery patterns should be given particular attention due to its significance and necessity to local forest management. These are what we propose to do in this doctoral research.

1.3 Objectives and methodology

1.3.1 Objectives

The objectives of this research can be summarized to be terms as follows:

1.3.1.1 Detection of forest disturbance and recovery

- Taking the “5.6 Fire” as an example, extract and map the burned forest area using Landsat TM imagery.
- Detect the forest disturbance and monitor post-fire forest recovery patterns based on multi-source and time series remote sensing data.
- Explore the impact of fire on forest ecosystem based on the inversion of forest ecological attributes.
- Investigate the effects of different post-fire forest restoration strategies and provide useful suggestions for local forest management.

1.3.1.2 Performance evaluation of multiple sensors

- Take use of the advantages of individual optical (Landsat/MODIS/AVNIR2) and SAR (PALSAR) technology in the monitoring of post-fire forest recovery.
- Evaluate and compare the performances of multiple remote sensing data in accuracy, applicability and efficiency for the retrieval of LAI.

1.3.2 Methodology

For the above objectives, the overall methodology of this research is illustrated in the technical flow chart (Fig. 1.4) as follows:

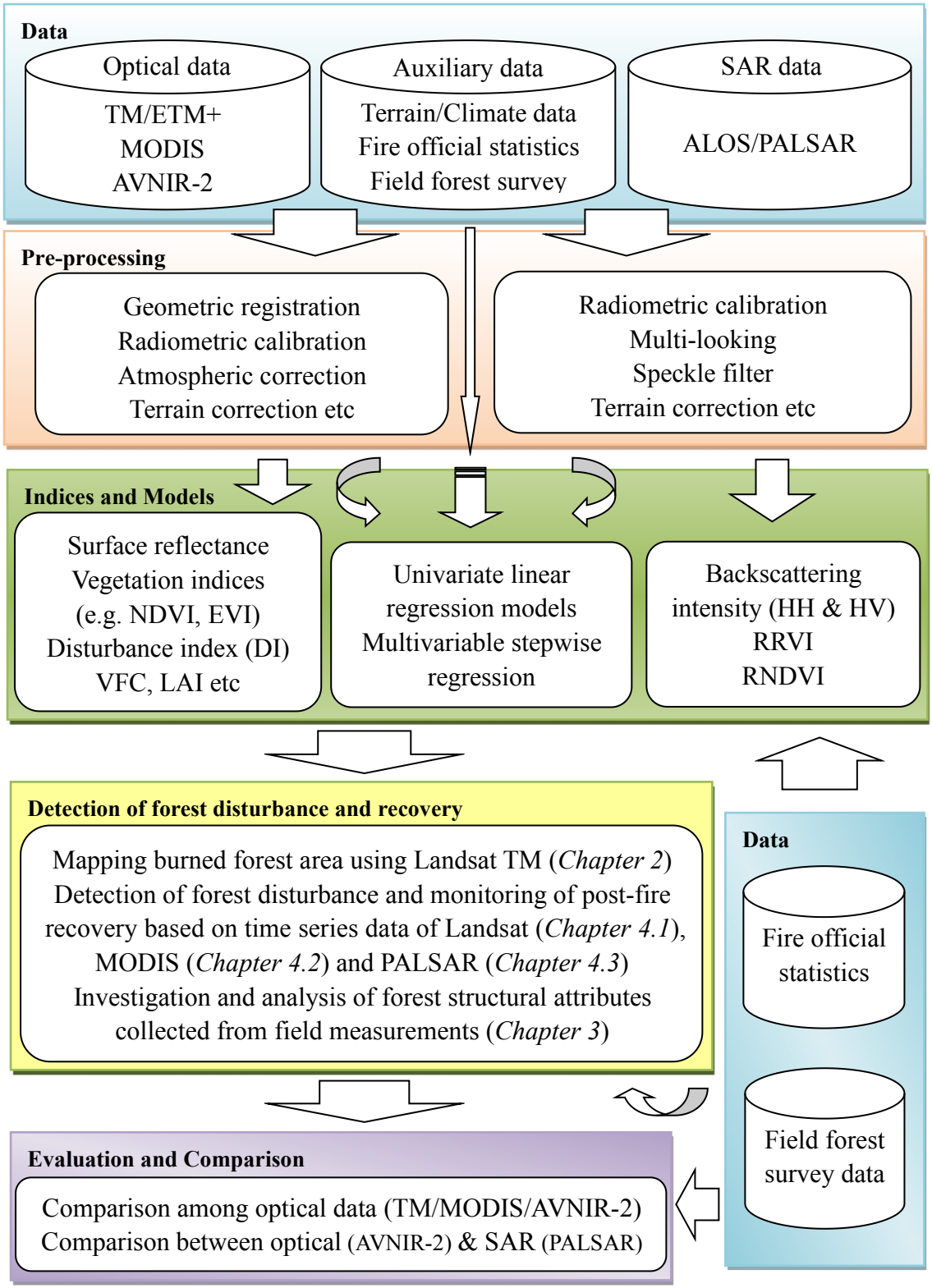

Figure 1.4 Technical flow chart of the overall methodology of this research.

2 Mapping burned forest area from Landsat TM data

2.1 Introduction

Detection of fire disturbance is a crucial process in land surface research, especially in fields related with global carbon emissions and climate change (Schroeder *et al.*, 2006, 2012). Fire activity and vegetation burning has been proposed as a primary mechanism for releasing carbon from terrestrial ecosystem to the atmosphere, with significant influence on regional and even global carbon budgets (Wotton *et al.*, 2010). Quantifying the distribution and frequency of forest fire disturbance helps to understand the changes in environment and climate, as well as serves the decision making for local forest management (Bergen *et al.*, 2009).

Extraction and mapping of burned forest area is one of the most common and basic applications among fire disturbance-related studies based on remote sensing. In various scales, the demand for the types of remote sensing data is significantly different because of the diverse technical characteristics, especially the spectral and spatial resolution. For example, at continental and global scales, the fire scar delineation and burned area mapping mainly rely on the low spatial resolution imagery which usually possess a wide swath width, including AVHRR (Kasischke *et al.*, 1993; French *et al.*, 1995; Remmel and Perera, 2001; Jiang *et al.*, 2008), MODIS (George *et al.*, 2006; Loboda *et al.*, 2007, 2011; Kasischke *et al.*, 2011a; Mouillot *et al.*, 2014), SPOT VEGETATION (Fraser and Li, 2002; Zhang *et al.*, 2003) etc.

On the other hand, remote sensing imagery with medium and high resolution, typically Landsat records are more suited for the extraction of burned forest area at regional and local scales. A great number of such studies have been conducted based on Landsat TM/ETM+ (Epting *et al.*, 2005; Bastarrika *et al.*, 2011; Matricardi *et al.*, 2013), IKONOS (Mitri and Gitas, 2008) imagery as well as ERS (Bourgeau-Chavez *et al.*, 2002), Radarsat (Goodenough *et al.*, 2011), Envisat/ASAR (Millin-Chalabi *et al.*, 2014), ALOS/PALSAR (Polychronaki *et al.*, 2013) data and so on.

Aiming at the study area of the Greater Hinggan Mountains, there were many studies to summarize and analyze the fire occurrence and fire-induced burned area, mainly using historical fire statistics. As described in chapter 1, Tian *et al.* (2010, 2011) found that in the 20 years from 1987 to 2006, totally 1059 fires occurred and was recorded, with a burned area of 2.81×10^6 ha, including 1.36×10^6 ha of forest area. Another observation on the same region concluded that there were about 1000473.06 ha of forest burned during the period of 1980-2005 (Zhang *et al.*, 2011). Furthermore, focusing on the “5.6 Fire”, the most serious forest fire in the history of P. R. China occurred in this area, as introduced before, it resulted in a burned land of 1.70×10^6 ha, including a forest-covered area of 1.01×10^6 ha according to the official statistics. However, Cahoon *et al.* (1994) detected the burn scar of the severe "5.6 Fire" using an AVHRR GAC 4-km image acquired on 29 July 1987, and then calculated the burned land of about 1.3 million hectares. The separation of forest vegetation from other land features, such as bare soil, water, buildings could not be achieved since the low spatial

resolution disabled the effective pixel spectral decomposition.

From the comprehensive comparison of the above results achieved either from official fire statistics or by low spatial AVHRR imagery, it can be found that it is still controversial about the actual burn scar and burned forest area caused by the "5.6 Fire". This issue needs to be addressed using more conclusive evidence. Compared to AVHRR imagery, the widely used Landsat data, characterized by more abundant spectral channels and much higher spatial resolution (Cohen and Goward, 2004; Pleniou and Koutsias, 2013), are particularly better suited to the fire scar delineation and burned forest area mapping in this scenario.

Based on Landsat TM/ETM+ data, a large number of algorithms, including supervised and unsupervised classification have been adopted to detect forest disturbances resulting from fires, logging and other causes (Michalek *et al.*, 2000; Epting and Verbyla, 2005; Comber *et al.*, 2012, Margono *et al.*, 2012). For serious stand-replacing forest disturbances, a much simpler method of threshold segmentation has also performed well, and been proven to be effective in the mapping of burned forest area (Loboda *et al.*, 2011; Sunderman and Weisberg, 2011). Thus, this study employs threshold segmentation based on four indices to accurately extract burned area from Landsat TM data. For more targeted comparison, threshold segmentation using single-band reflectance was conducted, as well as supervised classification of all features and forest areas alone; the accuracies of all these methods were evaluated and compared. Finally the optimal method for burned forest area extraction was selected, and the estimated areas were compared with official statistical values.

2.2 Data and methods

2.2.1 Landsat data

Since the "5.6 Fire" occurred in as early as 1987, very limited satellite remote sensing data have the temporal coverage over the occurrence. In addition to the NOAA AVHRR imagery with a 1-km and even lower resolution, only Landsat TM data with spatial resolution of 30 m (multispectral) can be utilized. The Landsat satellites follow a repetitive, circular, and sun-synchronous, near earth orbit. The technical characteristics of the sensors aboard Landsat 4-5 were shown in Table 2.1.

Table 2.1 Technical characteristics of the sensors aboard Landsat 4-5.

Satellite	Sensor	Band	Wavelength range (μm)	Spatial resolution (m)	Swath width (km)	Revisit cycle (days)
Landsat 4-5	MSS	4 (Green)	0.50 – 0.60	82	180	18
		5 (Red)	0.60 – 0.70	82		
		6 (Near IR)	0.70 – 0.80	82		
		7 (Near IR)	0.80 – 1.10	82		
	TM	1 (Blue)	0.45 – 0.52	30	185	16

2 (Green)	0.52 – 0.60	30
3 (Red)	0.63 – 0.69	30
4 (Near IR)	0.76 – 0.90	30
5 (Mid IR)	1.55 – 1.75	30
6 (Thermal)	10.4 – 12.5	120
7 (Mid IR)	2.08 – 2.35	30

Considering the "5.6 Fire" burned from May 6 to June 2, 1987, we selected Landsat-5 TM images which were acquired just after the fire was extinguished. The burn scar was so large that two scenes were needed (Table 2.2). They were provided by the USGS-EROS (Earth Resources Observation and Science centre). The overall technique flow chart of burned forest area mapping was shown in Fig. 2.1.

Table 2.2 The Landsat-5 images used for extraction in this study.

Year	Date	Path/Row	Sensor
1987	June 15	122/23	TM
1987	June 24	121/23	TM

2.2.2 Data pre-processing

Regarding pre-processing of the TM data, the two scenes were first processed by geometric correction, terrain correction, radiometric calibration, and atmospheric correction (based on the moderate resolution atmospheric transmission model-4). Following these, surface reflectance images could be acquired. The scene of path 121 row 23 was then normalized to the scene of path 122 row 23 to minimize the impact of potential sun-sensor-view angle effects (Schroeder *et al.*, 2006). Finally the two scenes were combined, using georeferenced mosaicking. Since there were some small burned patches located in Russia about which we had no knowledge of the field survey and statistics, to reduce their impacts, we extracted the fire perimeter within the Greater Hinggan Mountain area of China using visual interpretation by the geographic information system (GIS) software, and then calculated the dimensions of the burn scar.

Additionally, some rivers, roads and developed areas were within the burned area while some were not, so in order to minimize their impacts on the extraction and mapping of the burned forest area, we extracted the rivers, roads and buildings by visual interpretation, and masked them out. In this way, only the forest area remained, facilitating the mapping of the burned forest area. The extracted fire perimeter, as well as rivers, roads and building areas were shown in Fig. 2.2.

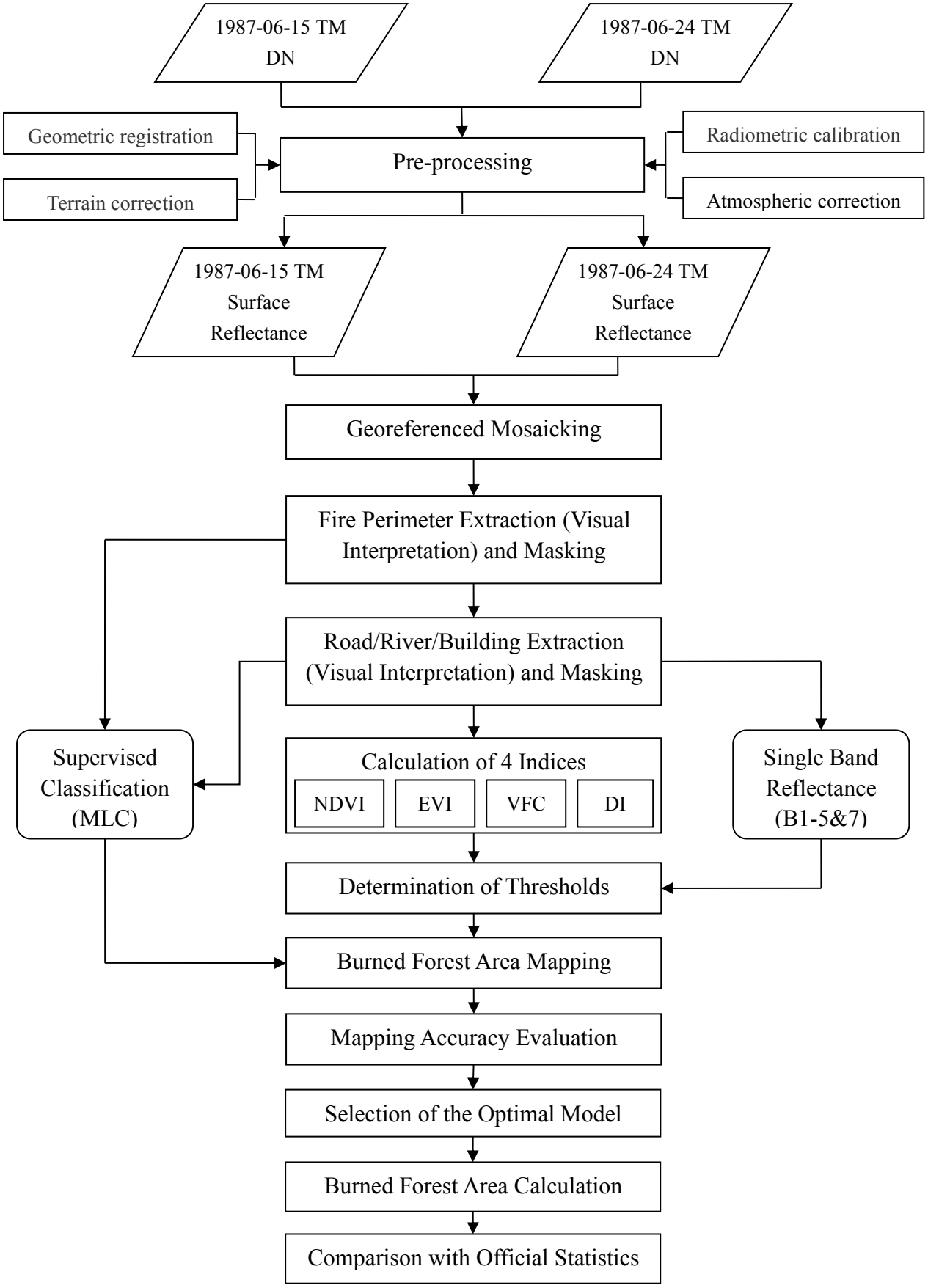

Figure 2.1 The overall technique flow chart of burned forest area mapping.

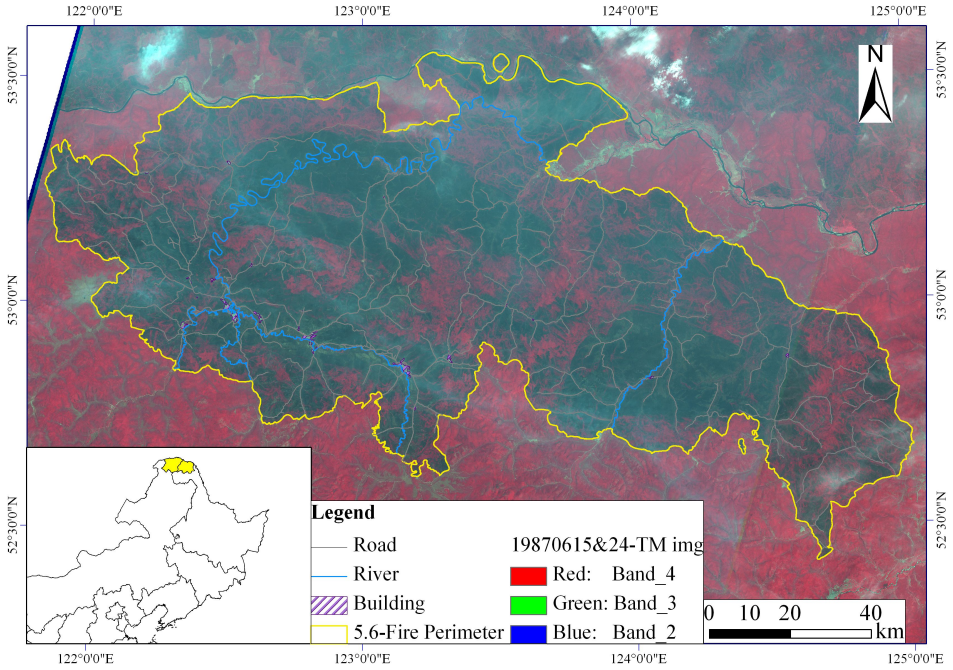

Figure 2.2 The fire perimeter and rivers, roads, building areas extracted by visual interpretation.

2.2.3 Calculation of the four indices

Vegetation indices (VI) are combinations of single bands of a remote sensing image, and are commonly used for a simple, effective and well-referenced characterization of ground vegetation status. It is intended for geographical mapping of the relative amounts of different vegetation components, which can then be interpreted in terms of ecosystem conditions (Carlson and Ripley, 1997; Guo, 2003; Koutsias *et al.*, 2009; Sharma *et al.*, 2013). Here we selected two VIs, the Normalized Difference Vegetation Index (NDVI) and the Enhanced Vegetation Index (EVI). Additionally, we calculated the Vegetation Fractional Cover (VFC) and Disturbance Index (DI) for comparison.

2.2.3.1 NDVI

NDVI is one of the oldest, most well-known, and most frequently used vegetation indices. The combination of its normalized difference formulation and use of the highest absorption and reflectance regions of chlorophyll make it robust over a wide range of conditions (Rouse *et al.*, 1974; Tucker, 1979). It can, however, saturate in dense vegetation conditions, when the leaf area index becomes high. It is defined by the following equation:

$$NDVI = \frac{(\rho_{NIR} - \rho_{\mathrm{Re}d})}{(\rho_{NIR} + \rho_{\mathrm{Re}d})} \tag{2-1}$$

where ρ_{NIR} and $\rho_{\mathrm{Re}d}$ indicate the reflectance of the near-infrared and red bands,

respectively. The calculated NDVI was shown in Fig. 2.3(a).

2.2.3.2 EVI

EVI was developed to improve the NDVI by optimizing the vegetation signals in high-LAI regions, by using the blue reflectance to correct for soil background signals and reduce atmospheric influences (Huete *et al.*, 1997). It is therefore more useful in the high-LAI regions. EVI is defined by the following equation:

$$EVI = \frac{2.5 \cdot (\rho_{NIR} - \rho_{\mathrm{Re}d})}{\rho_{NIR} + c_1 \cdot \rho_{\mathrm{Re}d} - c_2 \cdot \rho_{Blue} + L} \tag{2-2}$$

where ρ_{NIR} and $\rho_{\mathrm{Re}d}$ have the same meaning as in Equation (2-1), and ρ_{Blue} indicates the reflectance of the blue band. We set c_1 = 6.0, c_2 = 7.5 and L = 1, following those values used in the production of MODIS product. The acquired EVI was shown in Fig. 2.3(b).

2.2.3.3 VFC

VFC, which defines the amount of vegetation on the land surface, plays an important role in the fields of resource surveys and environment management, as well as climate change monitoring (Jiang *et al.*, 2008). Many methods have been developed to estimate VFC, among which, the linear spectral mixture analysis (SMA) (Fernandez-Manso *et al.*, 2012) has been widely favored. In actual applications, we often use vegetation indices in place of reflectance of a single band to take full use of multi-band information (Cao *et al.*, 2011; Chen and Cao, 2012). NDVI was selected in this case, and the calculation of VFC was performed using the following equation:

$$f_{cover} = \frac{NDVI - NDVI_{soil}}{NDVI_{veg} - NDVI_{soil}} \tag{2-3}$$

where f_{cover} is the VFC, and $NDVI_{veg}$ and $NDVI_{soil}$ are the NDVI values of pure forest and pure soil pixels in the study area, respectively. The acquired VFC was shown in Fig. 2.3(c).

2.2.3.4 DI

DI is derived from the Tasseled Cap transformation (Crist and Cicone, 1984; Healey *et al.*, 2005; Chen *et al.*, 2012). It is a linear combination of the three Tasseled Cap indices: Brightness (B), Greenness (G) and Wetness (W). However, as there are variations in the acquisition date between the images, the detection model should be designed to be relatively insensitive to phenology and BRDF (bidirectional reflectance distribution function) variation. Thus spectral normalization steps should be taken, which use within-image statistics to normalize radiometric change. The normalized equations are as follows:

$$\begin{aligned} B_n &= (B - B_\mu) / B_\sigma \\ G_n &= (G - G_\mu) / G_\sigma \\ W_n &= (W - W_\mu) / W_\sigma \end{aligned} \tag{2-4}$$

where B_μ, G_μ, and W_μ represent the mean Tasseled Cap Brightness, Greenness and Wetness of the dense forest for a particular scene, respectively, B_σ, G_σ, W_σ are the corresponding standard deviations, and hence B_n, G_n and W_n indicate the normalized Brightness, Greenness and Wetness, respectively. Here the "dense forest of a particular scene" that was used for normalization was selected from the corresponding NDVI image based on the criterion $NDVI \geq NDVI_{95\%}$.

After the three component indices were normalized, they can be combined linearly to acquire the DI (Healey *et al.*, 2005) as follows:

$$DI = B_n - (G_n + W_n) \tag{2-5}$$

The DI transformation is based on the observation that disturbed stands of forest typically have a higher Tasseled Cap brightness value and lower greenness and wetness values than undisturbed forest areas. A disturbed forest area that shows a high positive B_n and a low negative G_n and W_n will give high DI values. Conversely, an undisturbed forest area should present low DI values. The estimated DI image was shown in Fig. 2.3(d).

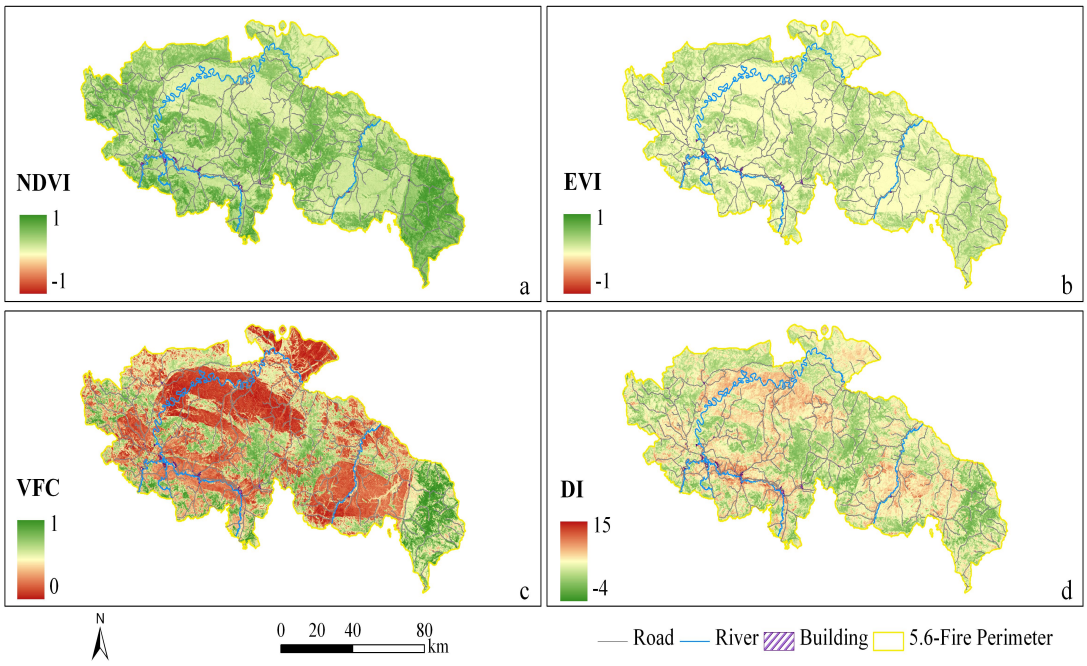

Figure 2.3 Maps of the burned area of (a) NDVI, (b) EVI, (c) VFC and (d) DI.

2.2.4 Determination of thresholds for the four indices

In order to determine the thresholds in each index which will permit the separation of burned forest from unburned forest, we selected samples in both the burned and unburned forest area, by a stratified random sampling method, and then plotted their distribution histograms from the NDVI, EVI, VFC and DI images. The results were shown in Fig. 2.4(a), (b), (c) and (d), respectively.

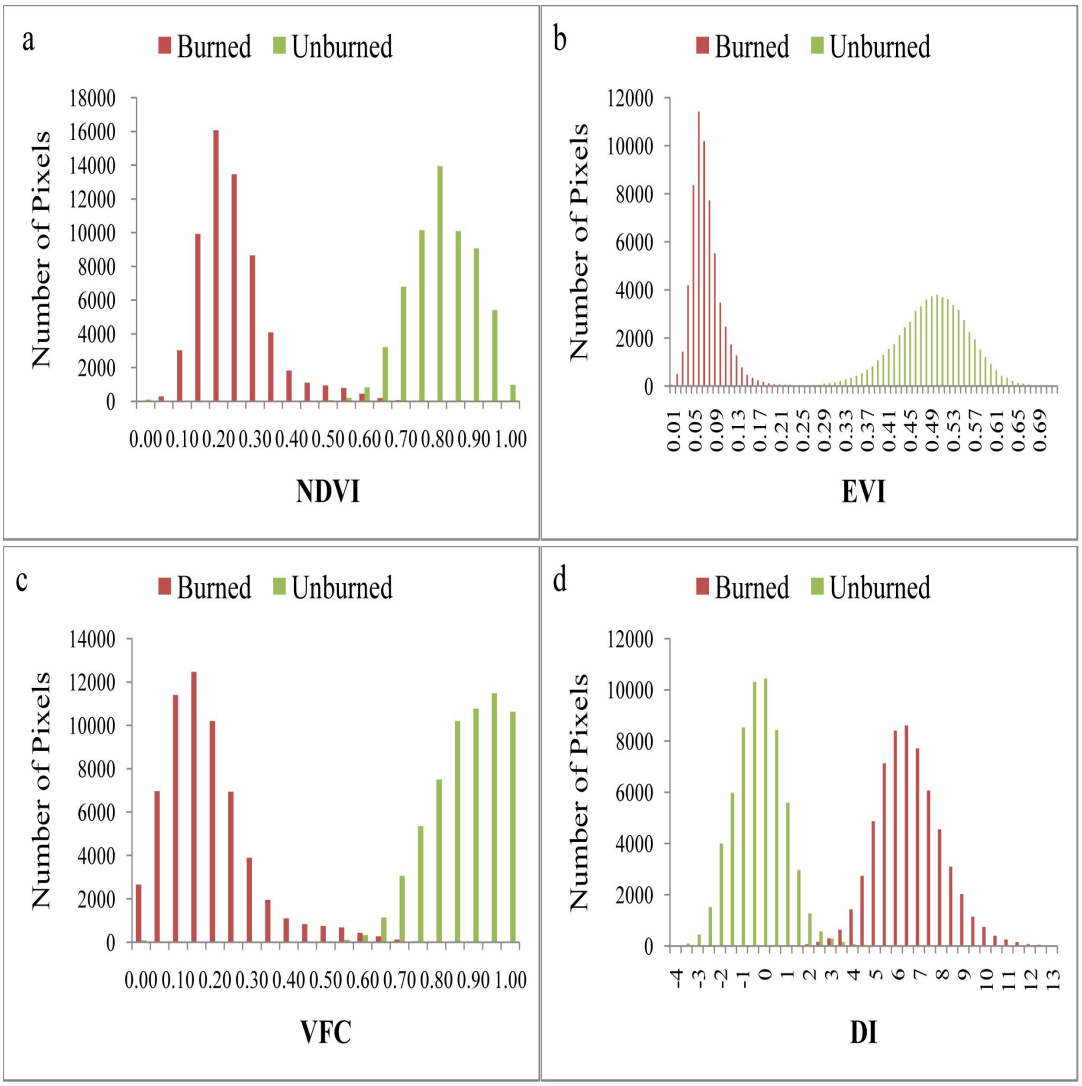

Figure 2.4 Histograms of burned and unburned forest area of (a) NDVI, (b) EVI, (c) VFC and (d) DI.

From these figures, it can be found that the histograms of the burned and unburned forest area were clearly separated from one another, making the threshold segmentation feasible. For accurate determination of the thresholds, we focused on the overlap area in each histogram, between the burned and unburned forest areas, and selected the optimal thresholds with which the highest accuracy of burned forest area mapping could be achieved.

2.2.5 Mapping by single-band threshold segmentation

The NDVI, EVI, VFC and DI indices, which incorporate information from different bands, gave different accuracies in their mapping of the burned forest area. As such, what may we expect if only the surface reflectance of single-band is used for mapping? For comparison, we performed a burned forest area mapping based on threshold segmentation of single-band reflectance.

The threshold for each band should be determined. Here the same samples used above were employed for threshold determination. The histograms for the six TM multispectral bands were plotted. Then the optimal thresholds were determined by the detection and evaluation iteratively.

2.2.6 Supervised classification

As methods of supervised and unsupervised classification are currently widely used to detect forest disturbances resulting from fires, logging and other causes (Castellana *et al.*, 2007; Comber *et al.*, 2012; Margono *et al.*, 2012), for further comparison, the mapping of burned forest area was also conducted using a supervised classification. Here the Maximum Likelihood Classifier (MLC) (Kavzoglu and Reis, 2008) was used to classify the surface reflectance images. In fact, we also trained some other classifiers, such as Parallelepiped, Minimum Distance, and Spectral Angle Mapper, however their classification accuracies did not show significant improvements, and thus here they have not been included.

Firstly, classification of all features was performed. The features selected in training samples included five classes: roads, rivers, buildings, burned forest and unburned forest. Additionally, as the mapping by threshold segmentation with these indices was achieved using only the forest area, from which the rivers, roads and buildings had been masked, the supervised classification of only forest area was also performed for a more targeted comparison. Thus only two classes, burned forest and unburned forest, were included in the training samples. Finally, these two types of classification were both carried out using six different band combinations: bands 2 and 5; bands 3 and 4; bands 4 and 7; bands 1, 3 and 4; bands 1, 2, 3 and 5; all 6 bands.

2.3 Results

2.3.1 Mapping using the four indices

From Fig. 2.5(a), (b), (c) and (d), it was concluded that the optimal thresholds for segmentation using NDVI, EVI, VFC and DI were 0.56, 0.24, 0.58 and 2.7, respectively. Based on the acquired thresholds for NDVI, EVI, VFC and DI, we mapped the burned forest area using each index, respectively. To fully verify and evaluate the mapping accuracy, we selected another group of test samples consisting of 2,023,605 burned forest pixels and 500,325 unburned forest pixels by visual interpretation following the stratified random sampling criterion. Using the index of Moran's I, the spatial autocorrelation of these burned and unburned forest pixels was

examined, respectively. The results indicated that the interpreted burned and unburned forest pixels were both randomly distributed and can be used for the accuracy assessment. The assessment results based on the whole collection of these pixels were shown in Table 2.3(a). As the reference samples used to estimate the accuracy were created using photo interpretation of the same Landsat image, usually high accuracies were justified.

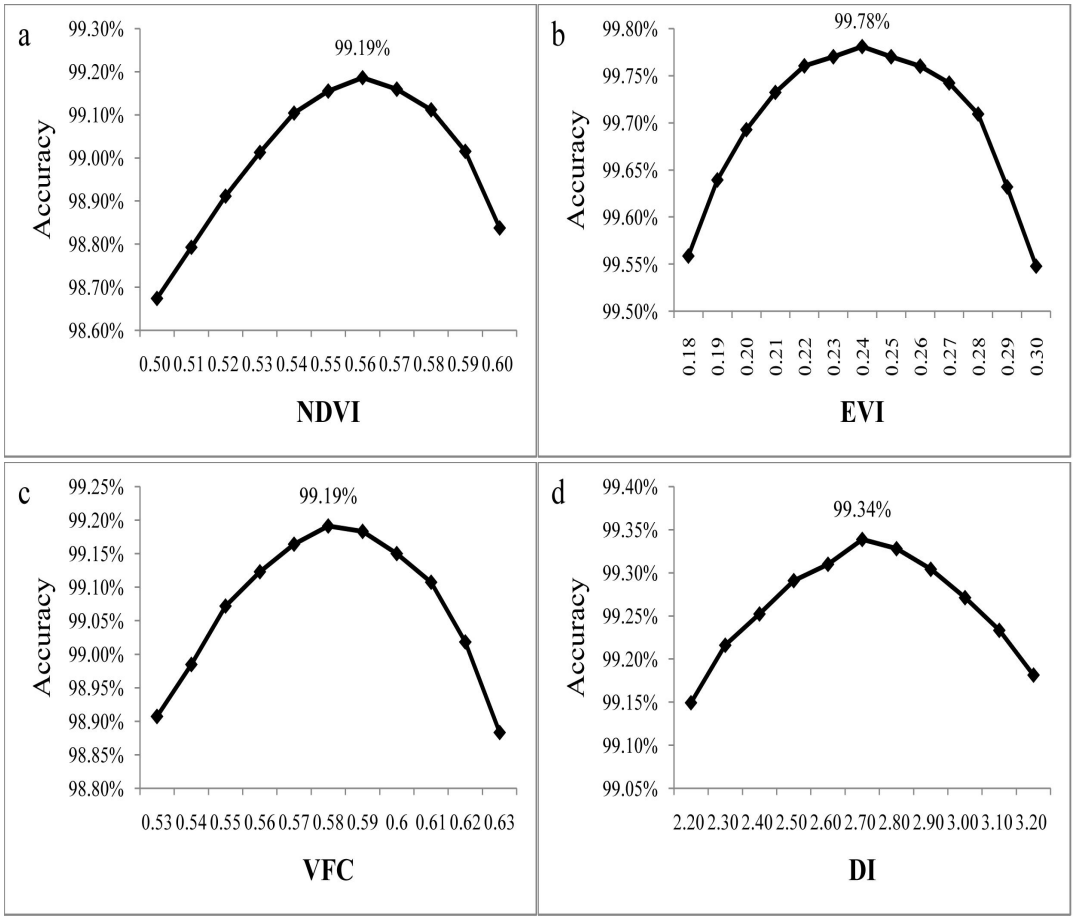

Figure 2.5 Determination of optimal thresholds by focusing on the overlap area of histograms of (a) NDVI, (b) EVI, (c) VFC and (d) DI.

Table 2.3 The accuracies of burned forest area mapping using: (a) four indices and (b) six TM bands.

Indices/Variables	Overall accuracy	Kappa coefficient
(a) Four indices		
NDVI	99.07%	0.9712
EVI	99.83%	0.9946
VFC	99.06%	0.9716
DI	99.44%	0.9824
(b) Six TM bands		
Band 1	70.18%	0.2098

Band 2	53.61%	0.1411
Band 3	80.62%	0.4703
Band 4	99.72%	0.9914
Band 5	46.03%	0.1253
Band 7	99.16%	0.9738

Using the test samples, the overall mapping accuracies of the NDVI, EVI, VFC and DI indices were found to be 99.07%, 99.83%, 99.06% and 99.44%, with corresponding kappa coefficients of 0.9712, 0.9946, 0.9716 and 0.9824, respectively. By comparison, it was found that the mapping accuracies using the four indices differed, and that their relative merits followed EVI > DI > NDVI ≈ VFC. To explore the causes of this difference, the spectral signatures of the burned and unburned forest area for the Landsat TM multispectral bands was plotted (Fig. 2.6).

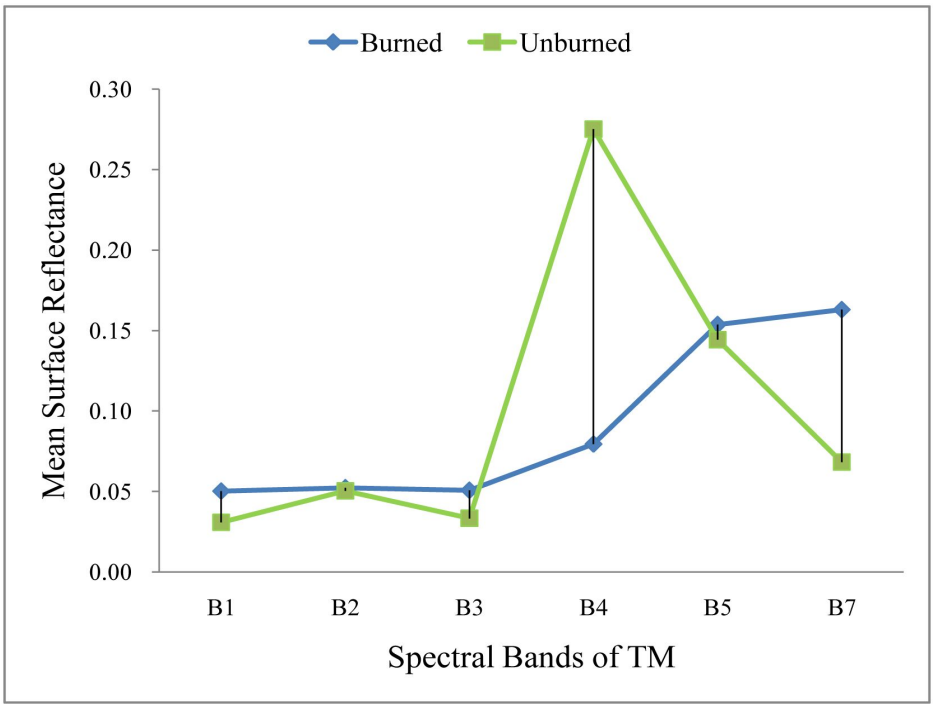

Figure 2.6 The spectral signatures of burned and unburned forest area for Landsat TM multispectral bands.

From Fig. 2.6, it was concluded that the differences in spectral characteristics of band 1, 3, 4 and 7 were significant, with band 4 most prominent. In contrast, the differences in band 2 and 5 were not significant. From the algorithms of the four indices (Equations (2-1)–(2-5)), we knew that NDVI incorporates information from band 3 and 4, and thus reflected the significant difference between the burned and unburned forest area in the two bands. EVI, which utilized the information from band 1, 3 and 4, had an improved performance over NDVI. Since VFC was acquired from NDVI, their accuracies were approximately equal. DI, derived from the Tasseled Cap transformation which made use of all TM multispectral bands (band 1–5 and 7), also

performed well in the mapping. However, as it incorporated the indistinct information from band 2 and 5, the accuracy of the DI mapping was less than that of EVI, although higher than those of NDVI and VFC.

2.3.2 Mapping using the six TM bands

The burned forest area was also mapped using the acquired optimal thresholds of 0.04, 0.04, 0.04, 0.15, 0.16 and 0.11 for band 1-5 and band 7, respectively. The same test samples were used for accuracy evaluation. From Table 2.3(b), it can be found that the overall mapping accuracies based on band 1-5 and band 7 were 70.18%, 53.61%, 80.62%, 99.72%, 46.03% and 99.16%, with corresponding kappa coefficients of 0.2098, 0.1411, 0.4703, 0.9914, 0.1253 and 0.9738, respectively.

From comparison among the bands, it was concluded that the mapping based on band 2 and band 5 had the lowest accuracy, followed by those of band 1 and band 3, while the mapping using band 4 and band 7 performed much better. This could be explained by Fig. 2.6, in which the spectral difference between burned and unburned forest areas was least in band 2 and 5, followed by that in band 1 and 3, while the difference in band 4 and 7 was among the most significant.

2.3.3 Mapping using supervised classification

With the results of the two types of classification, the same test samples as used above were taken as ground truth references for error analysis and accuracy evaluation. The overall accuracies and kappa coefficients were calculated (Table 2.4).

Table 2.4 Mapping accuracies of (a) all features classification (5 classes), and (b) only forest classification (2 classes) using six different band combinations.

Band combinations	Overall accuracy	Kappa coefficient
(a) All features classification (5 classes)		
Bands 2&5	47.95%	0.1864
Bands 3&4	91.54%	0.7996
Bands 4&7	93.86%	0.8500
Bands 1&3&4	93.06%	0.8310
Bands 1&2&3&5	90.40%	0.7711
All 6 bands	95.18%	0.8800
(b) Only forest classification (2 classes)		
Bands 2&5	52.78%	0.1599
Bands 3&4	99.49%	0.9841
Bands 4&7	99.73%	0.9915
Bands 1&3&4	99.51%	0.9847
Bands 1&2&3&5	95.42%	0.8629
All 6 bands	99.71%	0.9910

From Table 2.4(a) and (b), it can be found that the classification accuracy based on the combination of bands 2&5 was the lowest, and was significantly lower than the accuracies from other combinations. This result can be explained by the little spectral difference between the burned and unburned forest areas in band 2 and 5, which was shown in Fig. 2.6. As there were significant differences in the spectral characteristics of burned and unburned forests in band 1, 3, 4 and 7, the classifications based on the combinations of bands 3&4, bands 4&7, as well as bands 1&3&4 were able to achieve more desirable results. The combination of bands 1&2&3&5 gave a lower classification accuracy than the above three combinations. It is probably because of the exclusion of band 4 from this combination, and thus the exclusion of the most significant information.

2.3.4 Area calculation and comparison with official statistics

Among all the mapping methods studied, including the six single-band reflectance threshold segmentation, four indices threshold segmentation and two types of supervised classification, the mapping by EVI threshold segmentation achieved the highest accuracy. As such, the burned forest area estimated using the EVI was determined to be optimal and taken as the final output. The burned and unburned forest area given by the EVI threshold segmentation, in addition to rivers, roads and building areas input by visual interpretation were shown in Fig. 2.7.

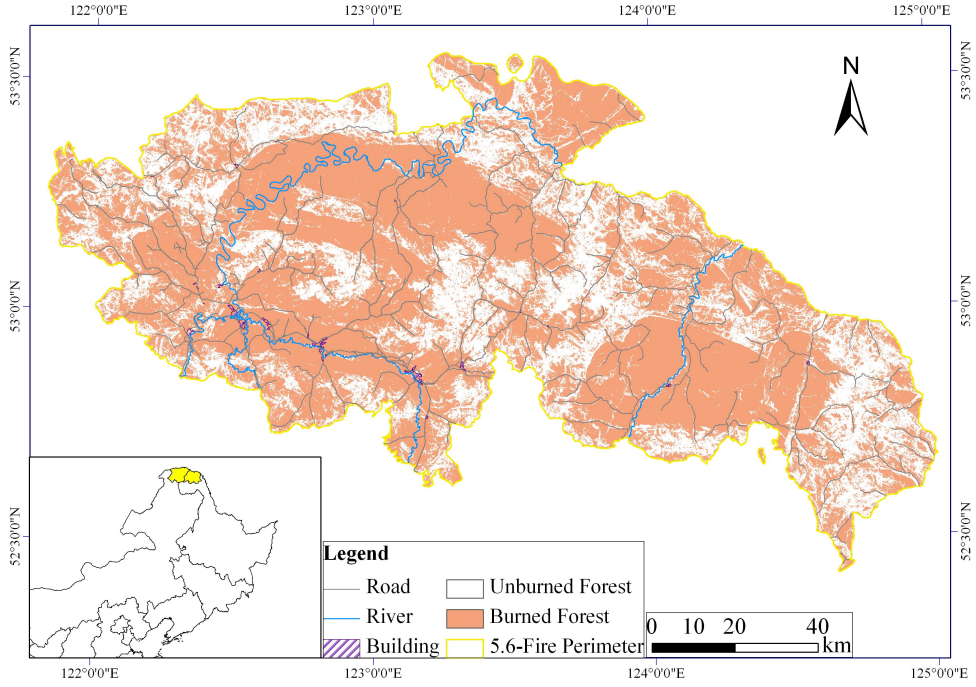

Figure 2.7 The burned and unburned forest area by EVI threshold segmentation as well as the rivers, roads and building areas by visual interpretation.

Based on the mapping result, we calculated the burned land area, using the fire perimeter from visual interpretation, and the burned forest area given by the EVI threshold segmentation, and compared them with values from official statistics (Fig.

2.8). The comparison revealed a discrepancy between the remote sensing extracted values, of 1.298 million and 0.862 million ha, respectively, and the official statistical values, of 1.70 million and 1.01 million ha, respectively. The official statistical values came from the measurement and estimation of area within the range delineated on the topographic map and forest form map. The delineation was achieved mainly by visual inspection in the field survey with the help of corresponding land use map.

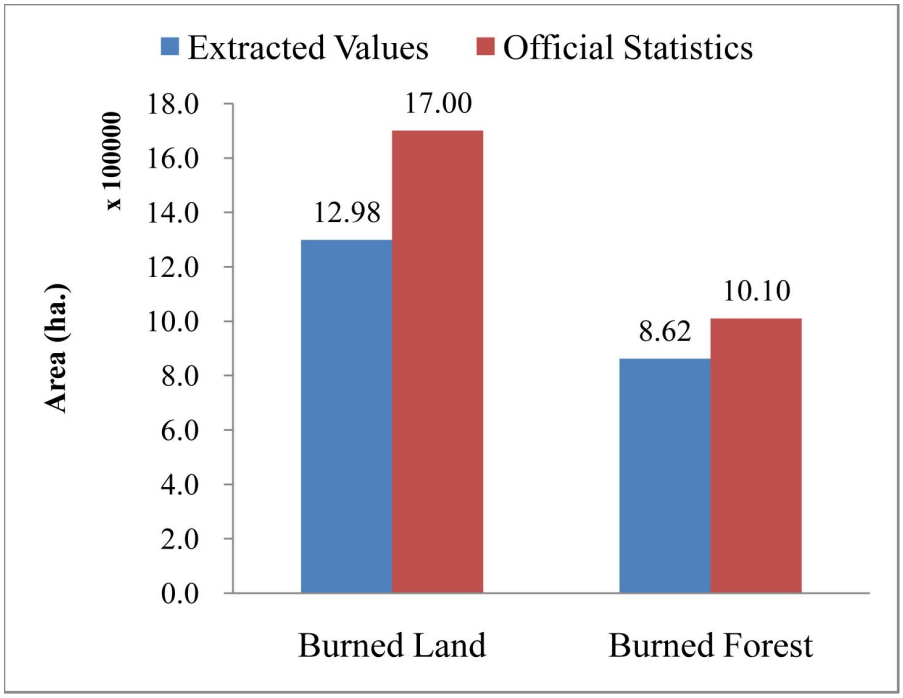

Figure 2.8 The comparison of burned land and burned forest area between remote sensing extracted values and official statistics.

Compared with human experience in the field survey and range delineation of fire scar, the mapping and calculation of burned area using remote sensing data appeared to be more objective, making the results more credible. In addition, due to the advantages of large-scale, multi-temporal and high-precision of remote sensing technology, the Landsat-based mapping was repeatable, less labour-intensive and more efficient, and proven to be an excellent choice of burned forest area mapping.

2.4 Discussion

2.4.1 Performance of spectral bands and indices

The burned land and burned forest area of the “5.6 Fire” were mapped from remote sensing images in this study. In this area, the discrepancy between the remote sensing extracted and official statistical values was found for the first time. This finding allows a more objective and accurate understanding of the losses caused by that fire and thus provides crucial information for the local forest monitoring and management.

Remote sensing approaches offer a feasible and effective tool for the detection of

forest disturbances in regional and even global scales (Masek *et al.*, 2008; Rykhus and Lu, 2011; Stroppiana *et al.*, 2012). In previous studies, a variety of spectral indices (such as DI by Healey *et al.*, 2005, NDVI and EVI by Stroppiana *et al.*, 2012, and NDVI, DVI, RVI, SAVI etc. by Veraverbeke *et al.*, 2012) have been utilized and compared, and being proven to achieve high accuracies. However, discussion on the causes of the variations in accuracies under certain circumstances still remains to be further explored.

In this study, four indices of NDVI, EVI, VFC, and DI were calculated for the burned forest area mapping. For comparison, the mapping using six TM multispectral bands was also performed individually by the same approach of threshold segmentation. The high accuracies achieved by the band 4 and band 7 were consistent with the findings in some previous studies (Koutsias and Karteris, 2000; Pleniou and Koutsias, 2013). However, here we found that the reflectance of band 5 was apparently not sensitive to forest fire disturbance. Actually, unlike Landsat band 7, in band 5, the spectral pattern of burned surfaces does not follow a unique pattern. This is consistent with the findings of the separability analysis by Maingi (2005) who concluded that information recorded in Landsat ETM+ band 7 was more informative than in ETM+ band 5 for the separation of old and new fire scars except for shaded deciduous forests. Some other studies carried out in the middle-infrared range indicate a varied behavior of burned areas (Pereira *et al.*, 1997; Arino *et al.*, 2001).

In particular, the comparison between the vegetation indices and the single spectral bands showed the accuracy of the mapping based on band 4 was even higher than that using NDVI, VFC and DI, and quite close to that by EVI. In addition, the mapping accuracy based on band 7 was also higher than that using NDVI and VFC although the magnitude of the difference was not significant. These results indicated that the accuracy of burned forest area mapping depends not upon the number of bands used, but on the proportion of significant information contained within the mapping application. This provides more consideration for the selection of indices or bands used for burned forest area mapping in the Greater Hinggan Mountain area.

2.4.2 Selection of classification principles

The MLC-based supervised classification was conducted to detect forest disturbance using different band combinations. Here we considered two groups of training samples. Except the samples consisting of all features, another group only included two classes of burned forest and unburned forest. The comparative study gave the result that the forest-only classification had higher accuracies than the all features classification. Especially, the classification accuracy from the combination of bands 4&7 was even higher than that from all six bands combination. This demonstrates that the classification accuracy is not only determined by the amount of significant information contained, but also influenced by any insignificant information included. The combination of bands 4&7 was demonstrated to be most suitable for the classification in this case, when only considering the forest area.

The above analyses indicate that simple indices or methods can also produce better performance than complex calculations under some specific conditions. It is probably

due to the blurring or lost of some original significant characteristics in the reorganization of more complex models or indices. Thus the complexity in the models is better to be avoided if simpler but also effective approaches exist, especially in actual applications.

The Landsat records are particularly useful for forest change monitoring, as they have unprecedented historical coverage, spanning 40 years of observations, as well as the necessary spatial and spectral resolutions, of up to 30 m and 7 bands, respectively. This permits the capture of most natural and managed disturbance events at regional and global scales (Wilson and Sader, 2002; Tucker *et al.*, 2004; Koutsias *et al.*, 2009; Kennedy *et al.*, 2012). In the following chapters, the monitoring of post-fire forest recovery can also be conducted based on these images, as well as with a combination of data from other sensors, including AVNIR-2, MODIS and PALSAR.

3 Field forest survey and data analysis

3.1 Introduction

Following severe fires, the forest ecosystems are remained to be recovered either under natural regrowth or by different degrees of human intervention in terms of seed planting or transplantation depending upon the local environmental conditions and forest utilization requirements (Gromtsev, 2002; Perry *et al.*, 2008; Dainou *et al.*, 2011; Camac *et al.*, 2013). In various forest ecosystems with different species and intensity of fire, the effects of forest restoration strategies were proven to be varied (Marzano *et al.*, 2013). Consequently it is necessary to investigate the effects of various restoration treatments and monitor the patterns of post-fire forest regeneration as it pertains to both post-fire ecological research and forest management (Bonan, 1989; Stueve *et al.*, 2009; Wotton *et al.*, 2010; Huang *et al.*, 2012; Otoda *et al.*, 2013).

Although there are already a large number of studies about forest fires and post-fire forest recovery (Asselin *et al.*, 2001; Díaz-Delgado and Pons, 2001; Shorohova *et al.*, 2009; Forkel *et al.*, 2012), most of them focus on species composition and forest succession (Uemura *et al.*, 1997; Schulze *et al.*, 2005; Gauthier *et al.*, 2010; Otoda *et al.*, 2013), as well as on the structural parameters and plant cover/tree density (Pausas *et al.*, 1999; Johnstone *et al.*, 2004; Moreira *et al.*, 2009, 2013; Ascoli *et al.*, 2013; Senici *et al.*, 2013). Thus far, relatively few studies have considered the forest ecosystem as a whole, including all life forms (such as arbor species, shrubs, and grasses) (Perry *et al.*, 2008), especially using quantitative indicators (Healey *et al.*, 2005). Here, we introduce a three-dimensional scaling parameter, leaf area index (LAI), which has been widely developed and validated in the interdisciplinary field of forest remote sensing combining forestry science with remote sensing technology (McMichael *et al.*, 2004; Chen *et al.*, 2010).

The leaf forms the main surface for matter and energy exchange between the plant canopy and atmosphere, and LAI, defined as half of the total green leaf area per unit horizontal ground surface area, is proposed as a key variable in the studies about terrestrial ecosystems and their development (Chen and Black, 1992; Arias *et al.*, 2007; Schleppi *et al.*, 2011). LAI can be used to characterize the canopy-atmosphere interface of an ecosystem, and is related to precipitation, atmospheric nutrient deposition and interception, canopy microclimate, radiation extinction, as well as water, carbon, and energy exchanges with the atmosphere (Chen *et al.*, 2010). It can be retrieved from remote sensing data, and measured using advanced canopy analyzer devices (Arias *et al.*, 2007).

The Greater Hinggan Mountain area has been regarded as a key focus for forest fire prevention and post-fire forest recovery monitoring because of the high incidence of forest fires, particularly the occurrence of the “5.6 Fire”, most serious forest fire in the history of P. R. China. After this fire, the local forestry bureaus have taken a series of measures to recover the forests and many favorable conditions have been created for speeding up ecological construction. During the recovery process, three different

restoration treatments were adopted for the regeneration of the forests in the burned area. The dynamics of forest regeneration varied depending on the treatment selected for regeneration.

In this chapter, taking the forests in three forestry bureaus (Xilinji, Tuqiang and Amuer) which suffered the largest biomass loss from the "5.6 Fire" as a focus, we investigated the post-fire forest recovery under different restoration treatments. A field survey was designed and a detailed statistical analysis on the collected data of structural parameters and LAI was performed. The objectives were to evaluate and compare the effects of different restoration treatments, based on which to determine which approach is most suitable for successional regeneration of local forest ecosystems. On the basis of the results, effective suggestions about post-fire forest recovery could be provided for reference in local forest utilization and management.

3.2 Data and methods

3.2.1 Three restoration treatments

Following the "5.6 Fire", three totally different restoration treatments, namely artificial regeneration, natural regeneration, and artificial promotion, were conducted for forest regeneration. As the name suggests, artificial regeneration indicates an active role of humans in the recovery process through removing all dead or damaged trees belonging to the pre-fire stand from the burned area, followed by complete replanting. In these sites, the coniferous species of *P. sylvestris* and *L. gmelini* were selected and a regular plant spacing (1.5 × 1.5 m or 1.5 × 2 m) was adopted according to field conditions. Natural regeneration means allowing the forests to regenerate completely naturally without any human intervention. Thus no any salvage logging or harvesting was conducted, allowing natural restoration to take place. The third approach, artificial promotion, indicates essentially natural regeneration with a select number of artificial aids, which include removing all dead trees and snags, clearing the burned area, weeding, and digging some pits to promote seed germination and growth naturally. In the years with adequate seeds (as the case of forest regeneration in this study), only pits with regular spacing were dug to promote seed rooting, while in a year lacking in seeds, on the basis of the digging, some supplementary measures of artificial seeding was also taken. In any case, no plantation by means of transplantation was performed.

3.2.2 Sampling design and field data collection

In order to investigate the forest restoration dynamics and compare the effects of different restoration strategies, we designed and performed a field forest survey within the burned area of the "5.6 Fire" during 12–18 July 2012, which was the 25th year after this fire. In this survey, we examined three forestry bureaus, Xilinji, Tuqiang, and Amuer, which covered over 85% of the burned forest area of the "5.6 Fire". We selected and investigated three plots of 10 m × 10 m in each forestry bureau under each type of restoration treatment. With respect to the plot size, in all plots under

artificial regeneration and artificial promotion treatments, the trees are evenly distributed within the plots and their surrounding areas, making the size of the plot effectively irrelevant. However, it was not such a case for the plots under natural regeneration. Thus, in future surveys, the size of sampling plots should be increased and the number of observations in each combination of treatment and region is also in need of augmentation. The field scene of forest ecosystems recovered under the three restoration treatments was shown in Fig. 3.1.

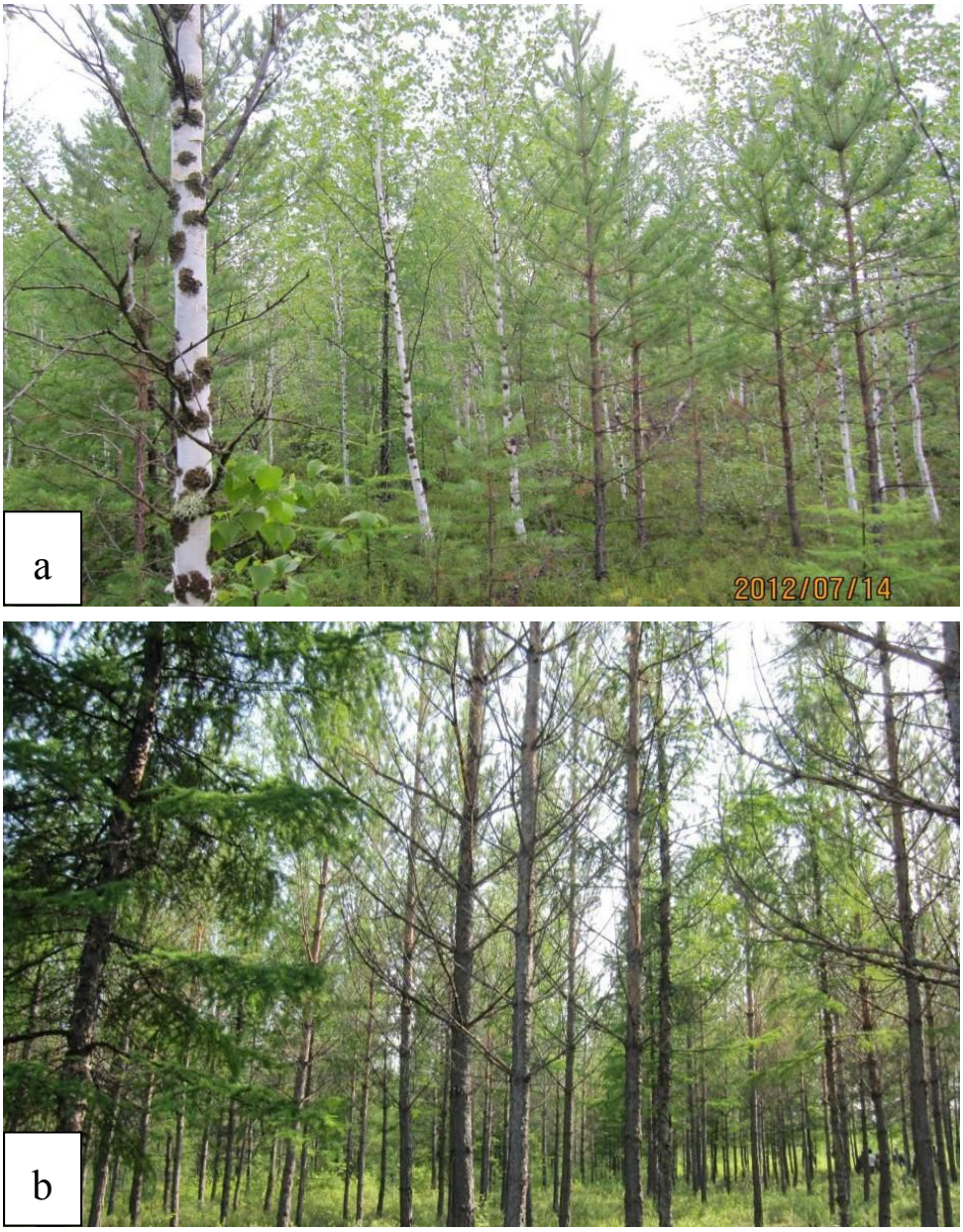

Figure 3.1 The field scene of forest ecosystems recovered under the three restoration treatments: (a) artificial promotion, (b) artificial regeneration and (c) natural regeneration.

Figure 3.2 Some photos showing the field working scene of some participants.

The coordinates of the four corners and the centre of each plot were measured using a differential global positioning system (DGPS). Within each regeneration plot, the species of each individual tree was recorded and the corresponding structural parameters including tree height, Diameter at Breast Height (DBH), and crown width (in the direction of both North-South and West-East) were measured using such devices as an altimeter rod, a tape measure, and a NIKON Forestry Pro 550. The young trees with DBH < 2 cm were recognized as seedlings and being counted; however, their structural parameters (tree height, DBH, and crown widths) were not measured and incorporated in the subsequent statistics. The dominant shrub species were also identified, but not measured. The LAI of each plot was measured using the LAI-2200 canopy analyzer with a height of just above the shrub under stable weather conditions (Chen and Cao, 2012). For all plots in the three forestry bureaus, forest regeneration began during the 1987–1989 period, regardless of the restoration treatments, and never suffered any disturbance thereafter. Some photos showing the field working scene of some participants were put in Fig. 3.2. The spatial distribution of these plots was shown in Fig. 3.3.

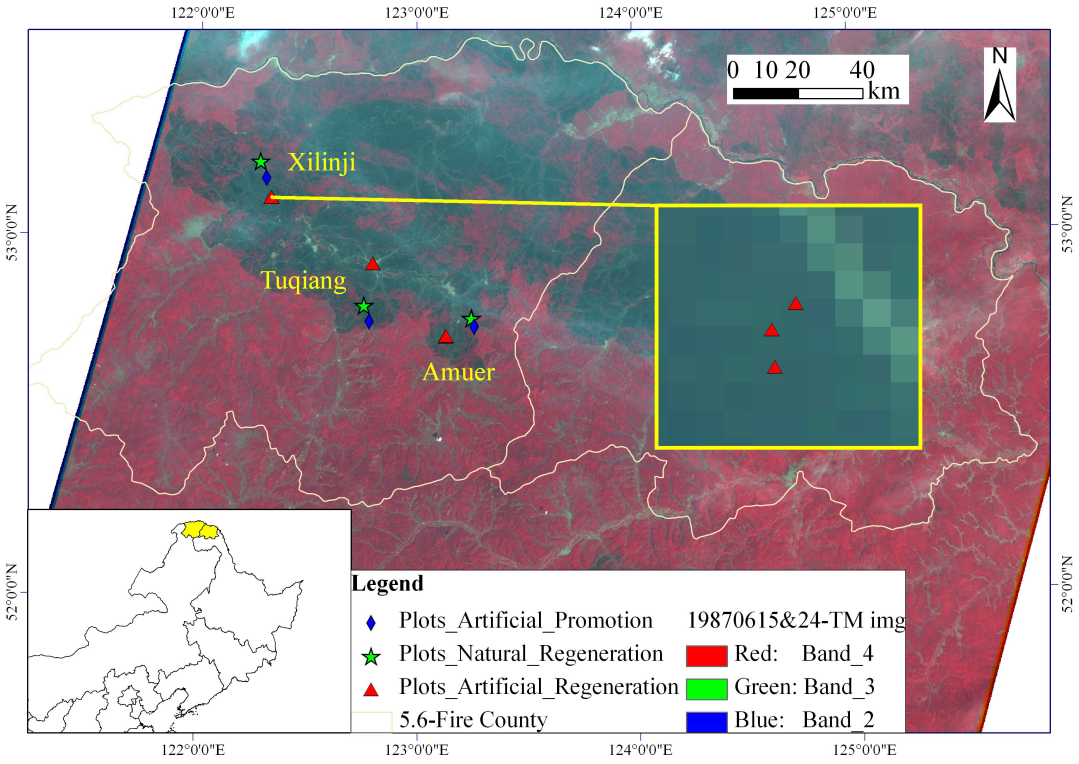

Figure 3.3 The spatial distribution of the experimental sites and survey plots within the burned forest area of the "5.6 Fire".

3.2.3 Statistical analysis

Fire severity is a crucial element for understanding and interpreting post-fire forest dynamics, as it is one of the main factors affecting post-fire forest regeneration (Schimmel and Granstrom, 1996; Keeley, 2009; Hollingsworth *et al.*, 2013; Camac *et*

al., 2013). For example, Hollingsworth *et al.* (2013) proposed that patterns of forest community composition were primarily related to gradients in fire severity, which could thus determine early patterns of community assembly because it has a greater influence than do environmental constraints. In this study, since all the dead and damaged trees had been removed from the burned sites under the artificial regeneration, it was difficult to measure the fire severity in all sites using field survey data (e.g. field-based CBI). As an alternative, we proposed taking the disturbance index (DI) (Healey *et al.*, 2005) as a proxy of fire severity. The DI image for the entire burned area of the "5.6 Fire" was acquired from Landsat imagery in chapter 2 (Chen *et al.*, 2013) and the values of all surveyed plots were extracted and analyzed. The results indicated that there was no significant difference in fire severity among the three forestry bureaus, and among the areas restored using the three restoration treatments. Therefore, in this chapter, we did not consider this factor for subsequent analyses and comparisons.

The species composition, structural parameters (tree height, DBH, and crown widths), and LAI of the forests in each forestry bureau under each type of restoration treatment were statistically analyzed. Firstly, the basic statistics (mean and standard deviation) of these attributes were calculated and compared. Then the quantitative analysis of variance (ANOVA) was performed to further demonstrate the comparison. In the ANOVA setting, it was hypothesized that no significant difference existed among different regions and restoration treatments. As the interaction effect of "treatment" by "region" was tested and proven insignificant in all these forest attributes, it was incorporated in the "error effect" to emphasize the "main effect" ("treatment effect" and "region effect") in the final model.

Here the factor of restoration treatment was taken as a fixed factor and the region effect was tested as a random factor. Before ANOVA, a test of normal distribution was performed by using Kolmogorov-Smirnov and Shapiro-Wilk statistics, and the equivalence of variances was tested through Levene's statistic. When the assumptions for the parametric statistical tests of normality and homoscedasticity on original data were not met, logarithmic transformation was carried out to meet ANOVA requirements. The *p* value (significant probability) was used to determine whether the difference was significant or not. When a significant effect was found (the null hypothesis was rejected), multiple comparisons (post-hoc test) among the three restoration treatments for all attributes were performed using the algorithm of Tukey's Honestly Significant Difference (HSD) and the results were further analyzed to explore the relative relationship between any two of the restoration treatments.

3.3 Results

3.3.1 Species composition

There were only four arbor species in the surveyed plots, which were the coniferous species of *P. sylvestris* and *L. gmelini*, as well as the broad-leaved species of *B. platyphylla* and *P. davidiana*. The species composition of regenerated forests in the

burned area under the three restoration treatments was quite different due to the varied effects of the three restoration treatments (Table 3.1).

It was found that there were only coniferous species of *P. sylvestris* and *L. gmelini* in the forest area under artificial regeneration. This result was determined by the species selection in the planting process. The species selection was made according to the local climatic and topographic conditions and considering the recommendations of local forestry engineers and technicians. Additionally, *P. sylvestris* and *L. gmelini* were relatively more suitable for human production, including the paper industry and construction activities, when compared to the broad-leaved species. In the forest area under natural regeneration, there were both the coniferous species (Mongolian pine and Larch) and broad-leaved species (Birch and Aspen), and the latter accounted for the main part. The dominant species in the completely naturally regenerated forest area was *P. davidiana* in Xilinji (78.02%), as well as *B. platyphylla* in Tuqiang (86.24%) and Amuer (84.61%). This suggested that the broad-leaved species had stronger resilience than coniferous species in the naturally regenerated forest area. Besides, from field records, it was observed more coniferous seedlings and shrub species in forest plots under natural regeneration. For the comparison studies, their structural parameters were not measured and included in the statistical analysis. In the forest area under artificial promotion, the coniferous species became dominant, which was the same as that in the artificially regenerated area.

Table 3.1 The species composition of forests in the forestry bureaus of Xilinji, Tuqiang, and Amuer under three different restoration treatments of artificial regeneration (AR), natural regeneration (NR), and artificial promotion (AP) (unit: %).

Restoration treatments	Coniferous species		Broad-leaved species	
	Pinus sylvestris	*Larix gmelini*	*Betula platyphylla*	*Populus davidiana*
(a) Xilinji				
AR	66.67	33.33	0.00	0.00
NR	6.59	10.99	4.40	78.02
AP	76.79	16.07	7.14	0.00
(b) Tuqiang				
AR	91.89	8.11	0.00	0.00
NR	3.67	9.17	86.24	0.92
AP	59.18	6.13	34.69	0.00
(c) Amuer				
AR	38.05	61.95	0.00	0.00
NR	3.13	10.94	84.61	1.32
AP	16.67	77.78	5.55	0.00

3.3.2 Tree height

The statistics of tree height in the three forestry bureaus, and all regions under the three restoration treatments, was performed and compared (Fig. 3.4). The results indicated that the average tree heights of forests under artificial regeneration was higher than those under natural regeneration and artificial promotion, with that of artificial promotion being the lowest. The ANOVA result (Table 3.2(a)) suggested that the difference in tree height was significant among the three restoration treatments ($p < 0.05$), but not among different regions ($p > 0.05$). Based on multiple comparisons by Tukey's HSD (letters of a and b on Fig. 3.4), it can be concluded that there was no significant difference in tree height between the restoration treatments of artificial promotion and natural regeneration, while they were both significantly lower than that of forest under artificial regeneration.

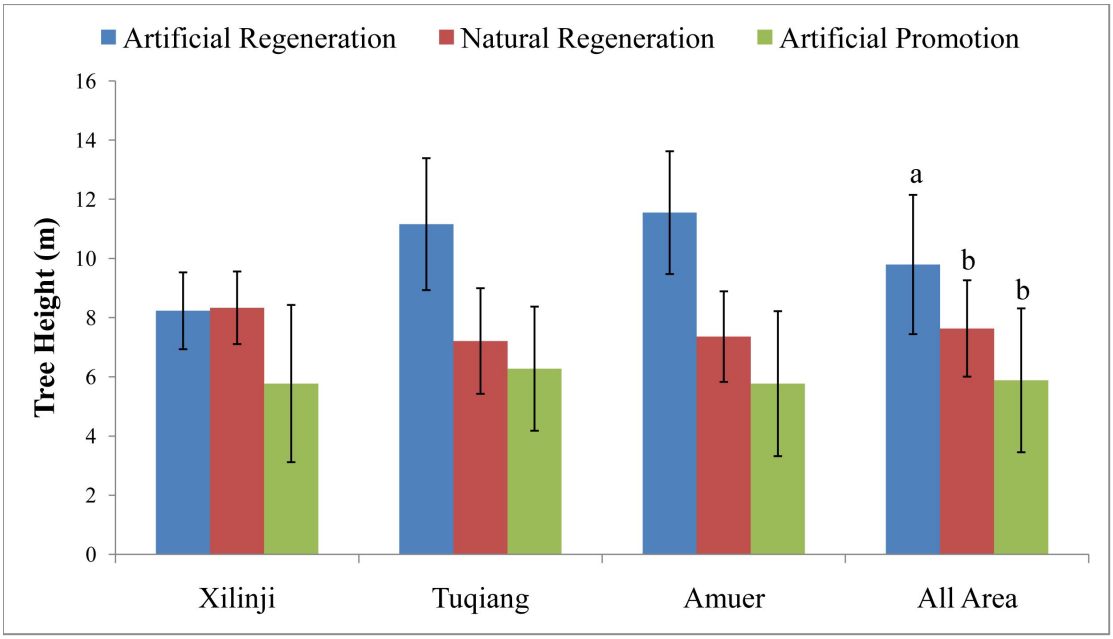

Figure 3.4 The statistics (mean±S.D.) and comparison of tree height in different regions under different restoration treatments. The letters a and b indicate the results of multiple comparison.

3.3.3 DBH

The statistics (Fig. 3.5) indicated that the recovered forest under artificial regeneration had a higher average DBH than those under the other two restoration treatments. As shown in Table 3.2(b), the difference in DBH among the three restoration treatments was extremely significant ($p < 0.01$). However, there was no significant difference in DBH among different regions ($p > 0.05$). The multiple comparison (Fig. 3.5) gave the result that there was no significant difference in DBH of forests under the treatments of artificial promotion and natural regeneration, however, they were both significantly lower than that under artificial regeneration. It was similar to the result of tree height.

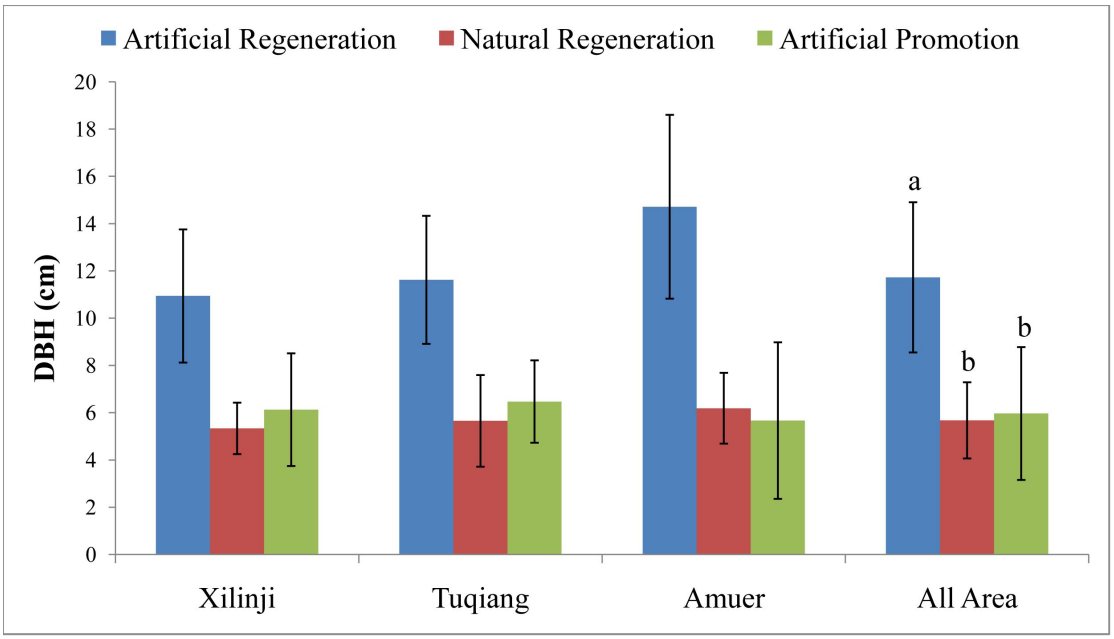

Figure 3.5 The statistics (mean±S.D.) and comparison of Diameter at Breast Height (DBH) in different regions under different restoration treatments. The letters a and b indicate the results of multiple comparison.

3.3.4 Crown width

3.3.4.1 Crown width in North-South

The statistics of crown width in the N-S direction (Fig. 3.6) suggested that the parameter differed in the three forestry bureaus. By qualitative comparison, crown width was larger for trees under artificial regeneration treatment than under the other two treatments. But ANOVA results (Table 3.2(c)) indicated that the difference among the three restoration treatments was marginally insignificant ($p \approx 0.05$) and that among the three regions was also insignificant ($p > 0.05$). Consequently, here further multiple comparison was not necessary. It was quantitatively different from the results of tree height and DBH. Since these sites were located in high latitudes, the subtle difference of solar radiation in the N-S direction may produce an impact on the dynamics of crown width.

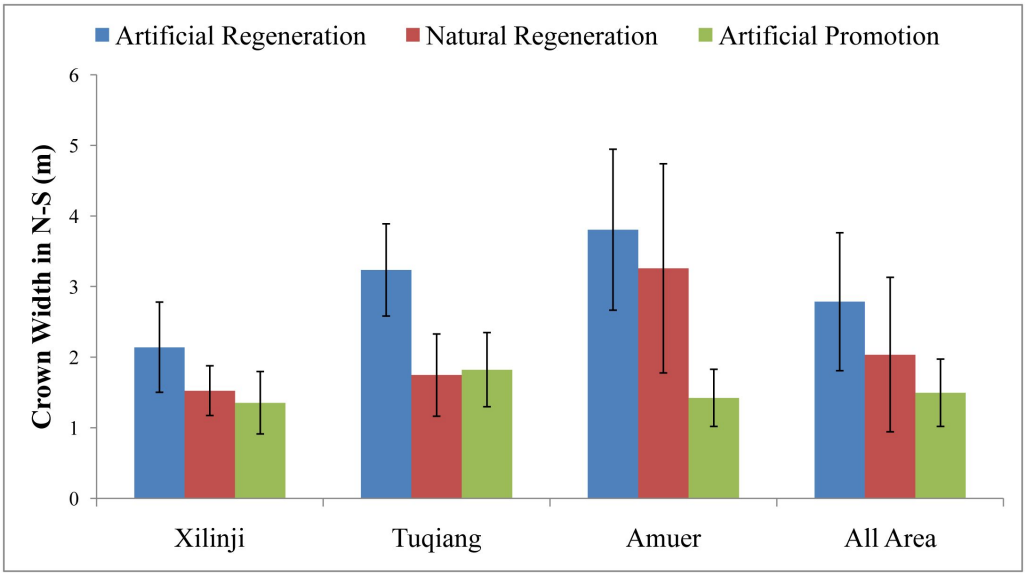

Figure 3.6 The statistics (mean±S.D.) and comparison of crown width in N-S direction in different regions under different restoration treatments.

3.3.4.2 Crown width in West-East

The statistics of crown width in the W-E direction were also analyzed (Fig. 3.7), from which we came to similar conclusion to that in N-S (Fig. 3.6). However, ANOVA results (Table 3.2(d)) indicated that the crown width in W-E had a marginally significant difference among the three treatments ($p \approx 0.05$), but not for the three regions ($p > 0.05$). By multiple comparison (Fig. 3.7), it could be concluded that there was a significant difference in crown width in W-E between the restoration treatments of artificial regeneration and artificial promotion. The differences between the two and natural regeneration were both insignificant.

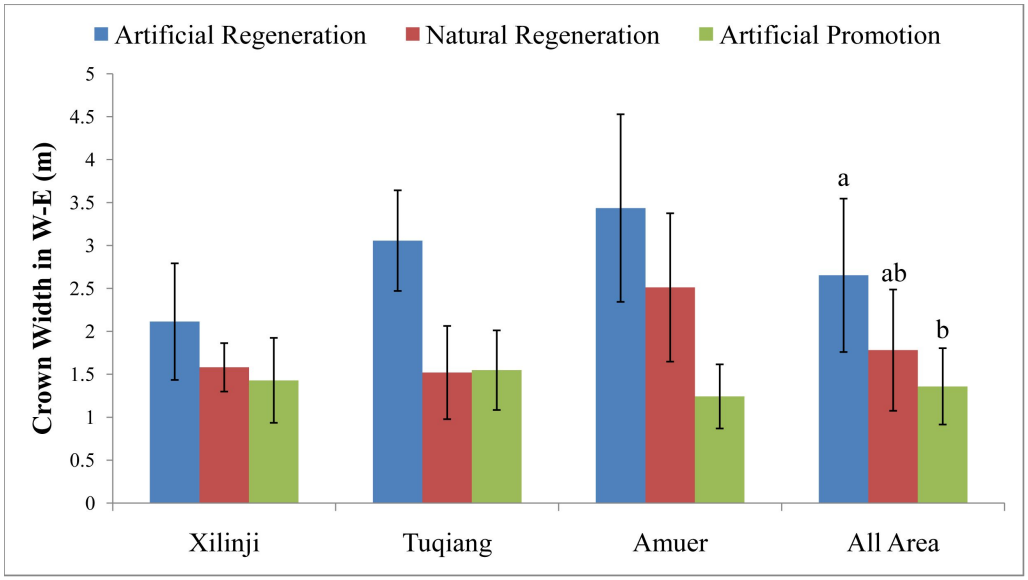

Figure 3.7 The statistics (mean±S.D.) and comparison of crown width in W-E direction in different regions under different restoration treatments. The letters a and b indicate the results of multiple comparison.

3.3.5 LAI

The statistical result (Fig. 3.8) suggested that the LAI of forest under natural regeneration was the highest. ANOVA results (Table 3.2(e)) indicated that there was no significant difference in LAI among different regions ($p > 0.05$), however, an extremely significant difference in LAI was observed among the three restoration treatments ($p < 0.01$). Multiple comparisons (Fig. 3.8) further indicated that a significantly higher LAI was achieved in forest under natural regeneration than under the other two restoration treatments. The average LAI of forests under artificial regeneration was a little higher than that under artificial promotion. It was completely different from the results of structural parameters (tree height, DBH, and crown widths). The structural parameters characterized the states of individual trees, while LAI was a characterization of the overall condition of forest within specific range of regions.

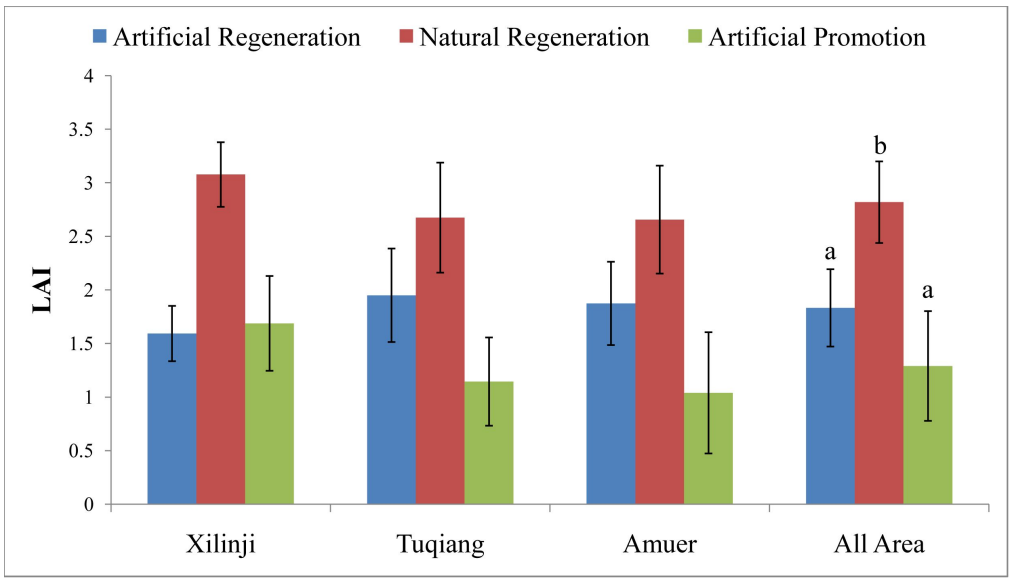

Figure 3.8 The statistics (mean±S.D.) and comparison of leaf area index (LAI) in different regions under different restoration treatments. The letters a and b indicate the results of multiple comparison.

Table 3.2 Tests of between-subjects effects (ANOVA) in the structural parameters (Tree height, DBH, and crown widths) and LAI. The "Treatment" and "Region" denote three forestry bureaus and three restoration treatments.

Source	Type III Sum of Squares	df	Mean Square	F statistics	Significant difference (p)
(a) Tree Height					
Treatment	29.233	2	14.617	9.294	0.031*
Region	1.202	2	0.601	0.382	0.705
Error	6.291	4	1.573		

(b) DBH					
Treatment	85.203	2	42.601	29.488	0.004**
Region	3.018	2	1.509	1.044	0.432
Error	5.779	4	1.445		
(c) Crown width in N-S					
Treatment	3.528	2	1.764	5.288	0.075
Region	2.004	2	1.002	3.003	0.160
Error	1.334	4	0.334		
(d) Crown width in W-E					
Treatment	3.351	2	1.676	7.603	0.043*
Region	0.712	2	0.356	1.616	0.306
Error	0.882	4	0.220		
(e) LAI					
Treatment	3.551	2	1.775	22.571	0.007**
Region	0.112	2	0.056	0.711	0.544
Error	0.315	4	0.079		

* $0.01 < p <= 0.05$; ** $p <= 0.01$.

3.4 Discussion

Forest fire is a common disturbance regime, and post-fire forest recovery plays a crucial role in a variety of fields, including climate change, carbon cycles and forest management which have been widely studied (Pausas *et al.*, 1999; Huang *et al.*, 2012; Senici *et al.*, 2013). Extensive studies have been conducted to investigate and compare the effects of different strategies on post-fire forest recovery (Moreira *et al.*, 2009, 2013; Beghin *et al.*, 2010; Ascoli *et al.*, 2013). For example, Moreira *et al.* (2009) compared two restoration treatments, direct planting and natural regeneration through resprouting, by focusing on the survival and size (height and basal diameter) of *Fraxinus angustifolia* and *Quercus faginea* in Central Portugal. The results suggested that, using natural resprouting may be a cheaper and more effective technique than direct planting to restore burned forests. Beghin *et al.* (2010) evaluated the impacts of five post-fire management options (no intervention; salvage logging; broadleaved plantation; *L. decidua* plantation; and *P. sylvestris* or *Pseudotsuga menziesii* plantation) on natural regeneration structure and composition, and found that density, size, and structural diversity of natural regeneration were higher in the area with no intervention. Aiming at our study area of the Greater Hinggan Mountain area, there were three different post-fire forest restoration strategies, artificial regeneration, natural regeneration, and artificial promotion, which had never been comparatively studied in previous research. Here, we proposed to evaluate and

compare the effects of the three restoration treatments on forest ecosystem using several forest attributes of structural parameters and LAI simultaneously.

On the basis of the field collected data, we concluded that there was significant difference in the dominant species of the forests under different restoration treatments. In the burned area under the treatment of artificial regeneration, the regenerated forest was dominated by the species selected for the planting. However, in the burned forest area, which was allowed to recover completely by natural regeneration, especially in boreal forests, broad-leaved species dominated in the initial stage after the disturbance event. This conclusion was demonstrated by many previous studies (Uemura *et al.*, 1997; Johnstone *et al.*, 2004; Schulze *et al.*, 2005).

Further analysis of the structural parameters (tree height, DBH, and crown widths) suggested that forest under the restoration treatment of artificial regeneration recovered significantly faster than those under the other two treatments. This probably resulted from the different species composition in forests under the three restoration treatments, which in turn, would affect the ecological functions and values of the ecosystems (Johnstone *et al.*, 2004; Gauthier *et al.*, 2010). However, the fact that the forest under natural regeneration recovered marginally faster than that under artificial promotion should be given attention as it indicated that the effect of artificial promotion is insignificant and hence its application as a restoration approach should be reconsidered.

As LAI reflects the “layers” of leaves within a certain area in various ecosystems and can characterize the canopy-atmosphere interface effectively, it can be used to indicate the vertical density of vegetation canopy in forest ecosystems (Arias *et al.*, 2007; Schleppi *et al.*, 2011). Besides, LAI benefits the comparison among different types of forest ecosystems. By the analysis of LAI under the three restoration treatments, it can be found that the completely naturally recovered forest had a higher canopy vertical density and relatively abundant vegetation types. The fact that the forest under artificial regeneration achieved a larger LAI than that under artificial promotion also raises a question on the necessity for the latter.

By the combined analysis of structural parameters and LAI, it can be concluded that the artificial regeneration treatment could be adopted in the actual forest management of post-fire recovery if the objective is timber production since the planted coniferous species of *P. sylvestris* and *L. gmelini* are more suitable for human utilization, including the paper industry and construction activities, than the broad-leaved species of *B. platyphylla* and *P. davidiana*. Additionally, a variety of other forest species can also be selected in consideration of local climate and soil conditions. However, when the aim of forest restoration is to promote species richness in local forest ecosystems, the burned forest area should be allowed to recover completely naturally without any anthropogenic interference. The restoration treatment of artificial promotion, which did not make sense and demonstrate its importance or necessity, should be carefully reconsidered. It could probably serve as a means of balance in forest management.

In previous studies, it was found that there is a transition in the dominant species of naturally regenerated forests, usually from dominance of broad-leaved pioneers in the

early period to that of conifers in the late-successional stage (Gromtsev, 2002; Johnstone *et al.*, 2004; Gauthier *et al.*, 2010; Otoda *et al.*, 2013), particularly in 60–180 years after the fire. Therefore, it is necessary to continue the field observations on forest regeneration in the future, as it has been only 27 years since the severe "5.6 Fire" occurred. This observation will be accomplished with the assistance of local forestry bureaus at an interval of five years. Moreover, we would attempt to investigate more sampling sites and increase the plot size in future field studies. Furthermore, the time series monitoring of forest disturbance and recovery would be focused in combination with remote sensing data (McMichael *et al.*, 2004; Masek *et al.*, 2008). In this synergy application, scale matching between the size of the field plots and spatial resolution of remote sensing images should be considered (Mitri and Gitas, 2013).

4 Forest disturbance detection and recovery monitoring

4.1 Based on Landsat TM/ETM+ data

4.1.1 Introduction

It has been demonstrated by many previous studies and emphasized for several times in the former chapters that serious fires will bring great damage to the whole forest ecosystem and it is thus necessary to identify the spatial and temporal trends in post-fire forest recovery for both ecological study and forest management (Schulze *et al.*, 2005; Beghin *et al.*, 2010; Corona *et al.*, 2012). The extensive Landsat records, are well suited for the detection of fire disturbance and monitoring of post-fire forest recovery due to their long historical coverage of about 40 years, the adequate spatial resolution of 30 m and abundant spectral bands (7 bands encompassing visible, infrared and thermal) which enable the capture of forest spectral changes at appropriate spatial and temporal levels (Masek *et al.*, 2008; Schroeder *et al.*, 2012; Han *et al.*, 2013).

Many previous studies adopted the Landsat TM/ETM+ imagery to monitor the forest regeneration patterns. For example, Song *et al.* (2007) used a forest succession model and a canopy reflectance model to produce spectral trajectories of forest succession and compared the simulated trajectories with those from Landsat TM imagery. Results indicated that the simulated trajectories captured the major characteristics of regional mean succession trajectory observed with TM-derived Tasseled Cap indices. Roder *et al.* (2008) selected a time series of 6 Landsat MSS, 13 Landsat-5 TM and 1 Landsat-7 ETM+ images, covering the period 1975-2000, to characterize post-fire vegetation dynamics in Mediterranean ecosystems using a indicator of photosynthetic active green vegetation cover from spectral mixture analysis. More specifically, a chronosequence of Landsat vegetation indices (NDVI and NBR) were analyzed as a surrogate of post-fire vegetation recovery at 16 years after fire (Epting and Verbyla, 2005).

Concerning the “5.6 Fire” occurred in 1987 in Northeastern China, the post-fire forest dynamics were detected in some studies, mainly using NOAA AVHRR imagery (Cahoon *et al.*, 1994; Yi *et al.*, 2013). Especially, when Yi *et al.* analyzed the AVHRR GIMMS NDVI to detect post-fire vegetation trends, another five scenes of Landsat imagery acquired in 1986-1987, 2000 and 2004 were taken as auxiliary comparison. However, only NDVI was tested. In contrast, here as many as 12 scenes of Landsat TM/ETM+ imagery covering the whole period of 1987-2011 were used for the monitoring of post-fire forest recovery. In addition to the commonly used vegetation indices (e.g. NDVI, EVI), a more effective index of DI was examined and evaluated. Furthermore, in consideration of the three forest restoration treatments introduced in chapter 3, the recovery trajectories under the three different strategies

were also tracked and compared. The results can be used to provide significant suggestions for policy makings in local forest management.

4.1.2 Data and methods

4.1.2.1 Landsat time series data

Landsat TM/ETM+ imagery were used in this study. The technical characteristics of Landsat 5 TM sensor were already shown in Table 2.1. Here only the corresponding characteristics of Landsat 7 ETM+ sensor were introduced in Table 4.1.

Table 4.1 Technical characteristics of the Landsat 7 ETM+ sensor.

Satellite	Sensor	Band	Wavelength range (μm)	Spatial resolution (m)	Swath width (km)	Revisit cycle (days)
Landsat 7	ETM+	1 (Blue)	0.450 – 0.515	30	185	16
		2 (Green)	0.525 – 0.605	30		
		3 (Red)	0.630 – 0.690	30		
		4 (Near IR)	0.760 – 0.900	30		
		5 (Mid IR)	1.550 – 1.750	30		
		6 (Thermal)	10.40 – 12.50	60		
		7 (Mid IR)	2.080 – 2.350	30		
		8 (Pan)	0.520 – 0.920	15		

The fire perimeter and burned forest area of the “5.6 Fire” were extracted in chapter 2. The entire burned forest area spanned two Landsat scenes (Path 121/122, Row 23), but it was difficult to acquire the two scenes simultaneously in each period. Considering that around 90% of the burned forest area was within the scene of path 122 row 23, we proposed to extract a sample area (Fig. 4.1) from Landsat path 122 row 23 for the recovery monitoring. For this scene 12 growing season (May-October) Landsat TM and ETM+ images were acquired between 1987 and 2011 to develop the time series (Table 4.2). These data were provided by the USGS-EROS. The overall technique flow chart of this monitoring was shown in Fig. 4.2.

Table 4.2 Landsat images used to develop the path 122 row 23 time series.

Date	Sensor
6/15/1987	TM
10/5/1993	TM
10/24/1994	TM
10/11/1995	TM
8/11/1999	ETM+

9/14/2000	ETM+
7/15/2001	ETM+
5/15/2002	ETM+
7/5/2006	TM
8/30/2009	TM
9/2/2010	TM
7/3/2011	TM

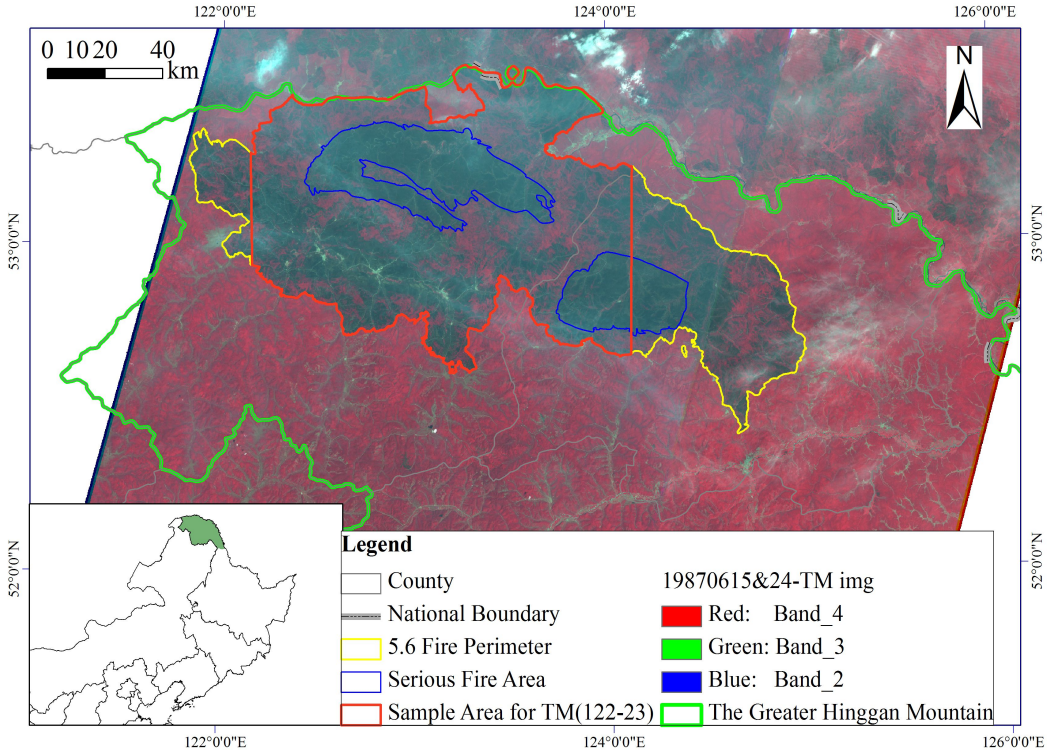

Figure 4.1 Location of the "5.6 Fire" perimeter as well as a sample area in Landsat path 122 row 23. The background is the mosaic of two Landsat TM scenes acquired in 1987 showing the burn scar in dark blue color.

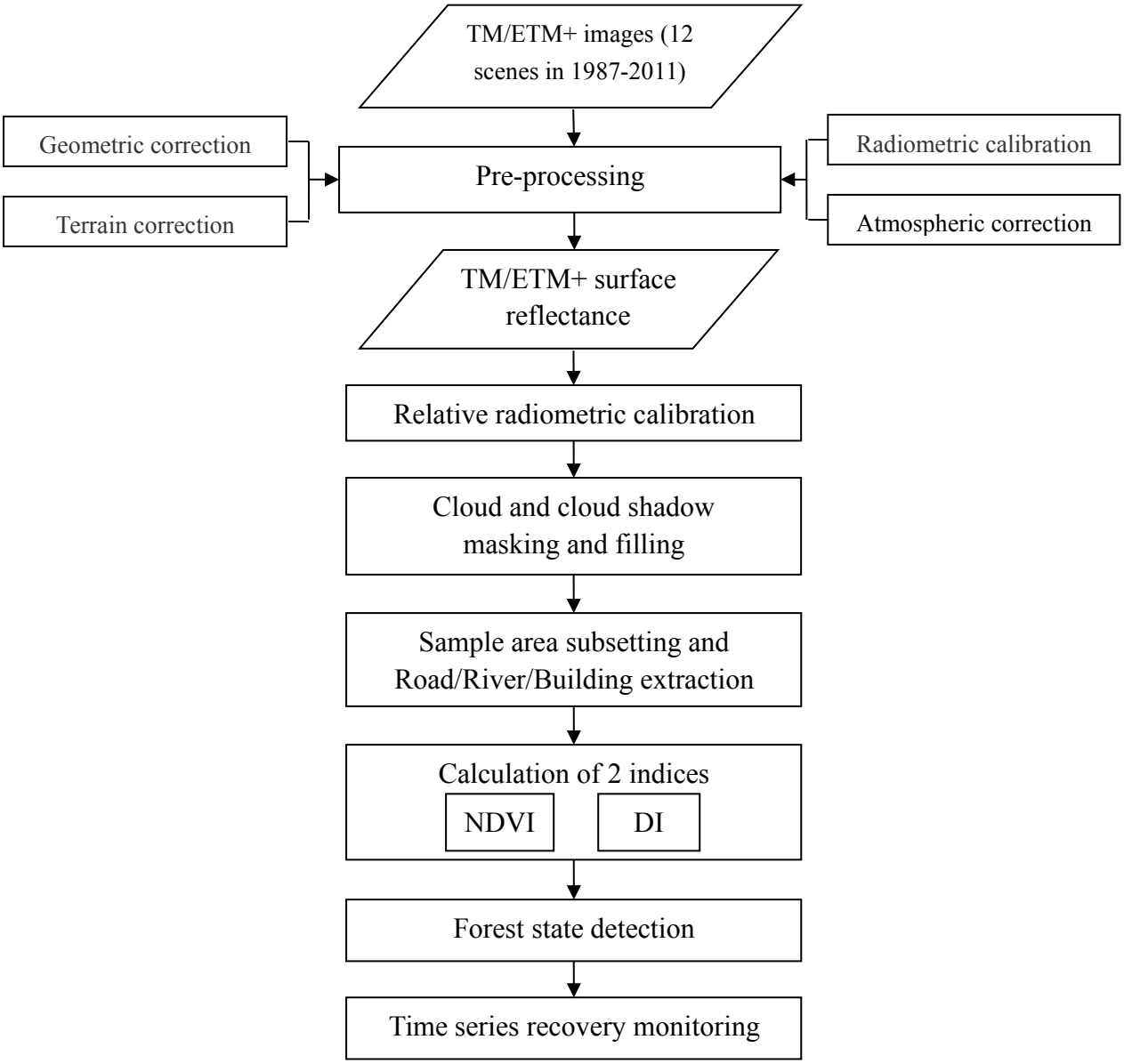

Figure 4.2 The overall technique flow chart of the post-fire forest recovery monitoring using time series TM/ETM+ data.

4.1.2.2 Data pre-processing and methodology

Prior to detection the images were pre-processed using the following steps. Firstly, the images were converted to surface reflectance through geometric and terrain correction, radiometric calibration, as well as atmospheric correction (based on MODTRAN-4). Then the reflectance images were normalized to a common reference scene to minimize the impact of sun-sensor-view angle effects. This made locating pseudo-invariant features (i.e., temporally stable areas of reflectance) necessary. It was achieved by the iterative multivariate alteration detection algorithm (Canty and Nielsen, 2008). Areas of cloud and cloud shadow were masked and then filled using an interpolation of the temporally nearest clear observations if necessary.

After all these pre-processing steps, the sample area of each scene was extracted. Here we first masked the rivers, roads and building area in each scene by visual interpretation and then extracted the burned and unburned forest area from the post-fire detection of the scene on 6/15/1987 (Chen *et al.*, 2013). The acquired surface reflectance of the sample area in the scenes acquired on 6/15/1987 and 9/14/2000 were shown in Fig. 4.3. The boundary of "Serious Forest Area" was extracted from the scene on 6/15/1987 and just for auxiliary understanding of the main burned area of the "5.6 Fire".

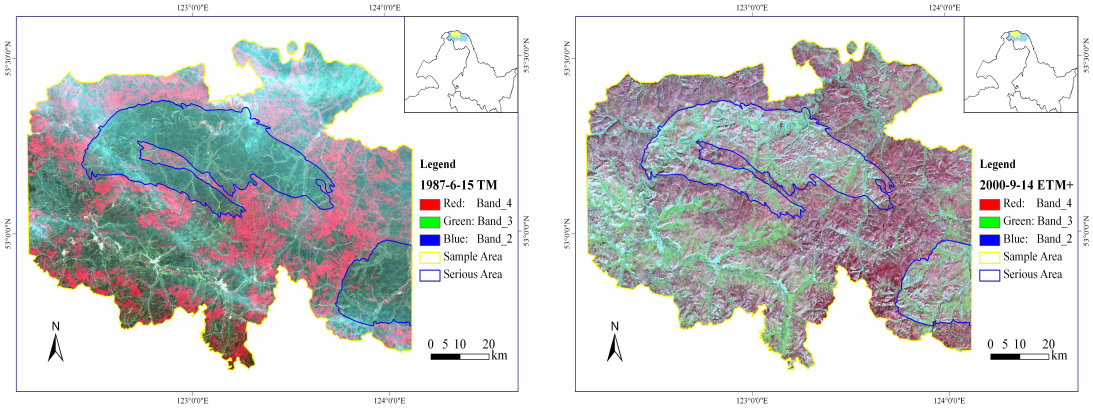

Figure 4.3 The pre-processed surface reflectance images of the sample area in the scenes acquired on 6/15/1987 (left) and 9/14/2000 (right).

Here we selected two indices of NDVI and DI. The detailed definitions of the two indices have been elaborated in section 2.2.3 (Equation 2-1 and 2-4, 2-5). It should be noted that there was one different processing in the spectral normalization of the Tasseled Cap Brightness, Greenness and Wetness when obtaining DI. In the section 2.2.3, a "dense forest for a particular scene" was determined to calculate within-image statistics for the normalization. Currently, as we had already extracted the burned and unburned forest area from the post-fire detection of image acquired on 6/15/1987 and 6/24/1987, to focus on the burned forest area, here the "dense forest for a particular scene" used for normalization was the same extracted unburned forest area.

Since the two indices could only be used as a relative description of the overall conditions of forest ecosystems with no corresponding parameters that could be measured by devices, it was difficult to directly compare the results with field survey data. Additionally, as there were already 27 years after the "5.6 Fire", and we had not collected forest attributes covering such a long period, the ground-based validation synchronized with the time series images appeared impossible. In spite of this, the collected forest attributes from the field survey in July 2012 will be used for some validation here. Also comparison of the recovery trajectories of forests under different restoration treatments was performed.

4.1.3 Results

4.1.3.1 Forest recovery in the burned area

The NDVI time series values of the sample area in all scenes were calculated. As there were 12 scenes which were too many to show all, only that on 9/14/2000 was illustrated (Fig. 4.4). In this figure, the rivers, roads and building areas were masked. Then the average NDVI values of the "burned forest" and "unburned forest" area were calculated and developed to be time series (Fig. 4.5).

From the two figures, it can be found that there were little difference in NDVI between the "burned forest" and "unburned forest" area. To illustrate quantitatively, the ANOVA of the two groups of NDVI values was performed and the result was shown in Table 4.3(a). It can be concluded that the difference in NDVI between the "burned forest" and "unburned forest" area was statistically insignificant (Sig. > 0.05). Additionally, from Fig. 4.5, we found that the NDVI was influenced by phenology as the values in October (1993-1995) and May (2002) were significantly lower than those in the peak growing seasons of July-September.

Table 4.3 The ANOVA result of NDVI and DI.

Difference Source	Sum of Squares	df	Mean Square	F statistics	Sig.
(a) NDVI					
Between Groups	0.042	1	0.042	1.148	0.296
Within Groups	0.796	22	0.036		
Total	0.838	23			
(b) DI					
Between Groups	48.611	1	48.611	14.397	0.001
Within Groups	74.280	22	3.376		
Total	122.891	23			

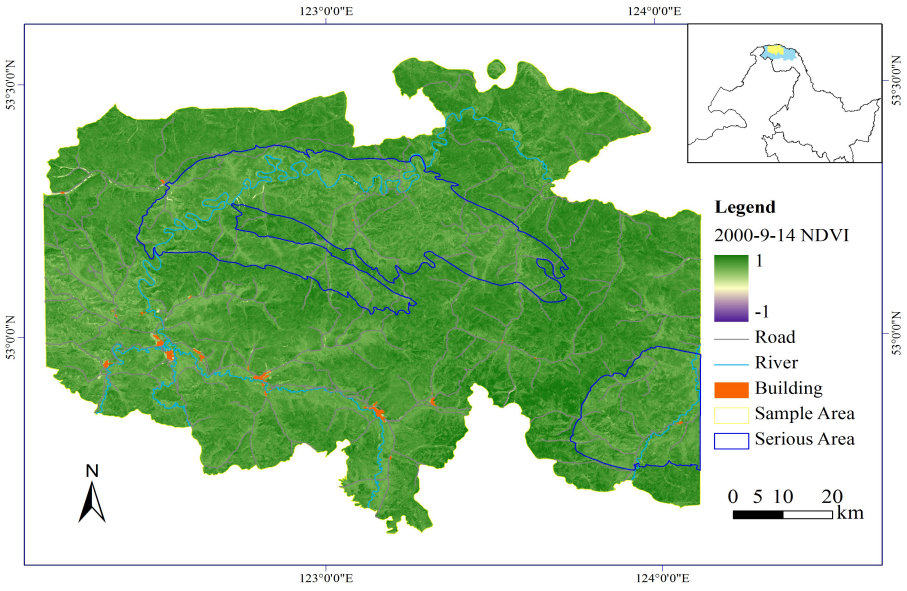

Figure 4.4 The NDVI image of the sample area in the scene acquired on 9/14/2000.

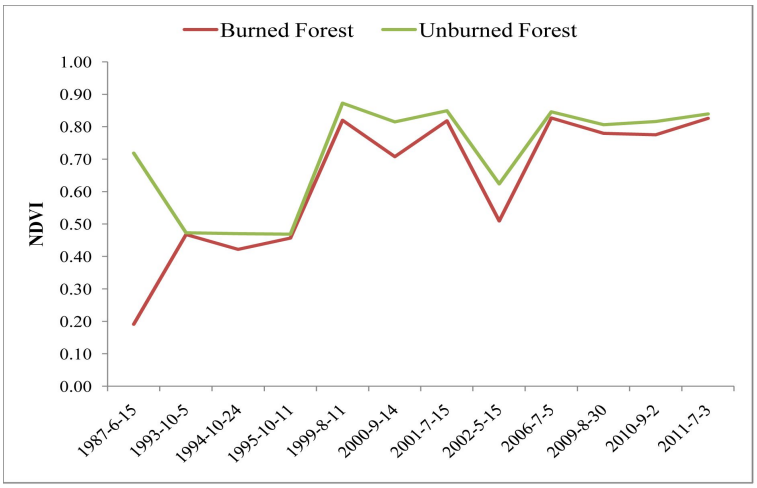

Figure 4.5 NDVI time series of the burned and unburned forest area of the "5.6 Fire".

The DI time series images were acquired. Here also the DI image on 9/14/2000 was shown in Fig. 4.6, where the rivers, roads, building area were the same as in Fig. 4.4. Since the "unburned forest" area was used for normalization in the calculation of DI, the corresponding DI values will all equal to 0 which appeared to be a straight line. In order to fully verify the trend of extracted DI, we used the "test samples" consisting of 2,023,605 burned forest pixels and 500,325 unburned forest pixels which were interpreted and used for evaluating burned forest area mapping accuracy in chapter 2. Then the average DI values of those sample pixels within the sample area were calculated, forming the time series (Fig. 4.7). In this figure, it can be found that the green line representing unburned forest area was not straight but curve and quite close to the "0 straight line", indicating all corresponding DI approximately equaled to 0.

From Fig. 4.6 and 4.7, we could visually find the difference in DI between the "burned forest" and "unburned forest" area, especially from the scene acquired in 1987. ANOVA was also conducted (Table 4.3(b)) and the result suggested that the difference in DI between the "burned forest" and "unburned forest" area was statistically extremely significant (Sig. < 0.01). It indicated that the serious "5.6 Fire" caused far-reaching impacts on the forest ecosystem. The forest was not completely recovered even after more than 20 years since the fire.

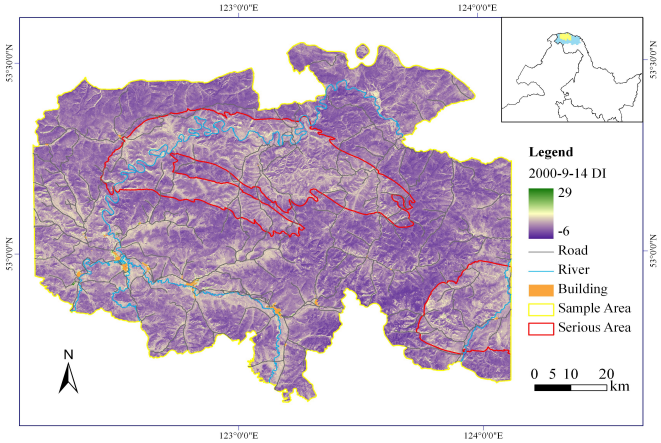

Figure 4.6 The DI image of the sample area in the scene acquired on 9/14/2000.

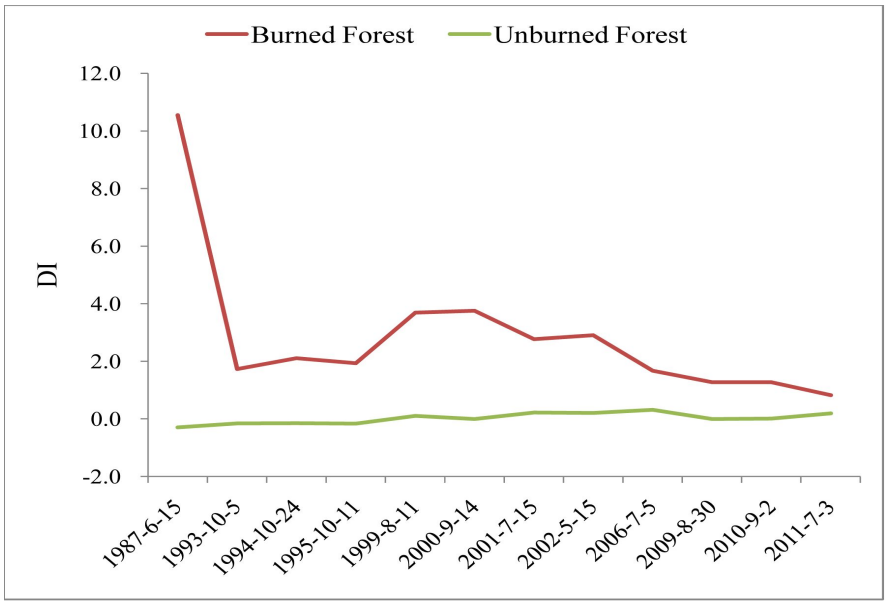

Figure 4.7 DI time series of the burned and unburned forest area of the "5.6 Fire".

Focusing on the DI of the "burned forest" area (red line in Fig. 4.7), the trend of DI which representing the trend of post-fire forest recovery could be observed. As forest area with a larger DI had a higher degree of being disturbed and the DI values in the year of 1999-2002 were apparently larger than those in other years, the forest probably suffered a new disturbance during this period for some reasons. But the specific causes still remained to be determined.

Finally, as no available TM images in the period of 1988-1992 were acquired, it was not possible to monitor the forest dynamics immediately after the "5.6 Fire", when the forest had been greatly recovered for natural and managed reasons.

4.1.3.2 Forest under different restoration treatments

As DI, but not NDVI, was proven suitable for the monitoring of post-fire forest recovery, it was selected to conduct the comparison of forest recovery under different restoration treatments. The DI values of the specific plots were extracted and averaged to characterize the forest growth under different treatments (Fig. 4.8).

Fig. 4.8 suggested that the forest recovery trajectories were different among the three restoration treatments. Compared to the other treatments, forests under natural regeneration presented a totally different recovery track. The much higher DI values in the early stage after fire indicated a relatively slower regeneration progress during this period. But after about 20 years, the recovery process had a breakthrough and the completely naturally recovered forest grew better than those under artificially assisted restoration. Some minor difference also existed in the DI values between the treatments of artificial regeneration and artificial promotion, which was statistically insignificant.

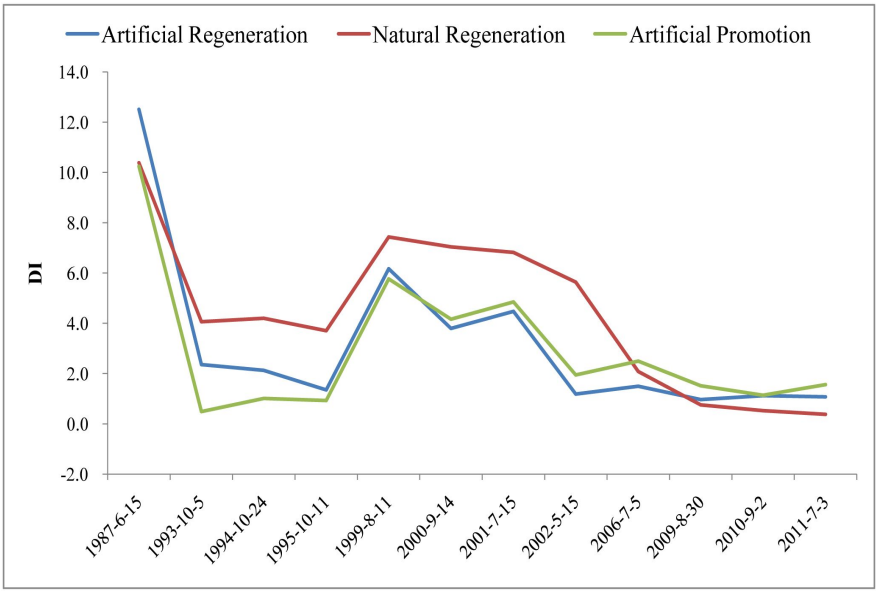

Figure 4.8 DI time series of post-fire forest recovery under different restoration treatments.

4.1.3.3 Comparison with field survey data

The field survey indicated that there were only coniferous species of Mongolian pine (*Pinus sylvestris*) and Larch (*Larix gmelini*) in the forest area under artificial regeneration. It was definitely decided by the species selection in the planting process. In the area under natural regeneration, there were both coniferous species and broad-leaved species, and the latter achieved complete dominance. But for the forest under artificial promotion, the coniferous species became dominant again.

The statistics of LAI of forests under the three restoration treatments was compared (Fig. 3.8). The result indicated that the LAI of forests under natural regeneration was the highest corresponding to the lowest DI value in 2011 (Fig. 4.8). The LAI of artificial regeneration was higher than that of artificial promotion. It was also consistent with the result from DI comparison. ANOVA results showed that an extremely significant difference was observed among the three restoration treatments ($p < 0.01$). Multiple comparisons further indicated that the forests under natural regeneration achieved a significantly higher LAI than those under the other two treatments (label a and b in Fig. 3.8). It reflected the overall trends of forest recovery under the three restoration treatments characterized by time series DI.

4.1.4 Discussion

4.1.4.1 Availability of different remote sensing indices

In this study, NDVI, one of the most widely used vegetation indices, was considered not suitable for the monitoring of post-fire forest recovery in the Greater Hinggan

Mountain area. Actually we had also calculated several other vegetation indices including EVI, ratio vegetation index, and soil adjusted vegetation index, however, the results were similar with that of NDVI. It was probably due to the limited bands (no more than three) used in the acquisition of these simple vegetation indices, making them relatively insensitive to the post-fire forest recovery detection, especially in long time series.

DI was proven to be a relatively effective approach to detect the forest disturbance and monitor its change. It relies on the physical characteristics of reflectance variations rather than statistical generalization from training samples, making it more reliable and widely applicable (Healey *et al.*, 2005; Masek *et al.*, 2008). The normalization of the spectral components using within-image statistics of unburned forest area makes DI relatively insensitive to BRDF variability and phenology and thus widely extend the data supply.

The Tasseled Cap transformation, where DI comes, is a standard transformation of the original Landsat spectral bands and can effectively capture the three major axes of spectral variation across the solar reflective spectrum (Crist and Cicone, 1984). It has been extended to some other sensors including IKONOS (Horne, 2003), MODIS (Lobser and Cohen, 2007). Consequently, the application of tracking forest disturbance and recovery by DI would be widely expanded across a variety of forest ecosystems using a wide range of data sources.

4.1.4.2 Applicability of the three restoration treatments

There have been many cases studying and comparing the effects of different post-fire forest restoration strategies (Moreira *et al.*, 2009; Beghin *et al.*, 2010; Ascoli *et al.*, 2013), while most only focused on the two ways of natural regeneration and direct tree planting. In previous studies, little was done aiming at the comparisons among the different restoration treatments of artificial regeneration, natural regeneration and artificial promotion, especially based on remote sensing data. In addition, long-term monitoring appeared to be quite necessary. In this study, taking the forest recovery after the “5.6 Fire” as an example, the forest recovery trajectories were monitored based on time series Landsat images and the effects of the three restoration treatments were compared.

The analysis results of structural parameters suggested that the coniferous species under artificial regeneration recovered significantly faster than those under the other two treatments. On the other hand, from the LAI which reflects the “layers” of leaves within a certain area, it was found that the completely naturally recovered forest had the highest canopy vertical density and relatively more abundant species. It was consistent with the results obtained from the remote sensing indices. This conclusion can provide a reference for local forest management.

4.2 Based on MODIS data

4.2.1 Introduction

Compared to Landsat TM/ETM+ imagery, MODIS which is a crucial instrument aboard the Terra and Aqua satellites has unique characteristics. Terra was launched on December 18, 1999 orbiting around the earth from north to south across the equator in the morning, while Aqua was launched on May 4, 2002 and passes south to north over the equator in the afternoon. Terra and Aqua MODIS are combining to view the entire earth's surface every 1 to 2 days with a 2330 km swath width, acquiring data in 36 spectral bands ranging from 0.4 to 14.4 μm. Two bands are imaged at a nominal resolution of 250 m at nadir, with five bands at 500 m, and the remaining 29 bands at 1 km.

Due to its great advantages in radiometric and temporal resolution, the MODIS original imagery and subsequently derived, abundant but free products have been widely used in almost every field associated with the Earth dynamics and processes occurring on the land (Friedl *et al.*, 2002, 2010; Li *et al.*, 2013), in the oceans (Wang *et al.*, 2007), and in the lower atmosphere (Levy *et al.*, 2013), especially in continental and global scales. When aiming at the forest disturbance mapping by MODIS, most studies are also in large scales because of the relatively coarse spatial resolution (Mildrexler *et al.*, 2009; Ferreira *et al.*, 2010). Simultaneously, as it provides global coverage every one to two days, the near real-time monitoring was intensively preferred (Hilker *et al.*, 2009; Xin *et al.*, 2013).

As expected, it has been used to detect forest fires and delineate burn scar in various forest ecosystems. For example, Li *et al.* (2004) found that the MODIS NIR channels centered near 1.24 and 2.13 μm are sensitive to changes in the surface properties caused by the fire and are not obscured by smoke which allow remote sensing recognition of burn scars in the presence of smoke. George *et al.* (2006) used thermal anomaly data in combination with the Normalized Difference SWIR to detect burned areas. Additionally, the MODIS burned area products (e.g. MCD45A1, MCD64A1) are also being used and validated (Chang and Song, 2009; Giglio *et al.*, 2010; Mouillot *et al.*, 2014).

As the “5.6 Fire” occurred in 1987 and the objective of this section is to monitor post-fire forest recovery with MODIS data over the whole burned forest area in long time series rather than the near real-time burn scar detection, some other MODIS imagery and products are in need. It has been observed such studies that Loboda *et al.* (2007) used MOD09A1 and MOD14 data to produce yearly maps of burned area of forests in Central Siberia. Cuevas-Gonzalez *et al.* (2009) selected time series MODIS NDVI and NDSWIR to investigate whether characteristic temporal patterns exist for stands of different ages in two types of evergreen needle-leaf and deciduous needle-leaf forests and whether their post-fire dynamics are influenced by variables such as pre-fire vegetation cover.

This study is centered on the hypothesis that the forest dynamics after the "5.6 Fire" can be detected by MODIS data. The main tasks are to monitor the temporal and spatial characteristics of post-fire forest dynamics using MODIS Land Cover Type data and investigate the responses of MODIS Vegetation Indices values to the forest types. The interannual variability in land cover type composition and distribution would be a useful reference for local forest monitoring.

4.2.2 Data and methods

4.2.2.1 MODIS Land Cover Type product

The MODIS data adopted included the Land Cover Type product (MCD12Q1) and Vegetation Indices products (MOD13A1). The MODIS Land Cover Type Yearly L3 Global 500 m SIN Grid product provides global maps of land cover at annual time steps and 500 m spatial resolution for 2001-present. It is produced from observations spanning a full year's input of both Terra- and Aqua-MODIS data through a supervised decision-tree classification algorithm in combination with a technique of boosting to improve classification accuracies.

This product incorporates five different land cover classification schemes, including the International Geosphere-Biosphere Programme (IGBP) global vegetation classification scheme (Belward *et al.*, 1999; Friedl *et al.*, 2002), the University of Maryland (UMD) scheme (Hansen *et al.*, 2000), the MODIS-derived LAI/fPAR scheme (Myneni *et al.*, 1997), the MODIS-derived Net Primary Production (NPP) scheme (Running *et al.*, 1994) and the Plant Functional Type (PFT) scheme (Bonan *et al.*, 2002). The primary land cover scheme which was defined by the IGBP and adopted in this study identifies 17 land cover classes, including 11 natural vegetation classes, 3 developed and mosaic land classes, and 3 classes of non-vegetated lands (Table 4.4). The v051 Land Cover Type products of the 2001-2012 periods produced with revised training data and certain algorithm refinements (Friedl *et al.*, 2010) were used here.

Table 4.4 IGBP Land Cover Units.

Class code	Class name	Class definition
Natural Vegetation		
1	Evergreen Needleleaf forest	Lands dominated by woody vegetation with a percent cover >60% and height exceeding 2 meters. Almost all trees remain green all year. Canopy is never without green foliage.
2	Evergreen Broadleaf forest	Lands dominated by woody vegetation with a percent cover >60% and height exceeding 2 meters. Almost all trees and shrubs remain green year round. Canopy is never without green foliage.
3	Deciduous Needleleaf forest	Lands dominated by woody vegetation with a percent cover >60% and height exceeding 2 meters. Consists of seasonal needleleaf tree communities with an annual cycle of leaf-on and leaf-off periods.

4	Deciduous Broadleaf forest	Lands dominated by woody vegetation with a percent cover >60% and height exceeding 2 meters. Consists of broadleaf tree communities with an annual cycle of leaf-on and leaf-off periods.
5	Mixed forest	Lands dominated by trees with a percent cover >60% and height exceeding 2 meters. Consists of tree communities with interspersed mixtures or mosaics of the other four forest types. None of the forest types exceeds 60% of landscape.
6	Closed shrublands	Lands with woody vegetation less than 2 meters tall and with shrub canopy cover >60%. The shrub foliage can be either evergreen or deciduous.
7	Open shrublands	Lands with woody vegetation less than 2 meters tall and with shrub canopy cover between 10-60%. The shrub foliage can be either evergreen or deciduous.
8	Woody savannas	Lands with herbaceous and other understory systems and with forest canopy cover between 30-60%. The forest cover height exceeds 2 meters.
9	Savannas	Lands with herbaceous and other understory systems and with forest canopy cover between 10-30%. The forest cover height exceeds 2 meters.
10	Grasslands	Lands with herbaceous types of cover. Tree and shrub cover is less than 10%.
11	Permanent wetlands	Lands with a permanent mixture of water and herbaceous or woody vegetation. The vegetation can be present in either salt, brackish, or fresh water.
Developed and Mosaic Lands		
12	Croplands	Lands covered with temporary crops followed by harvest and a bare soil period (*e.g.*, single and multiple cropping systems). Note that perennial woody crops will be classified as the appropriate forest or shrub land cover type.
13	Urban and built-up	Land covered by buildings and other man-made structures.
14	Cropland/Natural vegetation mosaic	Lands with a mosaic of croplands, forests, shrublands, and grasslands in which no one component comprises more than 60% of the landscape.
Non-Vegetated Lands		
15	Snow and ice	Lands under snow/ice cover throughout the year.
16	Barren or sparsely vegetated	Lands with exposed soil, sand, rocks, or snow and never has more than 10% vegetated cover during any time of the year.
0	Water	Oceans, seas, lakes, reservoirs, and rivers. Can be either fresh or salt-water bodies.

4.2.2.2 MODIS Vegetation Indices product

MODIS global vegetation indices are designed to provide consistent spatial and temporal characterization and comparisons of vegetation conditions. Global

MOD13A1 data are produced every 16 days at 500 m spatial resolution as a gridded level-3 product. They include two indices of NDVI and EVI. In this study, the products of the tile h25v03 from Julian Day 193 (July 11/12) during 2001-2012 were collected and analyzed together with the IGBP Land Cover Type products.

As the fire perimeter and the burned forest area of the "5.6 Fire" had been extracted in chapter 2, the images of land cover type and vegetation indices (NDVI and EVI) were extracted using corresponding boundaries after they were re-projected from sinusoidal to UTM/WGS-84 projection.

4.2.3 Results

4.2.3.1 Land cover type

The area percentage of 17 land cover units defined by IGBP during the period 2001-2012 was calculated and compared (Fig. 4.9). From this figure, it can be found that the class of "Mixed forest" in the IGBP scheme dominated in this region, followed by the lands with "Cropland/Natural vegetation mosaic". On the whole, the area of "Mixed forest" gradually increased throughout the 12 years (from 46.34% in 2001 to 80.50% in 2012), while that of "Cropland/Natural vegetation mosaic" decreased from 30.46% in 2001 to 5.94% in 2012. It just reflected the vegetation transition from the mosaic of croplands, forests, shrublands, and grasslands to pure forests during the forest regeneration after the "5.6 Fire".

As there were as many as 17 classes in the IGBP scheme, for ease of understanding and use by the scientific community and public, we summarized them into four high-level land cover categories, namely "Forests", "Savannas & Shrublands & Grasslands", "Cropland/Natural vegetation mosaic" and "Others". The former two were the summarization of five forest classes (No. 1-5), several savannas/shrublands/grasslands classes (No. 6-10), respectively. The "Cropland/Natural vegetation mosaic" just corresponded to the No. 14 class in the original IGBP scheme and the "Others" included all the remaining land cover units. The area percentage of the four high-level land cover classes during 2001-2012 was also calculated (Fig. 4.10). The results indicated that the "Forests" area increased from 50.29% in 2001 to 89.35% in 2012. The area change of different classes in this period revealed the recovery of forests in the burned area. Certainly the anomaly of "Forests" and "Savannas & Shrublands & Grasslands" in 2005-2007 should be noted.

Since the fire severity differed in different regions, to identify the temporal and spatial change of recovered forests, we mapped the spatial distribution of forest of the 12 years (Fig. 4.11). By time series comparison, it was found that the regenerated forest mainly existed in the severely burned area which was also shown in Fig. 4.1. This comparison directly reflected the post-fire forest spatial dynamics.

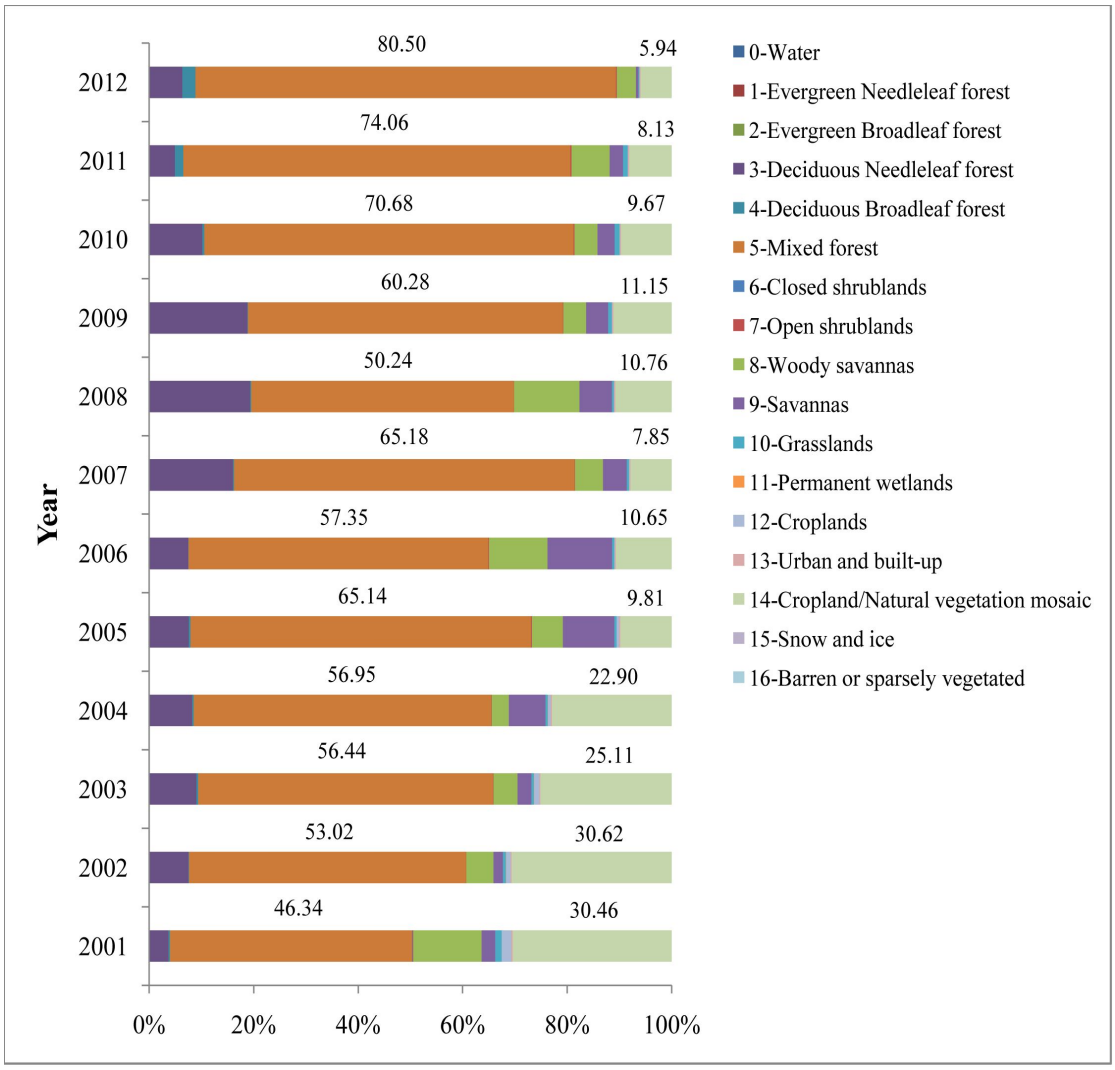

Figure 4.9 The area percentage of 17 land cover units during the period of 2001-2012 in the IGBP classification scheme.

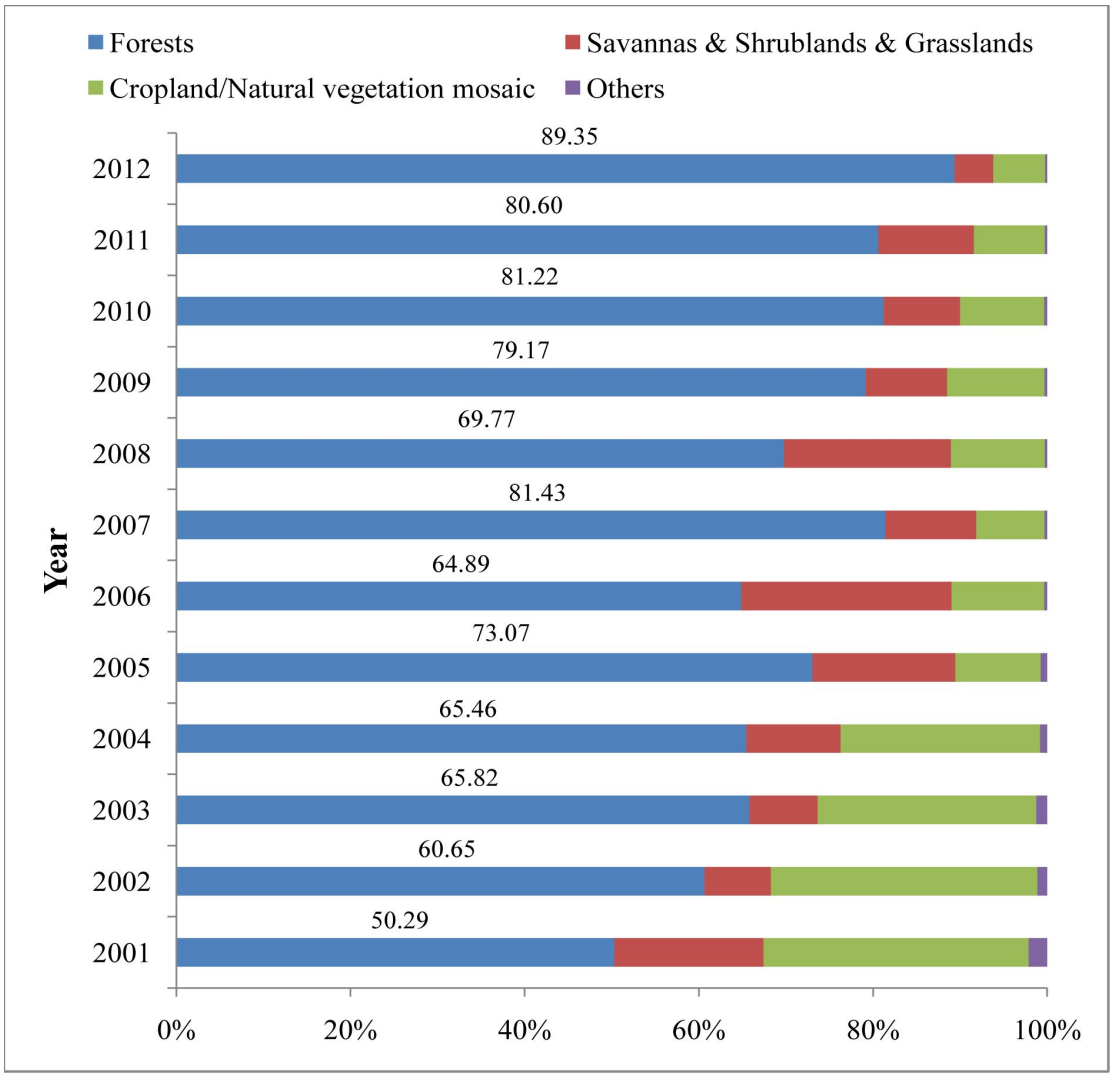

Figure 4.10 The area percentage of 4 high-level land cover classes during the period of 2001-2012.

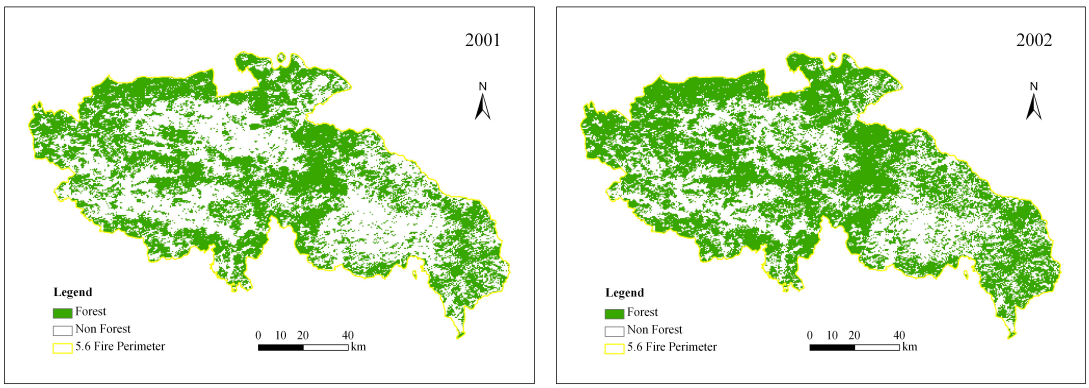

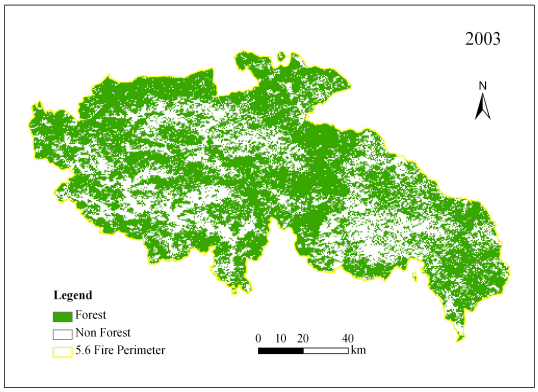
2003
N
Legend
Forest
Non Forest
5.6 Fire Perimeter
0 10 20 40
km

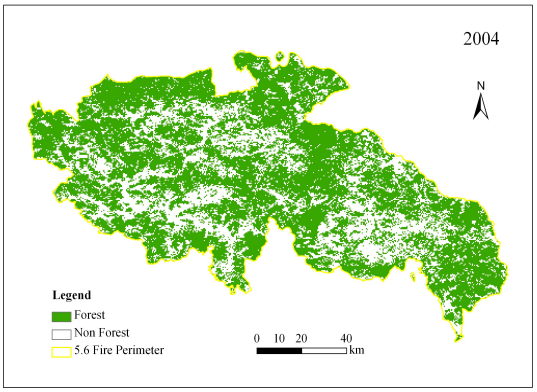
2004
N
Legend
Forest
Non Forest
5.6 Fire Perimeter
0 10 20 40
km

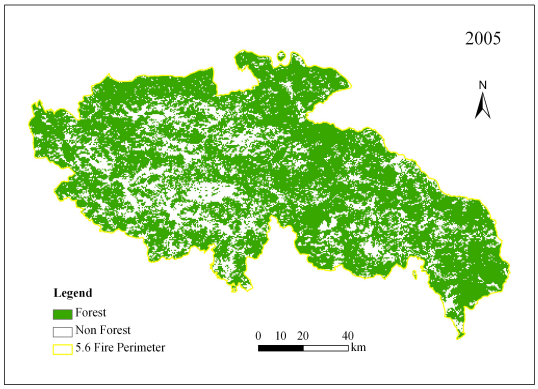
2005
N
Legend
Forest
Non Forest
5.6 Fire Perimeter
0 10 20 40
km

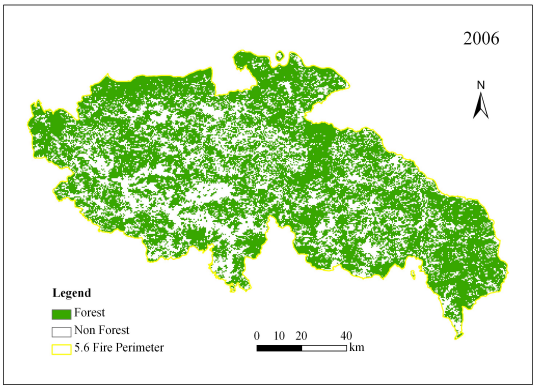
2006
N
Legend
Forest
Non Forest
5.6 Fire Perimeter
0 10 20 40
km

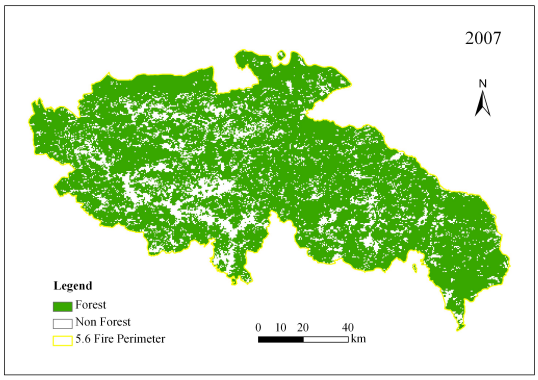
2007
N
Legend
Forest
Non Forest
5.6 Fire Perimeter
0 10 20 40
km

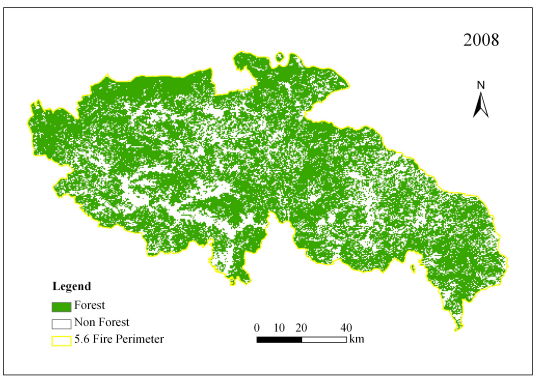
2008
N
Legend
Forest
Non Forest
5.6 Fire Perimeter
0 10 20 40
km

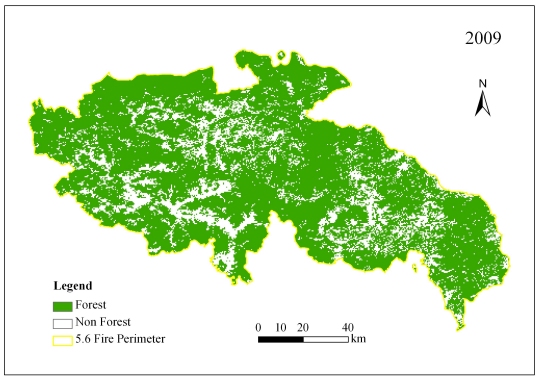
2009
N
Legend
Forest
Non Forest
5.6 Fire Perimeter
0 10 20 40
km

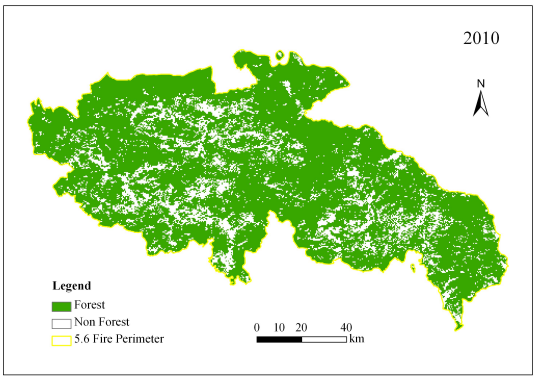
2010
N
Legend
Forest
Non Forest
5.6 Fire Perimeter
0 10 20 40
km

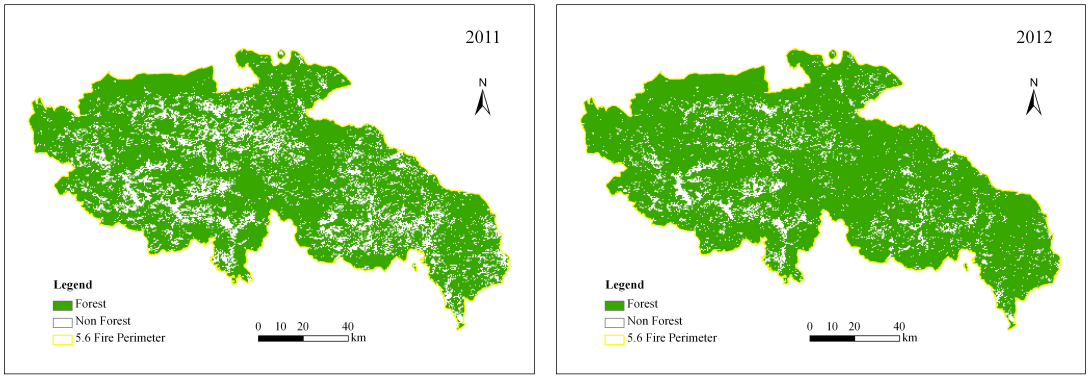

Figure 4.11 The spatial distribution of forest and its change in the burned area of "5.6 Fire" during 2001-2012 in the IGBP classification scheme.

4.2.3.2 Vegetation indices

As MODIS vegetation indices (NDVI & EVI) are well suited for the mapping of global and regional vegetation conditions and have been used in products displaying land cover and land cover changes, here they were used to identify different types of forests and land cover vegetation classes.

NDVI

Since there was little "Evergreen Broadleaf forest" in the study area, we only detected the other four types of "Evergreen Needleleaf forest", "Deciduous Needleleaf forest", "Deciduous Broadleaf forest", and "Mixed forest" in IGBP scheme. The annual NDVI values of the four forest types in the peak growing season of 2001-2012 were calculated and compared (Fig. 4.12). By ANOVA, it was concluded that there were extremely significant differences among the NDVI of the four types of forests (Table 4.5(a), $p < 0.01$). It indicated that the four types of forests in this region can be seperated by MODIS NDVI. The comparison also suggested that the broadleaf forest had a significant higher NDVI than needleleaf forest ($p < 0.05$).

When the 17 IGBP land cover units were summarized to 4 high-level classes, the NDVI values of the former 3 types of land cover vegetation were also extracted and compared (Fig. 4.13). By ANOVA, it was found that there were extremely significant differences among the NDVI of the "Forests", "Savannas & Shrublands & Grasslands", and "Cropland/Natural vegetation mosaic" (Table 4.5(b), $p < 0.01$). From multiple comparisons, it can be found the NDVI of "Forests" was significant higher than the other two, and that of "Cropland/Natural vegetation mosaic" was the lowest.

To further explore the impact of fire on local forest and monitor the post-fire forest restoration, the forest located in the burned and unburned area of "5.6 Fire" was recognized and their NDVI values were compared. Through the quantitative analysis (Table 4.5(c)), it was found that the difference in NDVI between the burned and unburned forests was extremely significant ($p < 0.01$), however, it remained statistically unchanged throughout the 12 years.

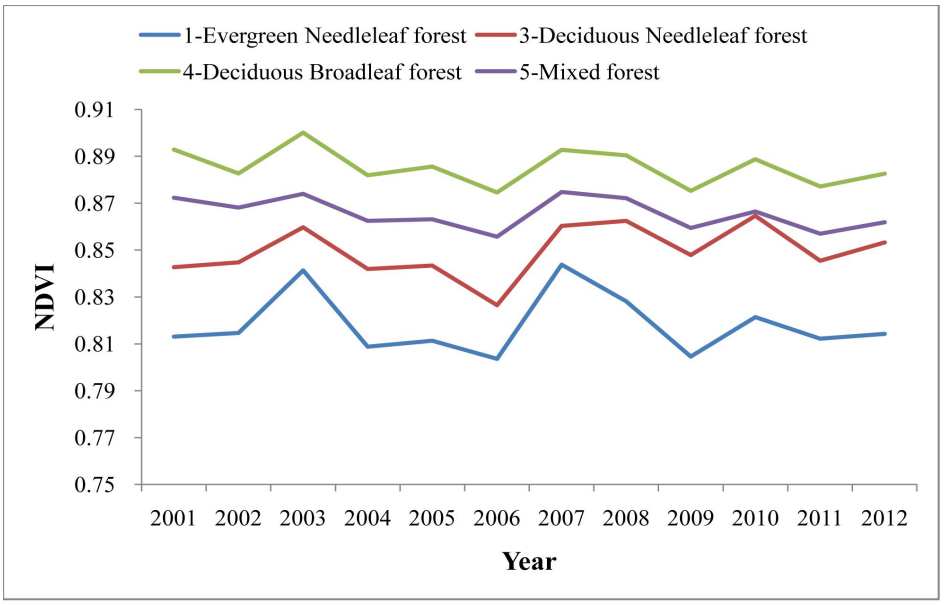

Figure 4.12 The NDVI of four types of forests (IGBP classification scheme) and their dynamics in the peak growing season of 2001-2012.

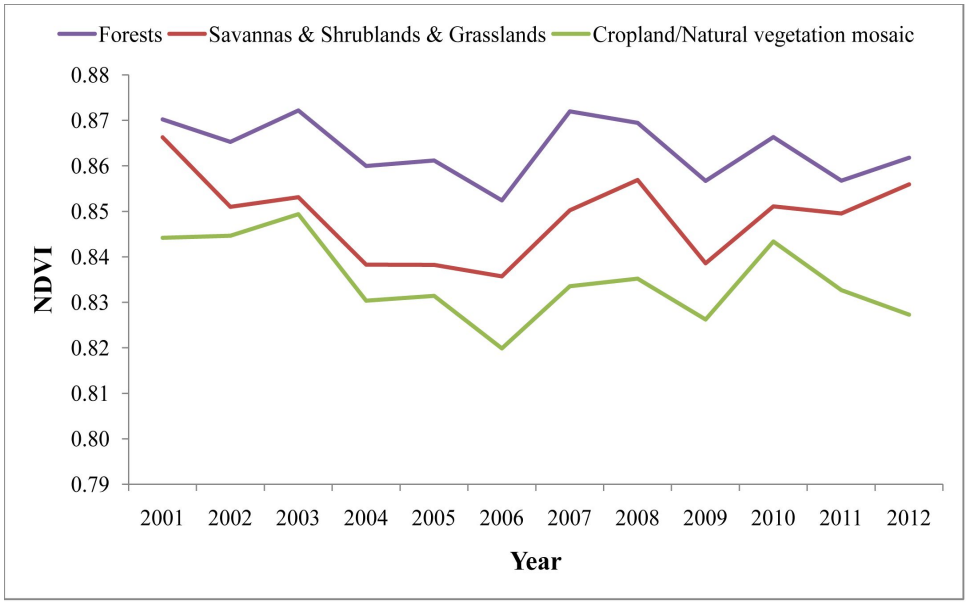

Figure 4.13 The NDVI of three types of land cover vegetation and their dynamics in the peak growing season of 2001-2012.

Table 4.5 ANOVA of NDVI.

Source	Sum of Squares	df	Mean Square	F statistics	Significant difference (p)
(a) Four types of forests (IGBP scheme)					
Between groups	0.0292	3	0.0097	96.4676	0.0000**
Within groups	0.0044	44	0.0001		
Total	0.0336	47			

(b) Three types of vegetation					
Between groups	0.0050	2	0.0025	35.9590	0.0000**
Within groups	0.0023	33	0.0001		
Total	0.0073	35			
(c) Burned & Unburned forests					
Regression analysis	0.0005	1	0.0005	369.7039	0.0000**
Residuals	1.24E-05	10	1.24E-06		
Total	0.0005	11			

** $p <= 0.01$.

EVI

The time series EVI of four forest types (IGBP scheme) and three high-level vegetation classes in the peak growing season of 2001-2012 were also calculated and compared. From Fig. 4.14 and Table 4.6(a), similar results as in MODIS NDVI can be obtained. But completely different results were acquired from Fig. 4.15 and Table 4.6(b). Here we found that no significant difference existed among the EVI of the three vegetation classes ($p > 0.05$). It indicated that the "Forests", "Savannas & Shrublands & Grasslands", and "Cropland/Natural vegetation mosaic" can not be discriminated using MODIS EVI.

The EVI of burned and unburned forests in the peak growing season of 2001-2012 were compared (Table 4.6(c)). Also similar results were obtained as in MODIS NDVI.

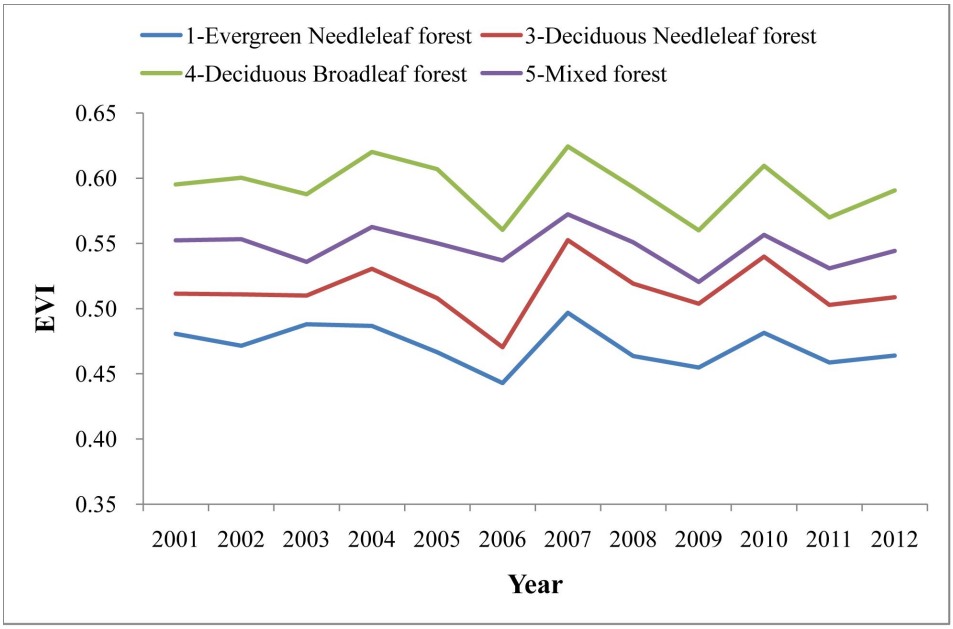

Figure 4.14 The EVI of four types of forests (IGBP classification scheme) and their dynamics in the peak growing season of 2001-2012.

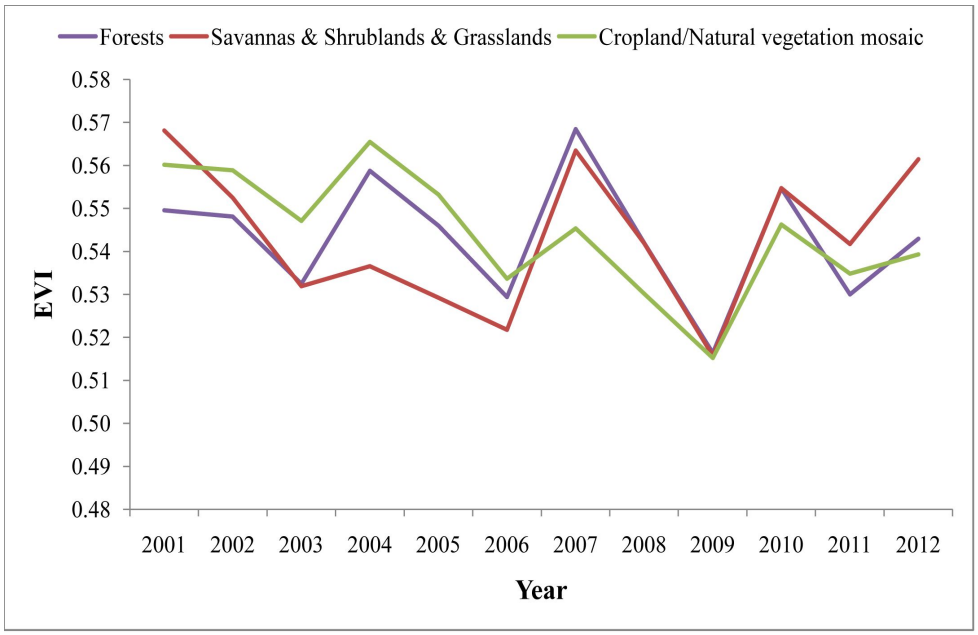

Figure 4.15 The EVI of three types of land cover vegetation and their dynamics in the peak growing season of 2001-2012.

Table 4.6 ANOVA of EVI.

Source	Sum of Squares	df	Mean Square	F statistics	Significant difference (p)
(a) Four types of forests (IGBP scheme)					
Between groups	0.0958	3	0.0319	96.0067	0.0000**
Within groups	0.0146	44	0.0003		
Total	0.1104	47			
(b) Three types of vegetation					
Between groups	6.09E-06	2	3.05E-06	0.0130	0.9871
Within groups	0.0077	33	0.0002		
Total	0.0077	35			
(c) Burned & Unburned forests					
Regression analysis	0.0022	1	0.0022	516.3113	0.0000**
Residuals	4.25E-05	10	4.25E-06		
Total	0.0022	11			

** $p <= 0.01$.

4.2.4 Discussion

Focusing on the forest recovery after the "5.6 Fire", this study identified the interannual variability of land cover type in the burned area and detected the responses of vegetation indices to different forest types based on MODIS data. Together with the yearly increase of "Forests" area and decrease of "Cropland/Natural vegetation mosaic" area, an anomaly in 2005-2007 can be observed. Further

examination indicated that it mainly resulted from the misclassification between forests and woody savannas/savannas which had no distinction in the definition of vegetation height. Additionally, we also observed the relatively high percentage of "Deciduous Needleleaf forest" in 2007-2009 which was because of the misclassification between this class and "Mixed forest" in the northwest of the burned area. It resulted from the data quality of original images with thin clouds in that area.

When comparing MODIS NDVI with EVI, it was found that they were both effective to separate the four types of forests, however, were not for the separation of three high-level vegetation classes. The differences among "Forests", "Savannas & Shrublands & Grasslands" and "Cropland/Natural vegetation mosaic" can be characterized by NDVI, but not EVI. Compared with NDVI, EVI which uses the blue band to remove residual atmosphere contamination minimizes canopy background variations and maintains sensitivity over dense vegetation conditions. But it also becomes more easily influenced by other factors including landscape fragmentation, seasonal change etc (Ferreira *et al.*, 2010; Samanta *et al.*, 2011).

The annual MODIS Land Cover Type product were produced by a full year's observations, while Vegetation Indices data used in the study were collected from the same period of each year, thus the NDVI and EVI time series values were influenced by the phenology. Here the impact of phenology was not eliminated since it had no influence on the comparisons among different forest types, different land cover vegetation, as well as between the burned and unburned forests.

Additionally, when detecting the difference between the burned and unburned forest area in MODIS VI, it was found that the difference in both NDVI and EVI remained unchanged throughout the 12 years, without any significant fluctuations. It suggested that the progress in restoration of burned forests during this period cannot be characterized by MODIS VI. Considering the long growth and regeneration cycle of boreal forest in this region, the relatively short period of 12 years appears to be a reason; however, the factor of low spatial resolution of MODIS Vegetation Indices products (500 m) is probably another cause.

Finally, as the Terra was launched on December 18, 1999, and Aqua was launched on May 4, 2002, the MODIS data are available only after 2000. But since the "5.6 Fire" occurred in 1987, there was as long as 13 years immediately after the fire which could not be covered by MODIS observations. In addition to the Landsat TM images, the AVHRR imagery was used in other studies (Yi *et al.*, 2013). The results indicated that the severely burned area exhibited a better recovery trend than the lightly burned regions but more detailed satellite analyses and field data were needed for a more convincing validation.

4.3 Based on ALOS/PALSAR data

4.3.1 Introduction

Rather than being sensitive to the spectral signatures of the targets, SAR is an active microwave sensor and is primarily sensitive to its roughness and structural composition and dielectric properties. Different land cover objects thus typically produce different backscattering characteristics which can be taken as a key feature when using SAR sensors for land cover analyses. For example, a smooth surface (e.g. still water) will give rise to little backscatter as most of the transmitted signals will be reflected away from the sensor, while a more structurally complex target (e.g. forest) will shows brighter as the signal interaction with the leaves, branches and trunks will result in a higher proportion of the signals being returned back to the sensor.

Compared to the X-band (e.g. TerraSAR-X) and C-band (e.g. ERS 1-2/SAR, Envisat/ASAR, Radarsat-1/2) radar sensors, the relatively long L-band wavelength of ALOS/PALSAR (23.6 cm) allows a penetration of microwave signals below the vegetation canopy (leaves appear transparent), to reveal information about the physical forest structures. PALSAR has both the co-polarized (HH and VV) and cross-polarized (HV and VH) channels which can be considered as "spectral bands" of SAR sensors and provide complementary information.

Regarding research involving with the detection of forest regeneration dynamics, most studies were performed using field survey data (Uemura *et al.*, 1997; Johnstone *et al.*, 2004; Otoda *et al.*, 2013), and in combination with a variety of optical imagery (Zhang *et al.*, 2004; Cuevas-Gonzalez *et al.*, 2009; Veraverbeke *et al.*, 2012). There were also some studies concerning fire scar identification and forest disturbance detection using SAR data although they are comparatively difficult to acquire, process and interpret (Ranson *et al.*, 2003; Tanase *et al.*, 2010b; Millin-Chalabi *et al.*, 2014).

PALSAR is relatively preferred due to its capability of deep penetration into forest structures, interacting with tree stems, large branches, and even ground. For example, Lucas *et al.* (2010) examined the relationship between PALSAR HH and HV backscattering coefficients and above ground biomass and concluded that the retrieval algorithms ideally needed to consider differences in surface moisture conditions and vegetation structure. Mari *et al.* (2012) used PALSAR backscatter information to estimate the effect of fire over different Mediterranean vegetation types. The results suggested that HH polarization exhibited a similar and continuous effect of increased backscatter after fire over different vegetation types, while for the HV polarization, a significant reduction was observed for sclerophyllous tree and coniferous forest. Some other similar studies were also performed using PALSAR FBD or ScanSAR data in co-polarized and cross-polarized polarization (Whittle *et al.*, 2012; Cornforth *et al.*, 2013; Polychronaki *et al.*, 2013).

Concerning the "5.6 Fire", no studies based on SAR data have been conducted focusing on the post-fire forest recovery, especially with respect to different

restoration strategies. As the optical images (Landsat TM/ETM+, MODIS) have already been used in above sections, for consistency and comparability, here the objective was to detect the post-fire forest dynamics under different restoration treatments and compare their different effects based on time series ALOS/PALSAR data. Both the HH and HV polarization were examined and evaluated.

4.3.2 Data and methods

4.3.2.1 ALOS PALSAR data

The ALOS satellite has been developed to mainly contribute to the fields of mapping, precise regional land coverage observation, disaster monitoring, and resource surveying. It enhances land observation technologies acquired through the development and operation of its predecessor of the Japanese Earth Resource Satellite-1 (JERS-1) and its successor of ALOS-2. The ALOS characteristics were shown in Table 4.7.

Table 4.7 The characteristics of ALOS satellite.

Item	Figure
Operation life	Jan. 24, 2006 – April 22, 2011
Launch vehicle	H-IIA
Spacecraft mass	Approx. 4 tons
Generated power	Approx. 7 kW (at End of Life)
Orbit	Sun-Synchronous Sub-Recurrent
	Repeat Cycle: 46 days
	Sub Cycle: 2 days
	Altitude: 691.65 km (at Equator)
	Inclination: 98.16 degree
Position determination accuracy	1 m (off-line)
Attitude determination accuracy	2.0×10^{-4} degree (with GCP)

ALOS is equipped with three sensors: the Panchromatic Remote-sensing Instrument for Stereo Mapping (PRISM), which is used to measure precise land elevation; the AVNIR-2, which observes the ground features in visible and near infrared channels; and the PALSAR, which is an active microwave sensor using L-band frequency to achieve cloud-free and day-and-night land observations (Fig. 4.16). The technical characteristics of PALSAR sensor under three observation modes were introduced in Table 4.8.

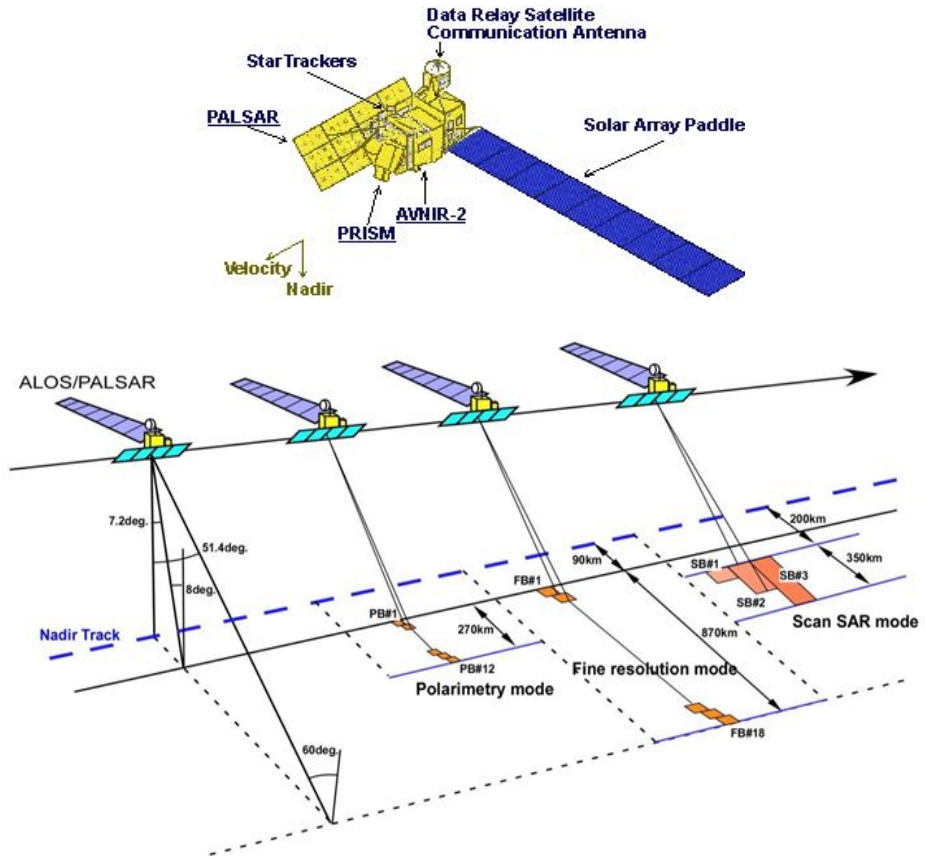

Figure 4.16 The three instruments onboard ALOS satellite (upper) and the PALSAR observation modes (lower).

Table 4.8 Technical characteristics of the PALSAR sensor.

Mode		Fine		ScanSAR	Polarimetric (experimental)
		FBS	FBD		
Chirp bandwidth		28 MHz	14 MHz	14 MHz, 28 MHz	14MHz
Polarization		HH or VV	HH+HV or VV+VH	HH or VV	HH+HV+VH+VV
Incident angle		8 – 60 deg.	8 – 60 deg.	18 – 43 deg.	8 – 30 deg.
Resolution	Range	7 – 44 m	14 – 88 m	100 m	24 – 89 m
	Azimuth	10 m (2 looks) 20 m (4 looks)		100 m	10 m (2 looks) 20 m (4 looks)
Swath width		40 – 70 km	40 – 70 km	250 – 350 km	20 – 65 km
Bit length		5 bits	5 bits	5 bits	3 or 5 bits
Data rate		240 Mbps	240 Mbps	120 or 240 Mbps	240 Mbps
Center frequency		1270 MHz (L-band)			
Radiometric accuracy		scene: 1 dB / orbit: 1.5 dB			

In consideration of the life period of ALOS PALSAR sensor and the availability of the three observation modes in the study area, only the data acquired under Fine resolution mode covering the vegetation peak growing season of 2006-2010 was available. Since that of 2006 had only single polarization (HH), those possessing dual

polarization (HH+HV) during the period 2007-2010 were utilized in this study (Table 4.9). These images were acquired during the same month (August) and provided by the JAXA EORC (Earth Observation Research Center).

Table 4.9 Time series ALOS/PALSAR data used in the forest dynamics detection.

Date	Polarization	Observation mode
8/5/2007 8/7/2008 8/10/2009 8/13/2010	HH and HV	FBD

4.3.2.2 Data pre-processing and methodology

The PALSAR data used here are the level 1.1 data which corresponds to Single Look Complex (SLC) products, provided in slant range geometry. The four scenes were pre-processed to backscattering intensity (Sigma0: σ°) images using the tools of NEST (Next ESA SAR Toolbox) and ASF (Alaska Satellite Facility) MapReady. The pre-processing flow chart was illustrated in Fig. 4.17.

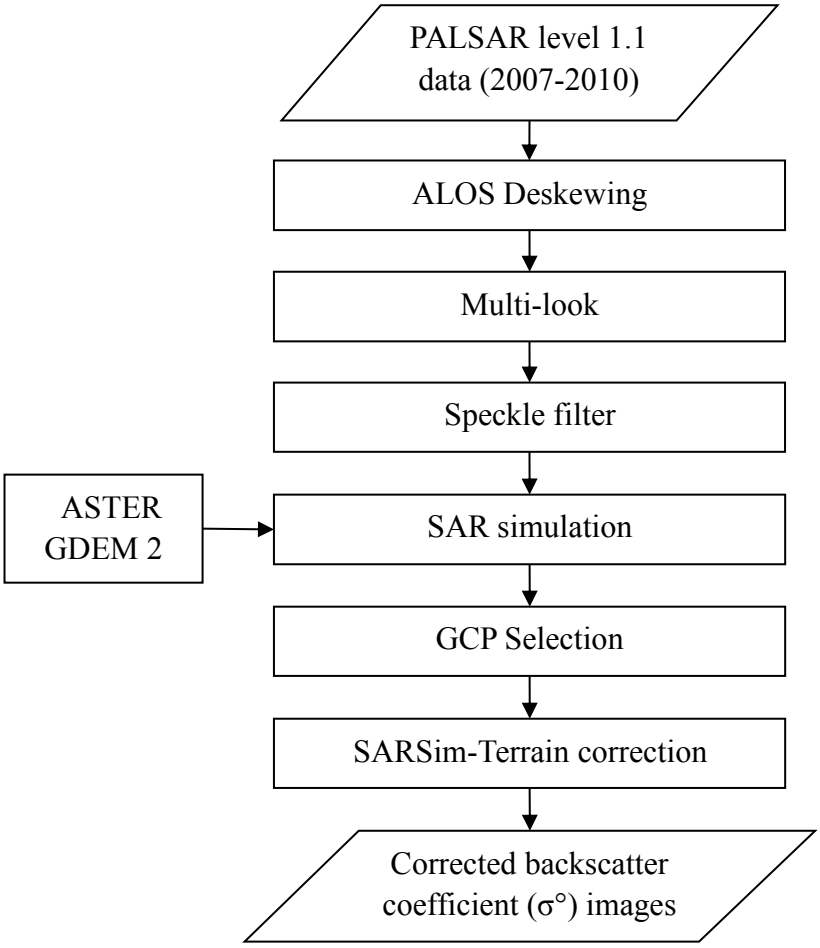

Figure 4.17 The pre-processing flow chart of the ALOS PALSAR data.

After these pre-processing steps, the backscattering coefficient images of Sigma0 were acquired. Taking the scene acquired on 8/5/2007 as an example, the histograms and scatter plot of Sigma0 in HH and HV polarization were plotted (Fig. 4.18). By comparison, it can be found that the Sigma0 of HH is higher than that of HV because HH backscattering contains more signals from ground surface and branch/trunk than HV.

SAR signals can be easily affected by terrain since it observes the ground in a side looking geometry. Due to the geometry-induced distortions in terms of foreshortening, layover and shadowing, terrain correction which removes these distortions by using the height information from a DEM becomes necessary. In this study, the ASTER GDEM 2 (Global Digital Elevation Model version 2) product was used for the terrain correction. The correction effect was shown in Fig. 4.19. The RGB composite subfigures showed the buildings in the urban area (upper) and the vegetation in the mountain area (lower). The left two subfigures are those after terrain correction, and those on the right represent situations before terrain correction.

In the upper two subfigures, the urban area in magenta revealed the strong HH signals backscattered by buildings (surface scattering), while the rivers in black indicated the extremely weak signals in both HH and HV polarization from the water. As HV polarization mainly represents signals from volume scattering (e.g. forest ecosystem), the green color in all these figures, especially the lower two, suggested the forest coverage. By the comparison of the forest area in the lower two subfigures between before (right) and after (left) terrain correction, it was concluded that terrain correction (both geometric and radiometric) effectively adjusted the position of ridge lines and valleys, as well as corrected the brightness of geometrically registered pixels by reducing the brightness of pixels in the slope facing the SAR sensor and increasing that in the opposite hillside.

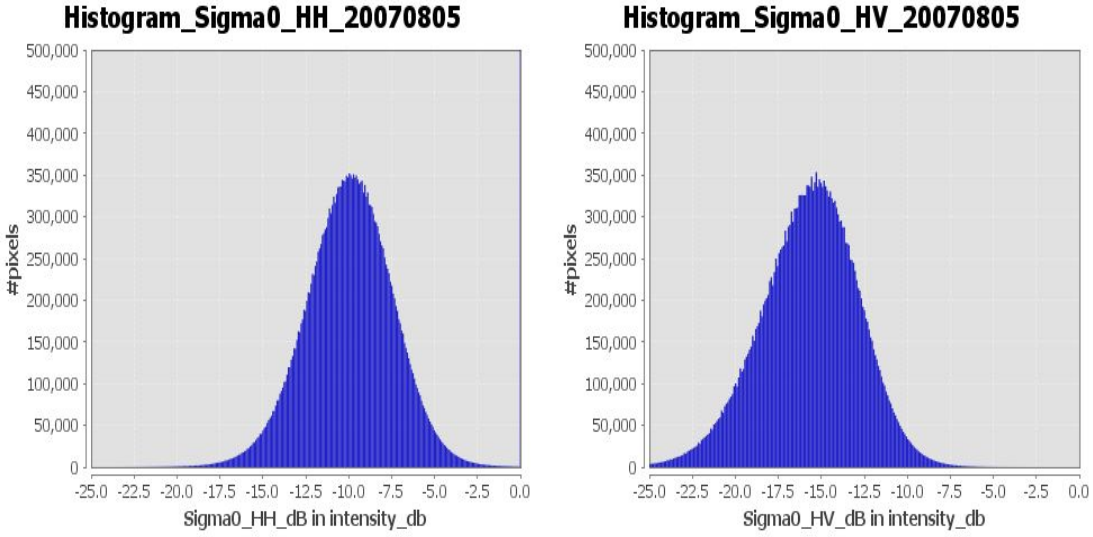

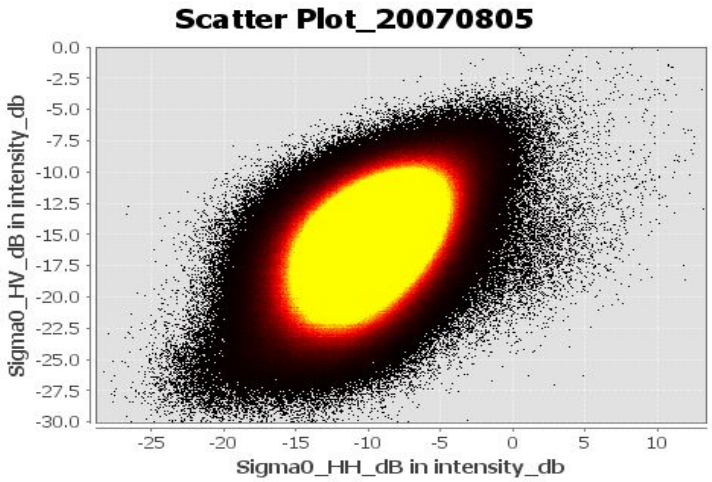

Figure 4.18 The histograms and scatter plot of processed PALSAR backscattering coefficient (intensity) of the scene acquired on 8/5/2007 (UL: histogram of HH; UR: histogram of HV; lower: scatter plot).

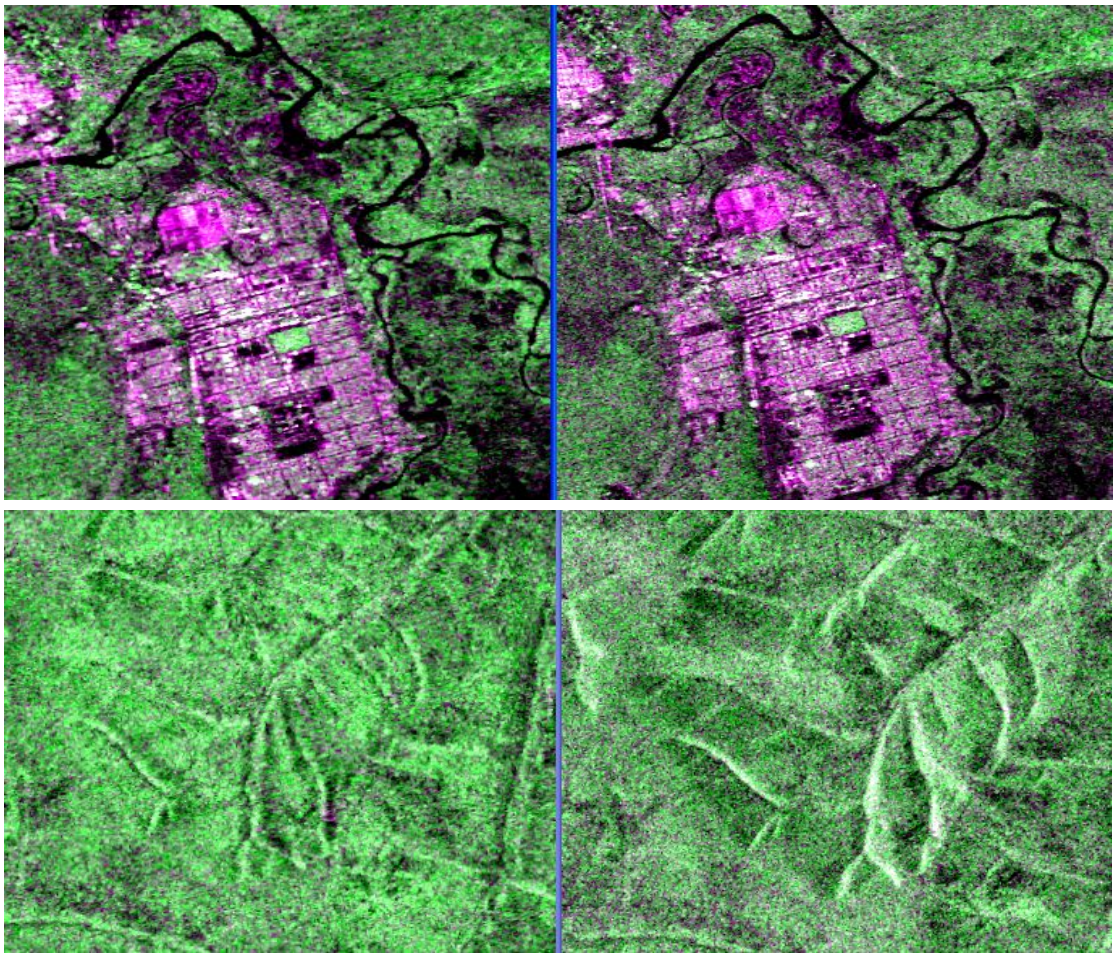

Figure 4.19 The acquired SAR backscattering coefficient (Sigma0: σ°) of the scene acquired on 8/5/2007 (R: HH; G: HV; B: HH). The upper are the urban area and the lower show the mountain vegetation; the left two subfigures are those after terrain correction and those on the right represent situations before terrain correction.

Since the swath width of PALSAR is relatively narrower compared to Landsat and MODIS sensors, the scene used in this study covers only two forestry bureaus of Tuqiang and Amuer with a spatial resolution of 10 m which well corresponds to the size of investigated plots in the field forest survey. Therefore, only the forest dynamics under different restoration treatments in the two regions were analyzed and compared. Due to the sensitivity of the radar backscattering signals to many factors, including forest canopy structure, terrain, surface moisture etc., based on ALOS PALSAR data, the forests in the plots located in the forestry bureaus of Tuqiang and Amuer will be examined and evaluated respectively.

4.3.3 Results

4.3.3.1 Forest dynamics in HH polarization

The statistics of backscattering coefficients (Sigma0: σ°) in HH polarization under three different restoration treatments in the two forestry bureaus of Tuqiang and Amuer were illustrated in Fig. 4.20. By one-way ANOVA, a quantitative comparison was conducted between the three groups (restoration treatments) during the period 2007-2010 for Tuqiang and Amuer respectively (Table 4.10).

From this table and figure, it can be found that there was difference in the HH backscattering coefficient among the three restoration treatments of Natural Regeneration (NR), Artificial Regeneration (AR) and Artificial Promotion (AP). For Tuqiang, the difference was significant (Sig. < 0.05), and for Amuer, it appeared to be extremely significant (Sig. < 0.01). By multiple comparisons, the Sigma0 of forest under NR was the strongest, and that of AR was larger than AP. The overall trends of Sigma0 in the two regions were different which was probably due to their specific environmental conditions.

Table 4.10 The one-way ANOVA result of backscattering coefficient (Sigma0: σ°) in HH polarization.

Difference Source	Sum of Squares	df	Mean Square	F statistics	Sig.
(a) Tuqiang					
Between Groups	21.252	2	10.626	3.891	0.030*
Within Groups	90.113	33	2.731		
Total	111.365	35			
(b) Amuer					
Between Groups	55.491	2	27.745	7.547	0.002**
Within Groups	121.321	33	3.676		
Total	176.812	35			

* $0.01 < p <= 0.05$; ** $p <= 0.01$.

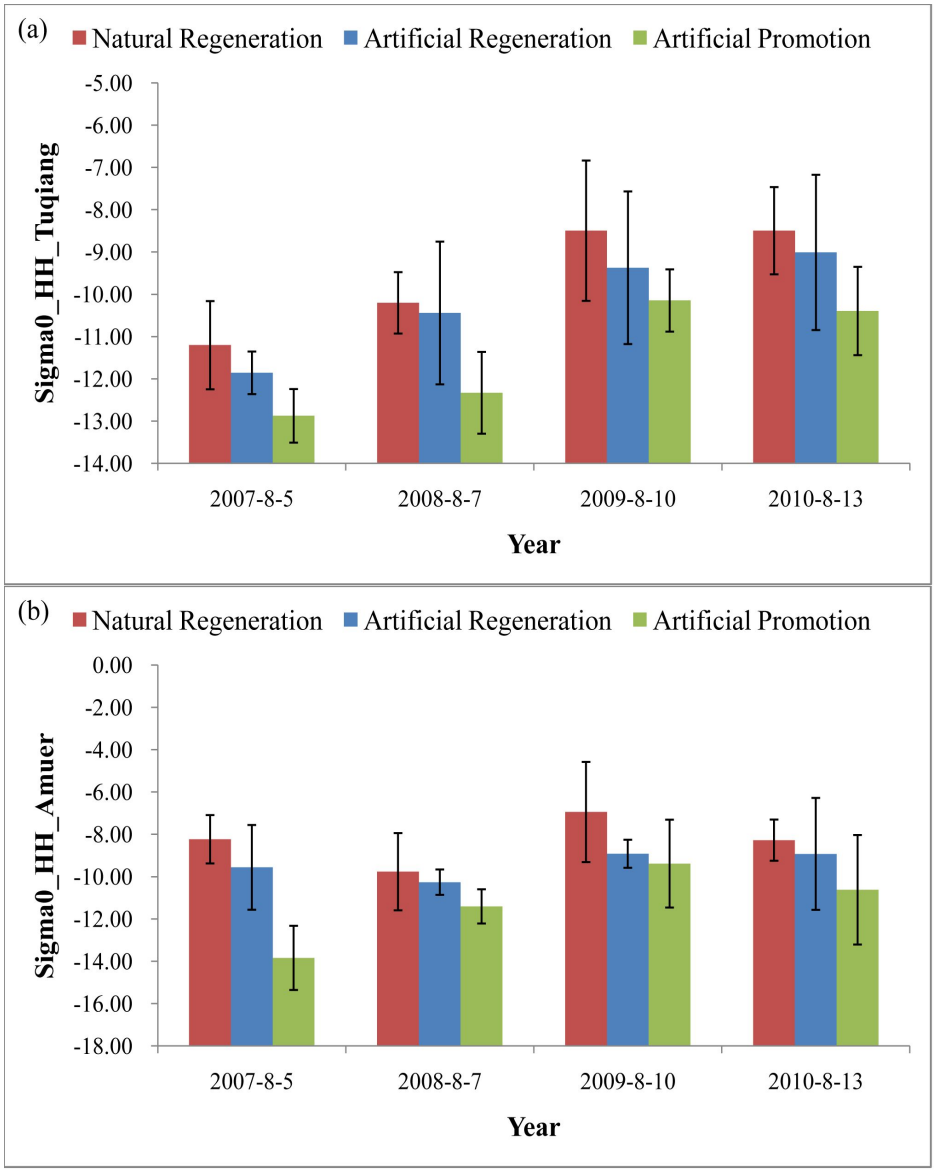

Figure 4.20 The statistics (mean±S.D.) and comparison of backscattering coefficient (Sigma0: σ°) in HH polarization under different restoration treatments in the forestry bureau of (a) Tuqiang; (b) Amuer.

4.3.3.2 Forest states in HV polarization

Similarly, the statistics of backscattering coefficients in HV polarization for the two forestry bureaus of Tuqiang and Amuer were shown in Fig. 4.21. Further comparison by one-way ANOVA among the three different restoration treatments was performed (Table 4.11). The probability value of 0.000 suggested that, for both the forests in Tuqiang and Amuer, extremely significant difference existed in HV backscattering coefficient among the three restoration treatments during the period 2007-2010.

Further multiple comparisons revealed the highest Sigma0 value in forest under NR and the lowest Sigma0 for AP. That of AR fell in between. It was consistent with the results achieved in HH polarization. Certainly, it can be found that the Sigma0 values

in HV polarization were comparatively lower than that in HH polarization (about 2-5 dB), even for the forest in the same region and under the same restoration treatment.

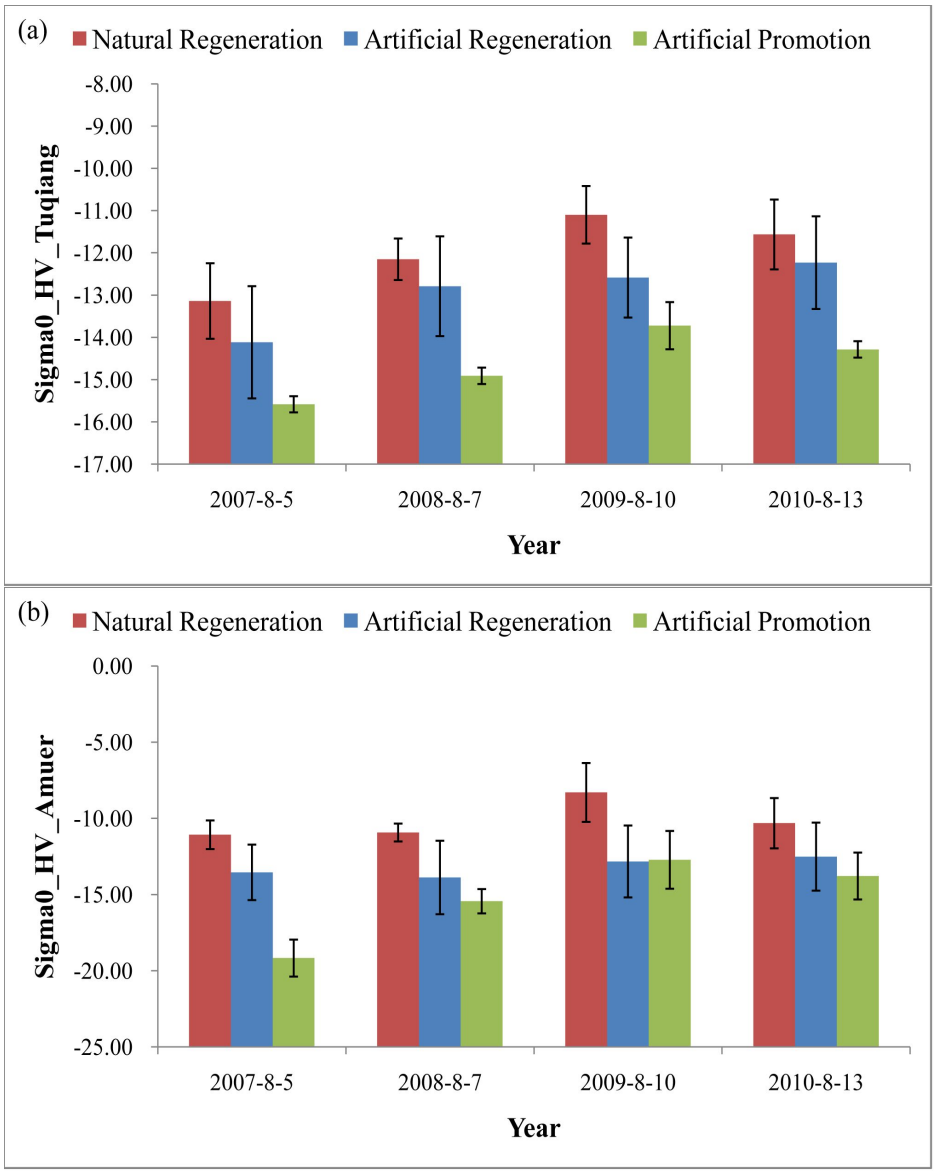

Figure 4.21 The statistics (mean±S.D.) and comparison of backscattering coefficient (Sigma0: σ°) in HV polarization under different restoration treatments in the forestry bureau of (a) Tuqiang; (b) Amuer.

Table 4.11 The one-way ANOVA result of backscattering coefficient (Sigma0: σ°) in HV polarization.

Difference Source	Sum of Squares	df	Mean Square	F statistics	Sig.
(a) Tuqiang					
Between Groups	42.881	2	21.440	18.921	0.000**
Within Groups	37.393	33	1.133		
Total	80.274	35			
(b) Amuer					

Between Groups	159.242	2	79.621	16.313	0.000**
Within Groups	161.069	33	4.881		
Total	320.311	35			

* $0.01 < p <= 0.05$; ** $p <= 0.01$.

4.3.3.3 Forest characterization by derived indices

The above analyses and comparison using backscattering coefficients in HH and HV polarization indicated that the two variables were both suitable for the forest identification among different restoration treatments. Nonetheless, it should be noted that the availability and efficiency differed depending upon the forest regions and detection period. More significant variables or indices should be developed and used to characterize the forest growth states under different treatments.

Considering the derivation and application of vegetation indices (e.g. NDVI, RVI, EVI) when using optical remote sensing imagery, we proposed to derive some similar indices from the radar backscattering coefficients. In the same way as RVI (Pearson and Miller, 1972) and NDVI (Rouse *et al.*, 1974; Tucker, 1979), it is possible to calculate two radar indices, namely Radar Ratio Vegetation Index (RRVI) and Radar Normalized Difference Vegetation Index (RNDVI). They are defined by the following equations:

$$RRVI = \frac{\sigma_{0HH}}{\sigma_{0HV}} \tag{4-1}$$

$$RNDVI = \frac{\sigma_{0HV} - \sigma_{0HH}}{\sigma_{0HV} + \sigma_{0HH}} \tag{4-2}$$

where σ_{0HH} and σ_{0HV} indicate the backscattering coefficient in HH and HV polarization, respectively. The two polarization modes act as the same role with the two spectral bands in red and near infrared wavelength.

The statistics of the two radar indices for the period 2007-2010 and the two regions of Tuqiang and Amuer were calculated and shown in Fig. 4.22 and 4.23, respectively. By visual comparison, it could be found that the two indices of RRVI and RNDVI had similar performance in this scenario of forest detection and identification.

The two groups of figures revealed a significant difference existed among the forest recovery trajectories under the three treatments of NR, AR and AP. A post-hoc test further indicated that, compared to the other two treatments, the forests under NR presented a completely different recovery trajectory characterized by both RRVI and RNDVI for both the two regions. The difference between NR and the other two treatments were relatively more apparent in Amuer than in Tuqiang. No significant difference was observed in both RRVI and RNDVI between the treatments of AR and AP. It was a conclusion that cannot be come to when using backscattering coefficient

in HH or HV polarization individually. This demonstrated the advantages of RRVI and RNDVI which utilize the significant information in HH and HV polarization simultaneously.

When looking back to the former chapters, it was found that the results acquired using radar indices were consistent with those achieved by DI (chapter 4.1) and LAI (chapter 3). The DI calculated from time series Landsat images also revealed a different recovery track between forests under NR and the other two treatments (Fig. 4.8). In that case, the minor difference in DI values between the treatments of AR and AP was proven to be insignificant. Similarly, the statistics and comparisons of LAI values collected from filed forest survey in 2012 gave the same conclusion (Fig. 3.8). The forests under NR showed a highest LAI, and the difference in LAI between the other two treatments was insignificant by a post-hoc test. All these indices and parameters provided independent and mutual corroboration for the characterization and delineation of forest recovery trajectories under different restoration treatments after the "5.6 Fire" occurred in the Greater Hinggan Mountain area.

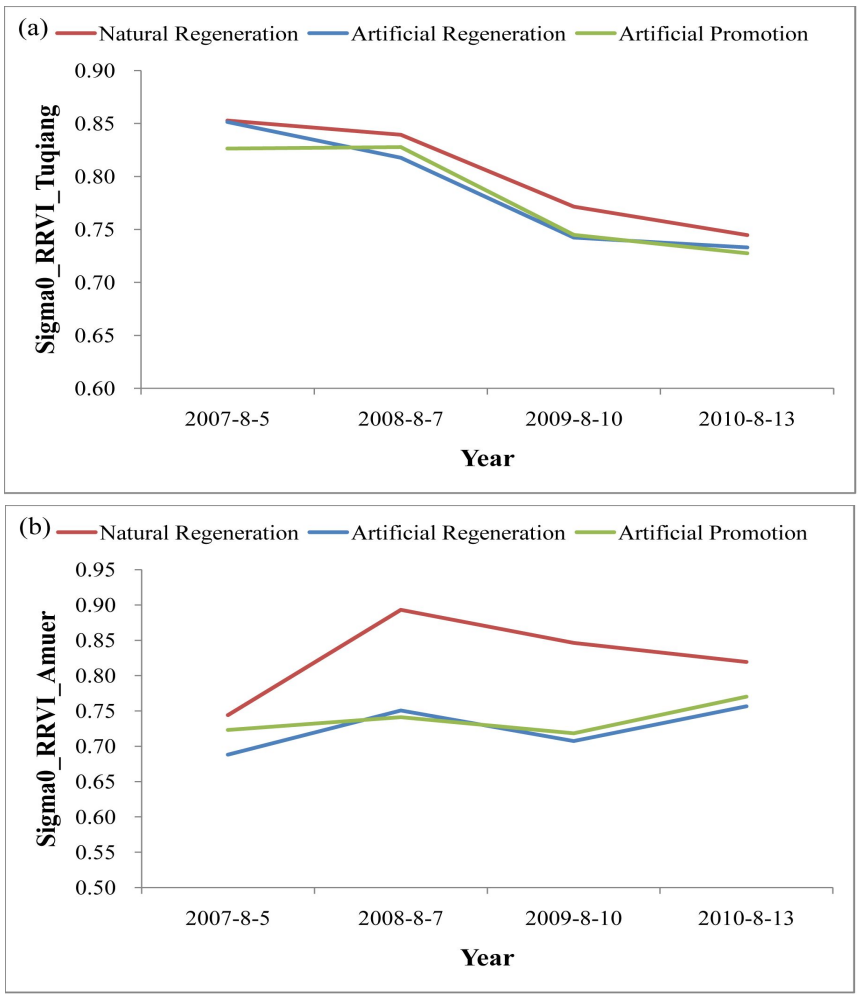

Figure 4.22 The comparison of backscattering coefficient ratio of RRVI under different restoration treatments in the forestry bureau of (a) Tuqiang; (b) Amuer.

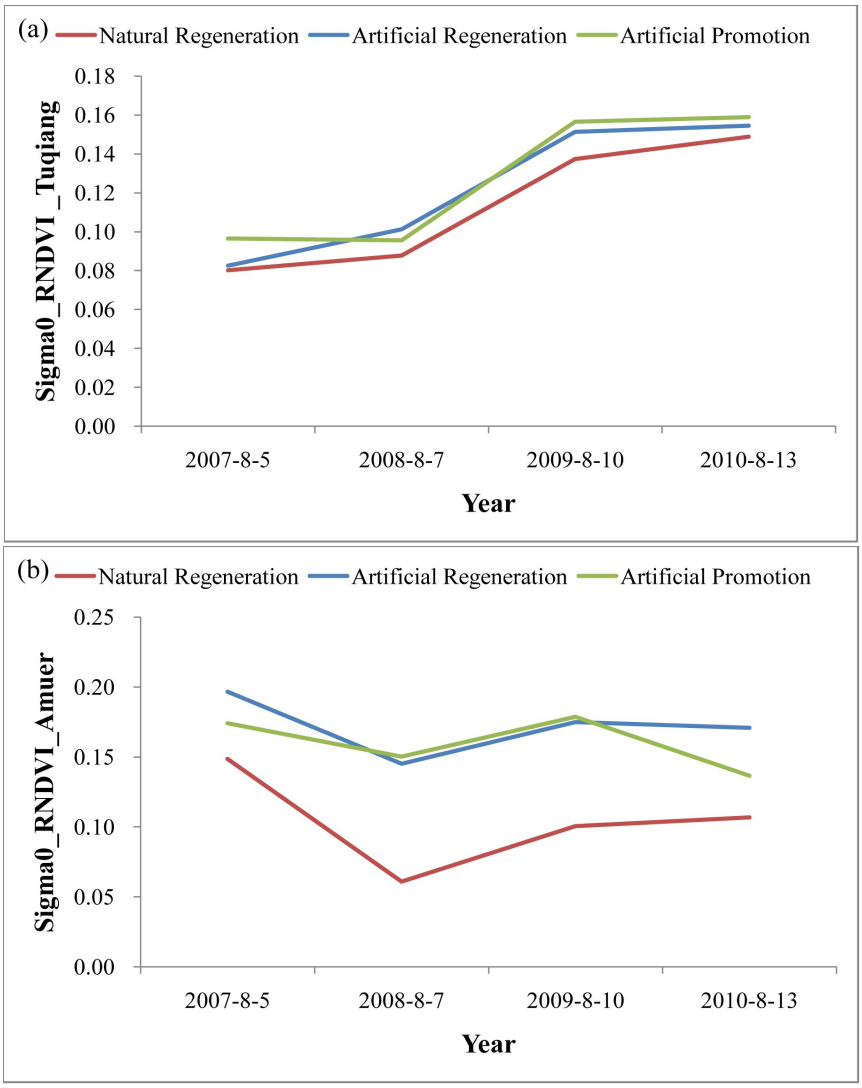

Figure 4.23 The comparison of backscattering coefficient ratio of RNDVI under different restoration treatments in the forestry bureau of (a) Tuqiang; (b) Amuer.

4.3.4 Discussion

4.3.4.1 Performance of different polarization modes

Similar with optical sensors, the polarization channels can be considered as the "spectral bands" of PALSAR, where the co-polarized (HH and VV) and cross-polarized (HV and VH) channels provide complementary characterization of the forest structures. The HH and VV signals typically interact with branches, stems and the ground layer (direct and specular backscatter), while the cross-polarized HV and VH backscatter generally are results of multiple scattering within the forest canopies (volume scattering) (Avtar *et al.*, 2012). In this study, by the comparison of ANOVA results, it was found that the Sigma0 in HV performed a little better than HH to discriminate the forest states under different treatments. Nevertheless, the analyses of Sigma0 in HH and HV polarization in this scenario of forest characterization gave the

similar results. This may due to the acquisition date of the PALSAR data, which was during 20+ years after the fire allowing a sufficient time for the forest to regenerate and thus resulting in a relatively intact forest structure. It is completely different from the situation of forest that immediately after a disturbance (e.g. fire, deforestation), especially a stand clearing event. Under that circumstance, there will be a sudden and considerable increase of Sigma0 in HH and decrease of Sigma0 in HV due to the absence of woody stems and large branches and presence of ground layer which could cause the increase of surface scattering and reduction of volume scattering (Isoguchi *et al.*, 2009; Mari *et al.*, 2012).

The backscatter intensity (Sigma0) in L-band SAR co-polarization (HH and VV) and cross-polarization (HV and VH) have been widely applied to estimate biophysical attributes, including biomass (Watanabe *et al.*, 2006; Mitchard *et al.*, 2009), tree foliage (Kobayashi *et al.*, 2012), tree height, DBH, and tree density (Suzuki *et al.*, 2013). A general and common finding is that the Sigma0 in HV exhibits a higher correlation with these filed measured parameters, especially with above-ground biomass than HH Sigma0. It also results from the comparatively higher sensitivity of Sigma0 in HV polarization to volume scattering.

In addition to the direct backscattering coefficients, polarimetric decomposition can provide more abundant components or variables to represent the physical characteristics of various targets and the corresponding scattering properties from them (Chowdhury *et al.*, 2013). The scattering mechanisms of even bounce, rotated dihedral and odd bounce from Pauli decomposition, the parameters of entropy (H), alpha angle (α) and anisotropy (A) from Cloude-Pottier decomposition (Cloude and Pottier, 1997), as well as the three components of even- or double-bounce scatter, canopy scatter and Bragg scatter from Freeman-Durden decomposition (Freeman and Durden, 1998) are typical polarimetric parameters which have been most widely used in forest identification and monitoring studies (Antropov *et al.*, 2011; Avtar *et al.*, 2012). However, all the polarimetric decompositions require quad-polarization (i.e. the whole collection of HH, HV, VH and VV) data. Due to the gap of the quad-polarization PALSAR data in the study area, the polarimetric decompositions cannot be conducted here to enable the forest identification.

4.3.4.2 Limitations and potential in future exploration

The forest structure is a dominant factor determining the forest backscatter intensity in this study. Additionally, radar backscattering signals can be affected by some other factors, with the most typical representatives of terrain and surface moisture conditions (Harrell *et al.*, 1995; Lucas *et al.*, 2010; Kasischke *et al.*, 2011b). In this case, the terrain effect has been greatly reduced by terrain correction, while the impact of surface moisture was not considered. It should be taken into account in future studies.

With the development of SAR technology, there is a new data collection and processing technique of Interferometric SAR (InSAR) which can also provide characterization of forest structural parameters by combining information of at least two complex-valued SAR images acquired from different orbit position or at different

times (Pinto *et al.*, 2013; Millin-Chalabi *et al.*, 2014). The interferometric coherence parameters (e.g. γ) can be used to estimate the similarity between two SAR images and are influenced by vegetation structure. Thus multiple PALSAR scenes covering the study area with appropriate baseline should be determined for the acquisition of interferometric coherence to retrieve the forest structural parameters, especially the tree height etc.

Considering that PALSAR is a L-band SAR sensor, and the SAR backscattering signals in different microwave bands will show varied properties, the combination use and comparison of L-band PALSAR with other SAR sensors (e.g. C-band ERS-2 and Envisat/ASAR) may give exciting results (Canisius and Fernandes, 2012; Tanase *et al.*, 2014). Because of the respective advantages of SAR and optical sensors, the synergy using of PALSAR data and optical imagery (e.g. AVNIR-2, Landsat) would be of particular interest and significance (Basuki *et al.*, 2013; Hoan *et al.*, 2013).

5 Performance evaluation and comparison

5.1 Introduction

With the development of remote sensing technology, a variety of satellites and sensors with different spatial, spectral and temporal resolutions have been developed rapidly, providing sufficient spatial and temporal coverage of high quality data at various scales. As a result, the potential of remote sensing techniques as a monitoring tool for forest ecosystem has been adequately recognized. Multi-source optical and SAR data have also been utilized to detect the forest disturbance and recovery under various circumstances (Tucker *et al.*, 2004; Wu and Peng, 2010; Bontemps *et al.*, 2012).

All remote sensing-based modeling are traditionally classified into two major categories: physical and statistical. Physical models follow the physical laws of the remote sensing systems and can be continuously improved by adding necessary knowledge. But it is usually difficult to make clear the physical mechanisms, and the appropriate models are potentially very complex. On the other hand, statistical models are based on correlation relationships between land surface measurements and remotely sensed variables. These models are usually site-limited; however, there are obvious advantages in terms of the conveniences for developing, effectiveness for calculations, and less demanding of input data (Liang, 2004).

In consideration of the limitations of specific physical models in data source and input variable requirements, the statistical modeling approaches are suited for various conditions due to their advantages (Rastmanesh *et al.*, 2010). Thus in this case, the simple linear regression model was determined for the performance evaluation and comparison among different optical sensors with varied resolution, as well as between optical and SAR data.

As introduced in chapter 3, LAI, as a crucial factor indicating the impacts of many biophysical processes (e.g. photosynthesis), has been regarded as an essential variable in terrestrial ecosystem monitoring, thus plays a key role in studies of many fields, including climate change, vegetation survey, as well as environment management (Chen *et al.*, 2010). It was selected as the field measured variable to be correlated with remote sensing spectral reflectance or transformations.

From the spectral characteristic of green vegetation which is a comprehensive reflection of its own biophysical features and environmental impacts, it is known that single-band reflectance can be used to establish regression models. However, as there are some differences in the wavelength range and bandwidth among different optical sensors, the direct comparison using single-band reflectance is not feasible and thus spectral indices should be derived and applied. As demonstrated in many studies, vegetation index (VI), a combination of single bands of remote sensing image, can be used as a simple, effective and experienced characterization of ground vegetation

states (Guo, 2003; Sharma *et al.*, 2013). Previous studies have shown that VI usually has a good correlation with a variety of physiological and ecological parameters of vegetation and thus be widely used to diagnose a range of vegetation biophysical parameters, including LAI, VFC, AGB etc (Chen and Cihlar, 1996; Xu *et al.*, 2010; Chen *et al.*, 2013). Therefore the VI was selected as remote sensing extracted variable to establish linear regression models.

In previous chapters, the remote sensing data of Landsat TM/ETM+, MODIS and ALOS PALSAR in time series had been used for the fire effect detection and forest recovery monitoring after the "5.6 Fire". As shown, these data possess considerably different temporal coverage and spatial resolution, and hence gave quite different performances. In order to make the performance evaluation and comparison among various sensors more direct and to the point, in this study, the linear statistical modeling was applied using field measured LAI values and remote sensing indices from ALOS AVNIR-2, Landsat-5 TM and MODIS NBAR, ALOS PALSAR data. These data was acquired at the relatively close dates in the year 2010. During the modeling, six diverse optical vegetation indices were selected for the evaluation and comparison among the three optical sensors, and two radar indices characterized by similar expression as the corresponding optical indices were determined for the comparison between optical and SAR sensors. The results seemed normal and natural which requiring further exploration and verification.

5.2 Data and Methods

5.2.1 Remote sensing and field survey data

In order to investigate and compare the accuracy of optical remote sensing data with different spatial resolution, here the multi-source optical images of ALOS AVNIR-2, Landsat TM/ETM+ and MODIS were selected for the comparative study. As described in Table 5.1, ALOS AVNIR-2 provides 10 m spatial resolution images with a repeat cycle of 46 days, while Landsat-5 TM possesses a spatial resolution of 30 m and temporal revisit cycle of 16 days, and MODIS aboard on Terra and Aqua satellites are together viewing the entire Earth's surface every 1 to 2 days, acquiring data in 36 spectral bands with ground resolutions of 250/500/1000 m. As these optical sensors have different main objectives and thus show their specific advantages in different fields, for more targeted research, the retrieval of LAI was focused and the same simple inversion method of statistical regression modeling was chosen for the comparative study. Considering data temporal coverage in the study area, we determined the year of 2010 as the time window of the three types of images.

The ALOS AVNIR-2 image was acquired on September 4th, 2010, and the Landsat-5 TM data was acquired on September 2nd, 2010. To keep the consistency in acquisition date as much as possible, the MODIS products of Nadir BRDF-Adjusted Reflectance data (NBAR, MCD43A4) covering August 29th-September 13th (from

Julian Day of 241) was used. A superimposed map of the three scenes from AVNIR-2, Landsat-5 TM and MODIS was shown in Fig. 5.1.

The LAI data collected in the field forest survey conducted in July 2012 were utilized to build the regression models and evaluate their accuracies. The difference of post-fire forest restoration treatments existed in the field sampling plots was not taken into consideration since there would be no sufficient data to conduct the modeling if considered. Although there is a gap between the remote sensing image acquisition date and field data sampling time, the research can still be conducted as the main objective is focused on the comparison of the performance of different optical sensors.

Table 5.1 Radiometric characteristics of ALOS AVNIR-2, Landsat-5 TM and MODIS NBAR data.

Satellite	Sensor	Bands	Wavelength range (μm)	Spatial resolution (m)	Swath width (km)	Repeat cycle (days)
ALOS	AVNIR-2	1	0.42 – 0.50	10 (at Nadir)	70 (at Nadir)	46
		2	0.52 – 0.60			
		3	0.61 – 0.69			
		4	0.76 – 0.89			
Landsat-5	TM	1	0.45 – 0.52	30	185	16
		2	0.52 – 0.60			
		3	0.63 – 0.69			
		4	0.76 – 0.90			
		5	1.55 – 1.75			
		6	10.4 – 12.5	120		
		7	2.08 – 2.35	30		
Terra/Aqua	MODIS	1	0.620 – 0.670	250	2330 (cross track)	1-2
		2	0.841 – 0.876			
		3	0.459 – 0.479	500		
		4	0.545 – 0.565			
		5	1.230 – 1.250			
		6	1.628 – 1.652			
		7	2.105 – 2.155			

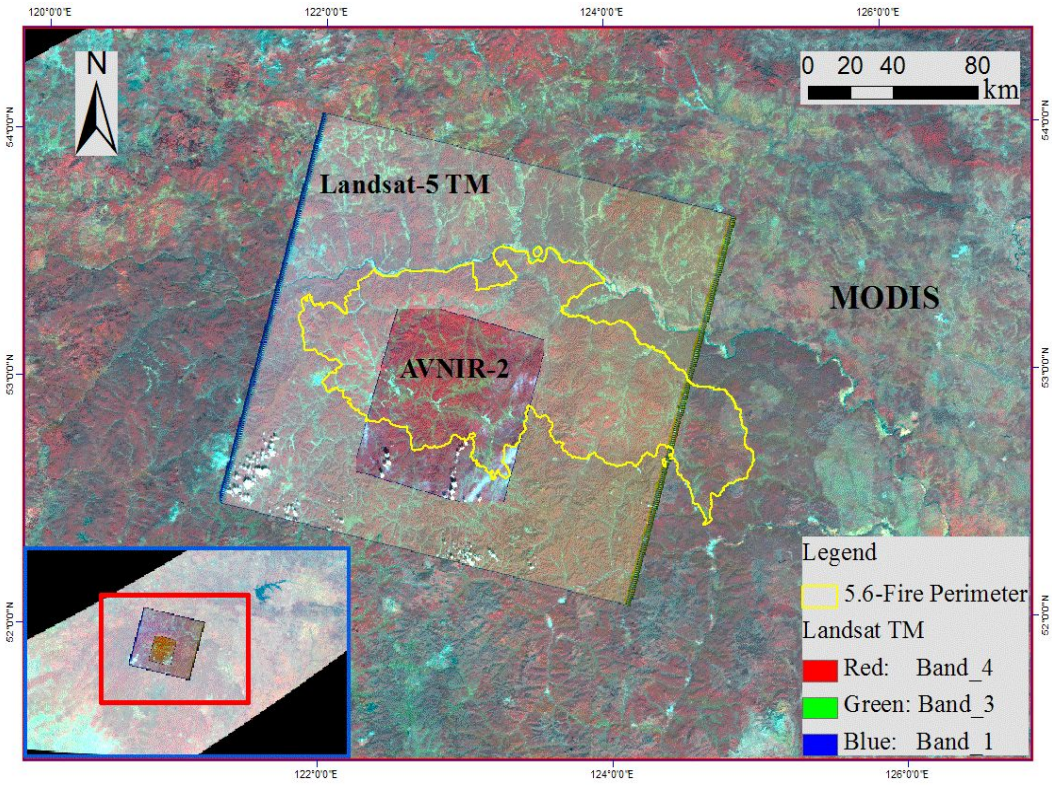

Figure 5.1 A superimposed map of three scenes from ALOS AVNIR-2, Landsat-5 TM and MODIS.

Regarding the performance evaluation and comparison between optical and SAR sensors, it seems very difficult due to their totally different physical mechanisms and the subsequent advantages. In order to minimize the unwanted effects of other uncontrollable factors, the optical sensor of AVNIR-2 and radar sensor of PALSAR aboard the same satellite of ALOS was determined for comparison. Considering the acquisition date of AVNIR-2 image, the PALSAR data was acquired on August 13th, 2010 which had already been used for the time series monitoring of forest dynamics in chapter 4.3. The same approach of linear regression modeling was adopted using the same collection of field measured LAI values. The AVNIR-2 and PALSAR images have the same spatial resolution of 10 m which just corresponds to the size of field sampling plots. This greatly facilitates the effective comparison. A superimposed map of the two images from ALOS AVNIR-2 and PALSAR was shown in Fig. 5.2.

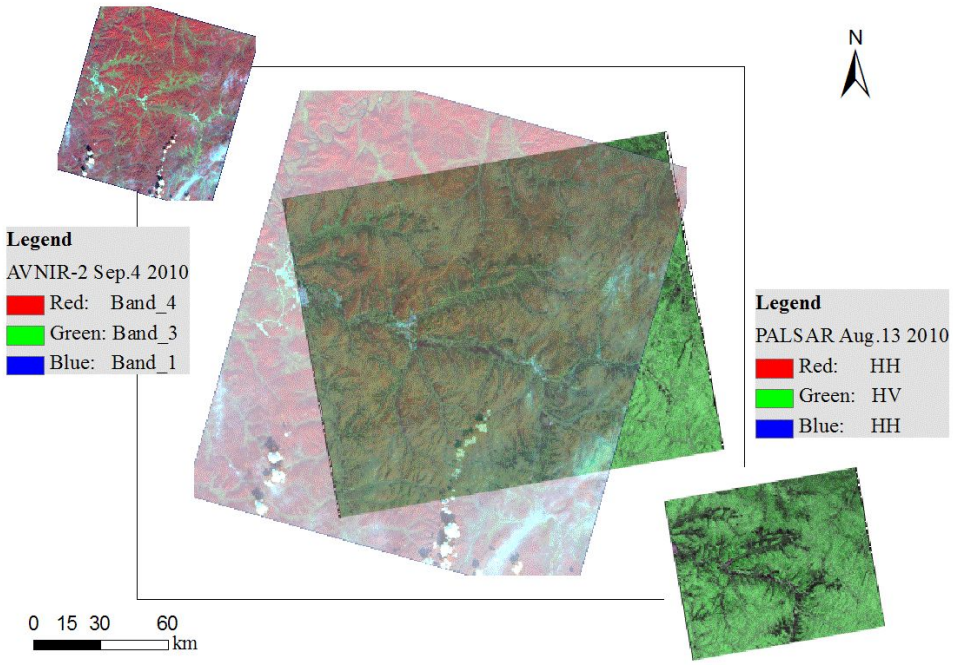

Figure 5.2 A superimposed map of two images from the optical sensor of AVNIR-2 and radar sensor of PALSAR aboard ALOS. For the overlap image in the middle, there is a transparency of 50%.

5.2.2 Data pre-processing

The ALOS AVNIR-2 and Landsat-5 TM images were pre-processed by geometric correction, orthorectification, radiometric calibration as well as atmospheric correction, respectively, after which, the surface reflectance of the study area was acquired. As the field sampling plots were located in the mountainous area with undulating terrain, the terrain correction was performed using ASTER GDEM data. The MODIS NBAR data has already standardized reflectance to a nadir view, thus minimizing artifacts in the sample related to variable geometry. Additionally, the NBAR spectral bands are comparable to those of Landsat TM, as summarized in Table 5.1. The ALOS PALSAR data had already been pre-processed following the flow chart shown in Fig. 4.17.

Since the ALOS AVNIR-2 and PALSAR imagery, Landsat-5 TM and MODIS NBAR data have totally different spatial resolutions of 10 m, 30 m and 500 m, respectively, while the LAI data were acquired from field survey sampling plots with size of 10×10 m, the images of Landsat-5 TM and MODIS NBAR were resampled to 10 m to make the spectral values extracted from optical images or backscattering coefficients from SAR data corresponding in spatial scale with the measured LAI values.

5.2.3 Multivariate selection and calculation

Based on the acquisition of pre-processed remote sensing images and the field measured LAI, we were able to carry out modeling. In this study, when establishing the relationships between optical vegetation indices (VIs) and field measured LAI, the impacts of soil background and atmosphere were considered and hence six indices were finally selected and statistically correlated to field measured LAI values. They are Ratio Vegetation Index (RVI) (Pearson and Miller, 1972), Difference Vegetation Index (DVI) (Jordan, 1969), NDVI (Rouse *et al.*, 1974), Soil-Adjusted Vegetation Index (SAVI) (Huete, 1988), Atmospherically Resistant Vegetation Index (ARVI) (Kaufman and Tanre, 1992) and EVI (Liu and Huete, 1995; Huete *et al.*, 1997), which are expressed as equation (5-1) to (5-6).

$$RVI = \frac{\rho_{NIR}}{\rho_{\mathrm{Re}d}} \tag{5-1}$$

$$DVI = \rho_{NIR} - \rho_{\mathrm{Re}d} \tag{5-2}$$

$$NDVI = \frac{(\rho_{NIR} - \rho_{\mathrm{Re}d})}{(\rho_{NIR} + \rho_{\mathrm{Re}d})} \tag{5-3}$$

$$SAVI = \frac{(1+L_1)\cdot(\rho_{NIR} - \rho_{\mathrm{Re}d})}{\rho_{NIR} + \rho_{\mathrm{Re}d} + L_1} \tag{5-4}$$

$$ARVI = \frac{(\rho_{NIR} - \rho_{RB})}{(\rho_{NIR} + \rho_{RB})} \tag{5-5}$$

$$EVI = \frac{2.5\cdot(\rho_{NIR} - \rho_{\mathrm{Re}d})}{\rho_{NIR} + c_1\cdot\rho_{\mathrm{Re}d} - c_2\cdot\rho_{Blue} + L_2} \tag{5-6}$$

where ρ_{NIR}, $\rho_{\mathrm{Re}d}$ and ρ_{Blue} denote the reflectance of the near-infrared, red and blue bands, respectively. Then $\rho_{RB} = \rho_{\mathrm{Re}d} - \gamma(\rho_{Blue} - \rho_{\mathrm{Re}d})$ and γ which indicating the radiation correction coefficient of optical path is assumed to the recommended value (by Kaufman) of 1. The parameter L_1 in Equation (5-4) indicates a soil adjusted coefficient which is normally assumed to be 0.5 for most regions. In Equation (5-6), we set c_1 =6.0, c_2 =7.5 and L_2 =1 which have been used in the acquisition of MODIS product.

To maintain consistency, the radar indices of RRVI and RNDVI, introduced in chapter 4.3, were utilized to conduct the linear regression modeling using PALSAR data. The expression of the two indices had been shown in equation (4-1) and (4-2).

After calculating the six optical VIs and two radar VIs, Pearson correlation analysis was performed. With those showing significant correlations, statistical regression models were established and ANOVA was conducted (Table 5.2).

5.3 Results

5.3.1 Univariate modeling using optical VIs

5.3.1.1 Based on ALOS AVNIR-2 data

Since the burned forest area is too large to be covered within one scene of ANVIR-2 image which possesses a swath width of 70 km (at Nadir), the AVNIR-2 data used here has a coverage over only the two forestry bureaus of Tuqiang and Amuer (the same as PALSAR data used in chapter 4.3), thus only totally 18 LAI sampling values can be utilized to establish the regression models. The modeling results were shown in Table 5.2(a) and Fig. 5.3. As expressed in the table, the correlation coefficient ($R > 0.7$) and determination coefficient ($R^2 > 0.5$) were all quite high and the Standard Error of the Estimate (SEE) was particularly little. The significant probability (Sig. < 0.01) indicated the validity and efficiency of these models. Among the six VIs, RVI which achieved the highest R (0.893) and R^2 (0.798) performed best, followed by ARVI ($R^2 = 0.718$) and NDVI ($R^2 = 0.652$). The regression model based on DVI had the lowest correlation.

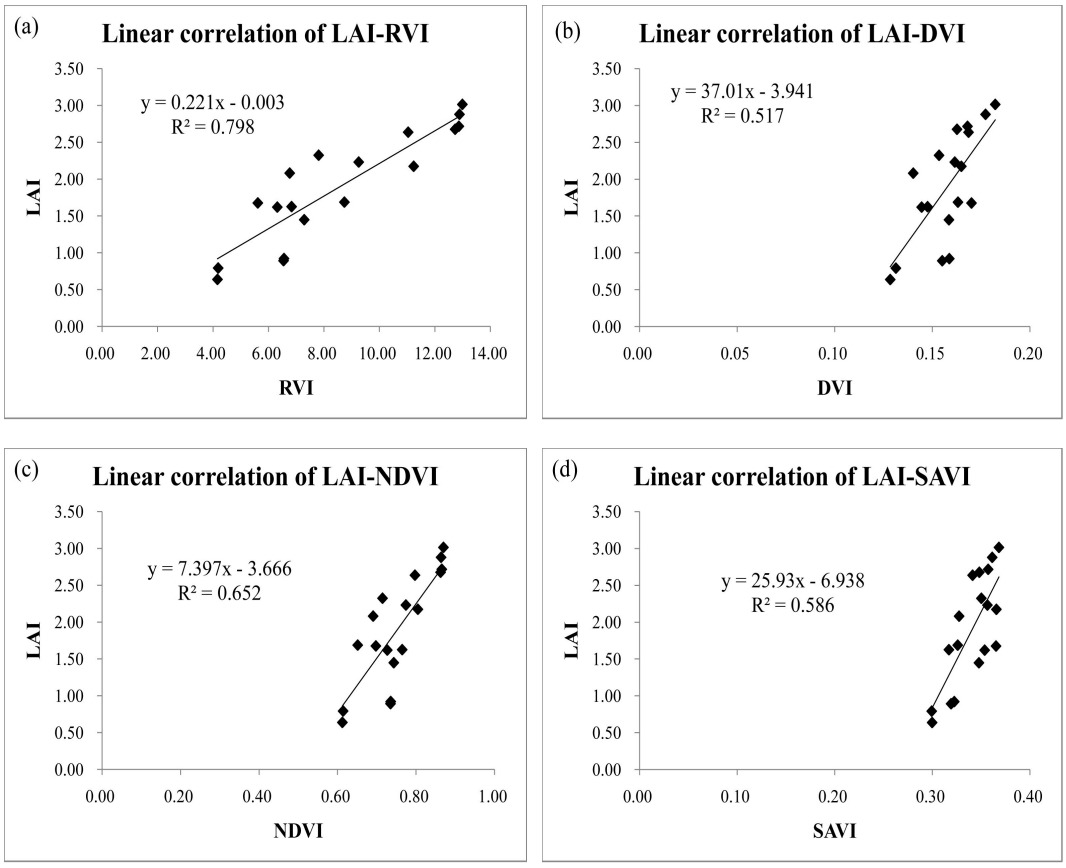

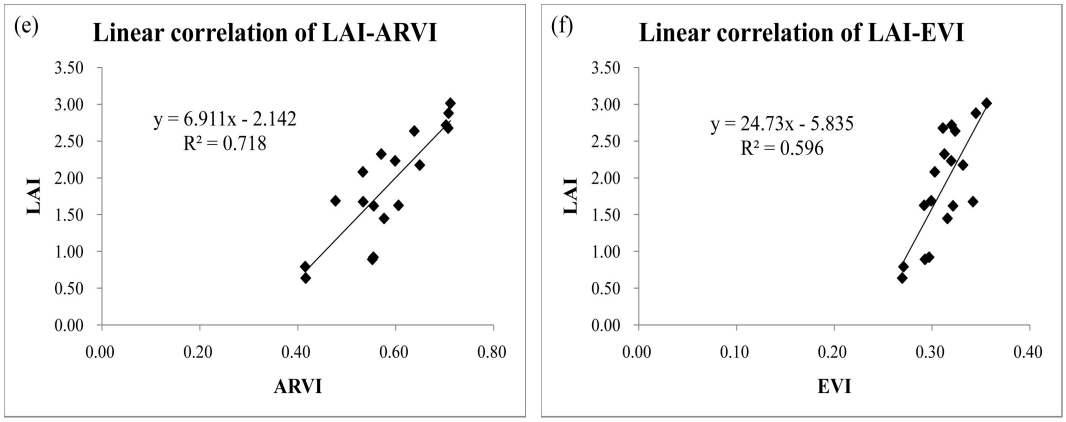

Figure 5.3 The linear regression models based on LAI and ALOS AVNIR-2 derived vegetation indices: (a) RVI; (b) DVI; (c) NDVI; (d) SAVI; (e) ARVI and (f) EVI.

5.3.1.2 Based on Landsat-5 TM data

The Landsat-5 TM covered all the 27 field forest survey plots which located in the three forestry bureaus of Xilinji, Tuqiang and Amuer, however, considering the situation of AVNIR-2-based modeling, the same 18 plot values from Tuqiang and Amuer were selected for correlation analysis to enable comparative studies. Based on the six VIs derived from TM, we established the linear models which were shown in Fig. 5.4. The model summary and ANOVA result were shown in Table 5.2(b), from which it could be conclude that the six VIs were also extremely significant and could be used to estimate the regional LAI individually (Sig. < 0.01).

Among the six VIs, it was still RVI that had the highest linear correlation with field measured LAI and simultaneously, DVI showed the least correlation. Compared to those from AVNIR-2-based VIs, the linear models established using TM-based VIs gave a worse performance which was characterized by lower R and R^2 as well as higher SEE. This may be due to the effect of spatial resolution. The inconsistency between the spatial resolution (30 m) and the size of field plots (10 m) can account for the reduced accuracy.

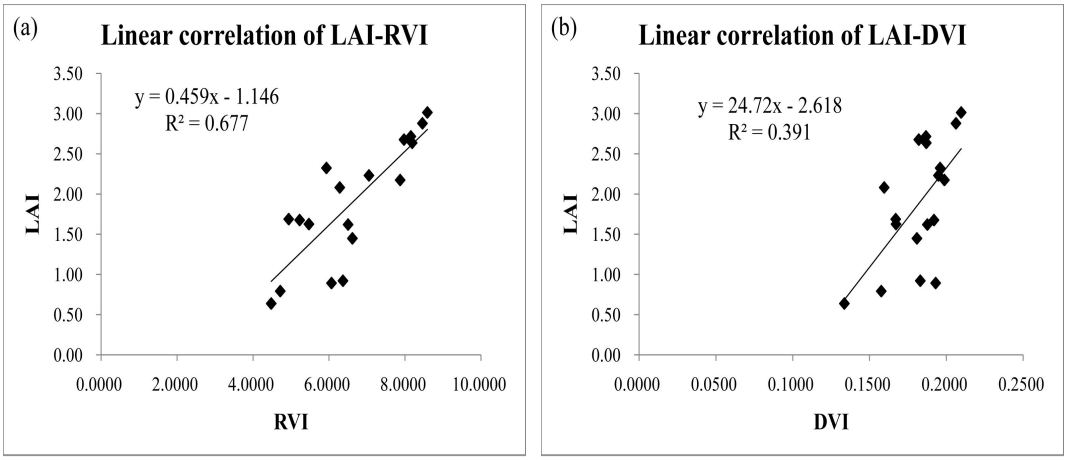

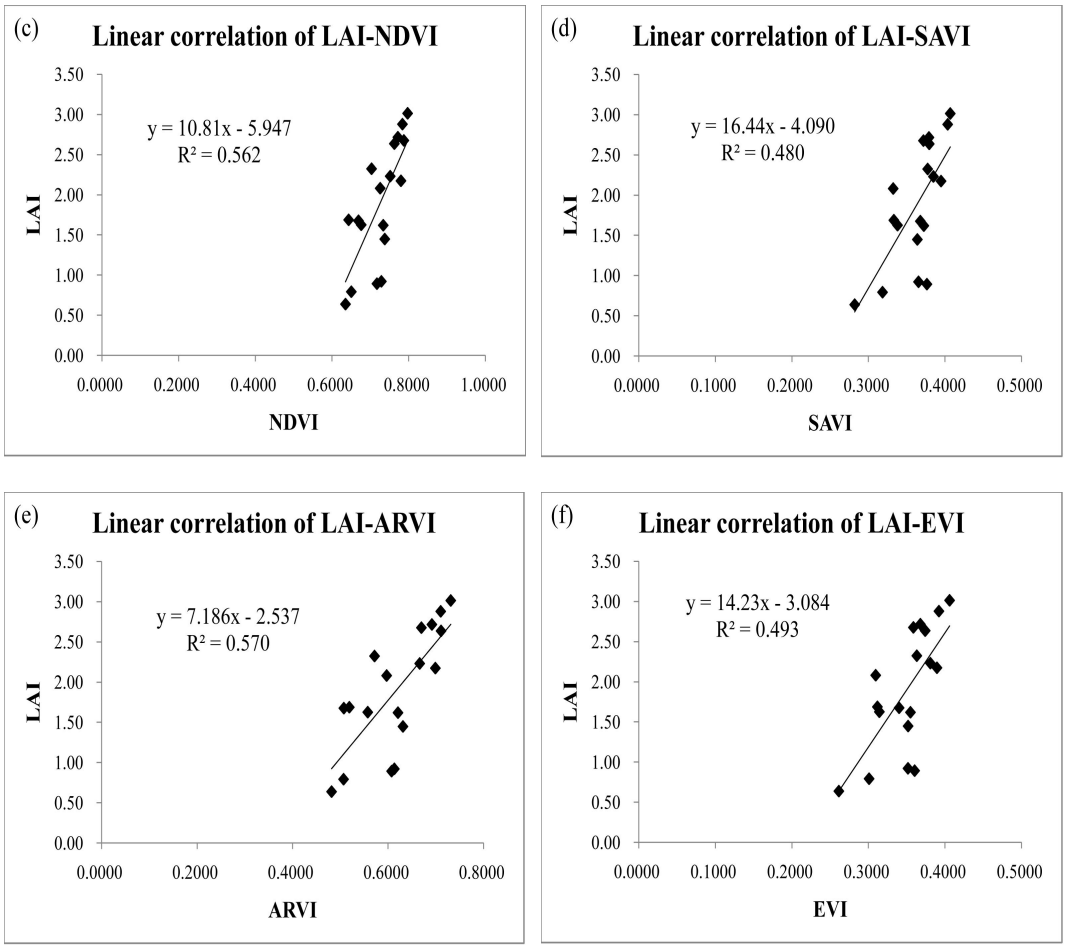

Figure 5.4 The linear regression models based on LAI and Landsat-5 TM derived vegetation indices: (a) RVI; (b) DVI; (c) NDVI; (d) SAVI; (e) ARVI and (f) EVI.

5.3.1.3 Based on MODIS NBAR data

Due to the broad swath width of up to 2330 km of MODIS sensor, the whole burned area (fire scar) including all field survey plots was within the MODIS coverage of one scene (h25v03). However, because of the low spatial resolution of the MODIS NBAR data (500 m) and relatively close distance between some plots, some two or even three field plots, especially those under the same restoration treatments, were within one MODIS pixel, and hence only 12 groups of LAI data could be identified in the MODIS image. For those gathered in the same pixels, the average LAI value was calculated to be correlated with corresponding VIs extracted from the image.

The linear correlation and modeling results were shown in Table 5.2(c) and Fig. 5.5 from which we found that the regression models based on VIs from MODIS NBAR were also significant (Sig. < 0.05). RVI still achieved the highest linear correlation with measured and partly averaged LAI while DVI showed the least. Compared with the results from AVNIR-2 and TM, the correlations were overall much lower and the SEE were much higher. It probably due to the reduction of the number of sample

points and the increase of inconsistency between the spatial resolution (500 m) and field plot size.

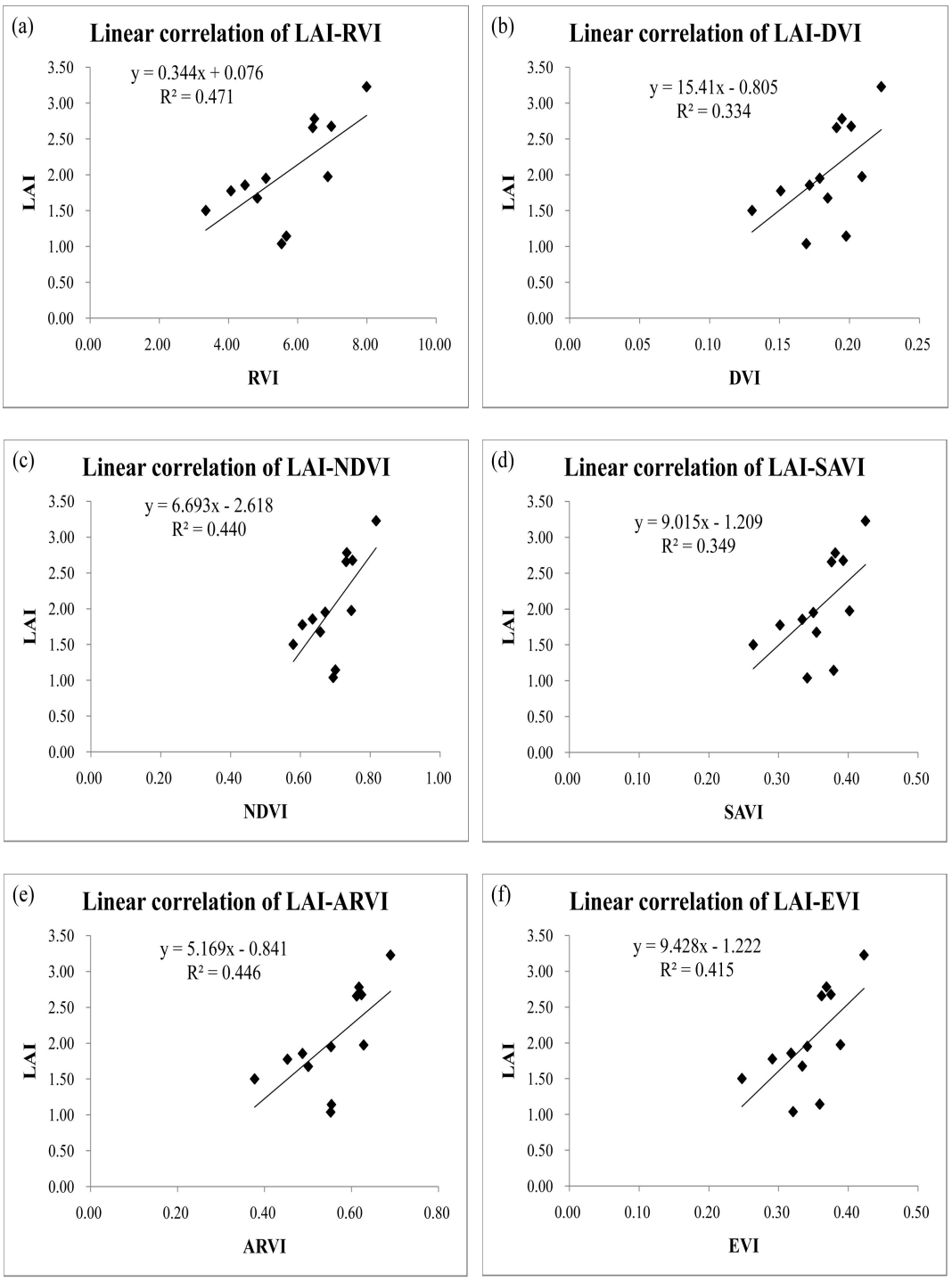

Figure 5.5 The linear regression models based on LAI and MODIS NBAR derived vegetation indices: (a) RVI; (b) DVI; (c) NDVI; (d) SAVI; (e) ARVI and (f) EVI.

Table 5.2 The model summary and ANOVA of single-VI-based models. The VIs were derived from (a) ALOS AVNIR-2; (b) Landsat-5 TM; (c) MODIS NBAR; (d) ALOS PALSAR data.

Independent variables [a]	R	R^2	SEE [b]	F statistics	Sig.
(a) ALOS AVNIR-2					
RVI	0.893	0.798	0.349	63.318	0.000**
DVI	0.720	0.517	0.539	17.186	0.001**
NDVI	0.808	0.652	0.458	29.987	0.000**
SAVI	0.766	0.586	0.499	22.733	0.000**
ARVI	0.848	0.718	0.412	40.853	0.000**
EVI	0.773	0.596	0.493	23.685	0.000**
(b) Landsat-5 TM					
RVI	0.823	0.677	0.441	33.585	0.000**
DVI	0.625	0.391	0.606	10.279	0.006**
NDVI	0.750	0.562	0.513	20.567	0.000**
SAVI	0.693	0.480	0.560	14.783	0.001**
ARVI	0.756	0.570	0.509	21.281	0.000**
EVI	0.702	0.493	0.553	15.538	0.001**
(c) MODIS NBAR					
RVI	0.687	0.471	0.518	8.920	0.014*
DVI	0.578	0.334	0.582	5.019	0.049*
NDVI	0.664	0.440	0.533	7.879	0.019*
SAVI	0.591	0.349	0.575	5.373	0.043*
ARVI	0.668	0.446	0.531	8.051	0.018*
EVI	0.644	0.415	0.545	7.094	0.024*
(d) ALOS PALSAR					
RRVI	0.834	0.695	0.429	36.465	0.000**
RNDVI	0.833	0.694	0.429	36.380	0.000**

[a] Independent variables include constant; Dependent variable is measured LAI.

[b] SEE: Standard Error of the Estimate.

* Significant correlation (0.01 < Sig. <= 0.05).

**Extremely significant correlation (Sig. <= 0.01).

The same as below.

5.3.2 Multiple-variable-based modeling

All above linear models are single-VI-based; however, multiple-variable-based models usually achieve a higher modeling accuracy and a lower error. Thus stepwise regression analysis was conducted to build empirical models for the LAI retrieval in SPSS 18.0, using the whole collection of all six VIs as the input independent variables. The stepwise regression analysis can automatically select the most significant variable(s) and produce the "best" regression model(s). The probability of F test in the model was set for variables to enter at <= 0.05 while to remove at >= 0.10. The modes outputted by this stepwise regression were shown in Table 5.3.

From this table, it was found that only partial variables (VIs) entered the multiple regression models, while most were removed due to insignificant impact or collinearity between variables. For VI calculated from different optical sensors, those entered the final models differed. For example, there were two multiple regression models produced when inputting VIs from ALOS AVNIR-2. RVI which having highest correlation with measured LAI entered both, and EVI was the other variable included in the second model. When taking the TM-based VIs as inputs, it would also produce two multiple regression models which were similar to those of AVNIR-2. The only difference lay in the replacement of EVI by ARVI. For the MODIS NBAR data, the output of stepwise regression analysis under the criteria setting was a form of univariate model. Compared with single-VI-based models, especially for AVNIR-2 and Landsat-5 TM, the multiple-VIs-based models showed higher accuracies and lower errors. Comparison of accuracies of the multiple regression models among the three optical sensors gave the same conclusion as that in univariate modeling analysis.

Table 5.3 The model summary and ANOVA of stepwise multiple-VIs-based model. The VIs were derived from (a) ALOS AVNIR-2; (b) Landsat-5 TM; (c) MODIS NBAR; (d) ALOS PALSAR data.

Independent variables [a]	R	R^2	SEE [b]	F statistics	Sig.
(a) ALOS AVNIR-2					
RVI	0.893	0.798	0.349	63.318	0.000**
RVI, EVI	0.921	0.849	0.311	42.193	0.000**
(b) Landsat-5 TM					
RVI	0.823	0.677	0.441	33.585	0.000**
RVI, ARVI	0.871	0.758	0.394	23.488	0.000**
(c) MODIS NBAR					
RVI	0.687	0.471	0.518	8.920	0.014*
(d) ALOS PALSAR					
RRVI	0.834	0.695	0.429	36.465	0.000**

5.3.3 Comparison of correlation between VIs

Since most vegetation indices rely on the spectral signatures of the same blue, red and near-infrared bands of one optical image, typically they had a strong correlation between one another. The result of stepwise regression analysis is a reflection of this autocorrelation to some extent. When building the linear regression models using the six VIs individually, some always performed better than the others. To explore and compare the correlation among VIs, the Pearson correlation was performed and the coefficients between any two of the six VIs derived from ALOS AVNIR-2, Landsat-5 TM and MODIS NBAR data were calculated (Table 5.4).

In this table, the figures in bold type indicated relatively high correlation. By summarizing and comparison within each sensor, it can be apparently found that RVI, NDVI, and ARVI formed one group, within which, a high correlation between each other can be achieved. Similarly, the remaining three indices of DVI, SAVI, and EVI also showed a relatively high correlation with each other and hence gathered into another group. However, when referring to their correlations with field measured LAI shown in Table 5.2, the two groups had completely different performance. The group consisting of RVI, NDVI, and ARVI always gave higher R^2 and lower SEE than those from the other group regardless of the data source.

Comparison among the three sensors showed that the absolute values of correlation among VIs were largely affected by the data source. The fact that those of MODIS were higher than TM, and that AVNIR-2 produced the lowest correlation revealed that an image with lower spatial resolution normally resulted in higher correlations between the same two indices. Based on optical data with varied spatial resolution, the difference in correlation within and between the two separated groups of VIs also differed. This reflected the significance of the data source in a way.

Table 5.4 The Pearson correlation coefficients between any two of the six vegetation indices from (a) ALOS AVNIR-2; (b) Landsat-5 TM; (c) MODIS NBAR data.

VI	RVI	DVI	NDVI	SAVI	ARVI	EVI
(a) ALOS AVNIR-2						
RVI	1					
DVI	0.794**	1				
NDVI	**0.903****	0.768**	1			
SAVI	0.677**	**0.805****	0.705**	1		
ARVI	**0.905****	0.775**	**0.973****	0.739**	1	
EVI	0.680**	**0.855****	0.708**	**0.948****	0.739**	1
(b) Landsat-5 TM						
RVI	1					
DVI	0.709**	1				
NDVI	**0.975****	0.725**	1			
SAVI	0.816**	**0.984****	0.830**	1		
ARVI	**0.982****	0.720**	**0.974****	0.826**	1	
EVI	0.854**	**0.961****	0.864**	**0.989****	0.873**	1
(c) MODIS NBAR						
RVI	1					
DVI	0.930**	1				
NDVI	**0.996****	0.934**	1			
SAVI	0.953**	**0.996****	0.955**	1		
ARVI	**0.983****	0.936**	**0.983****	0.961**	1	
EVI	0.958**	**0.991****	0.960**	**0.994****	0.968**	1

5.3.4 Comparison with PALSAR indices

As PALSAR is aboard the same satellite of ALOS with AVNIR-2, they have the same spatial coverage over the two forestry bureaus of Tuqiang and Amuer, the same 18 LAI sampling values were utilized to establish the linear regression models based on the two radar indices of RRVI and RNDVI. The modeling results were shown in Table 5.2(d) and Fig. 5.6. As shown, the correlation coefficient and determination coefficient were both high (R^2 = 0.695 for RRVI and 0.694 for RNDVI). The significant probability represented the efficiency of the modeling. Compared to the results obtained in AVNIR-2 based linear regression modeling using the indices of RVI (R^2 = 0.798) and NDVI (R^2 = 0.652), there was no significant difference between them.

Through the Pearson correlation between the two indices, a strong collinearity was found (R = 0.998). Thus only one variable was included when multiple-variable stepwise regression analysis was performed (Table 5.3(d)).

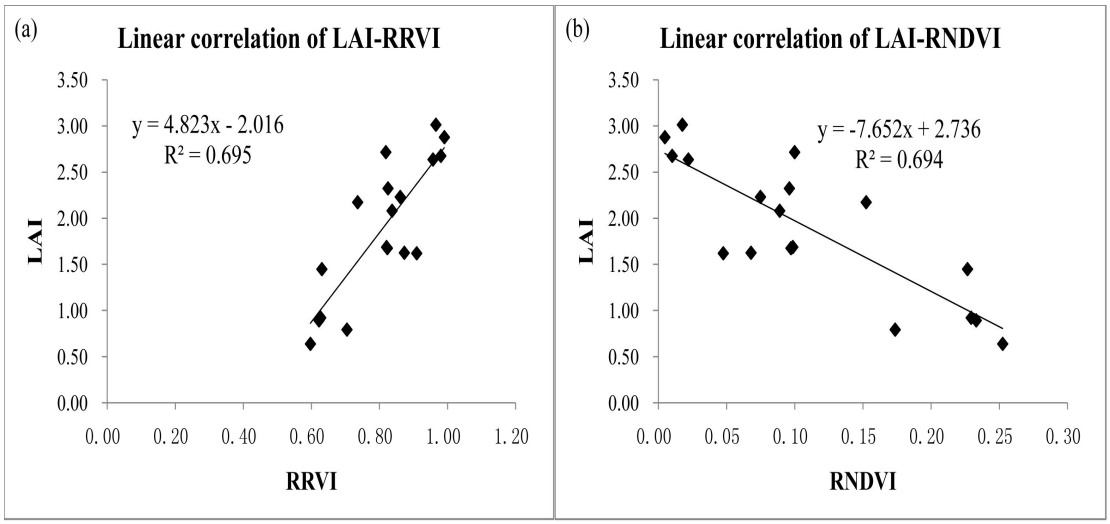

Figure 5.6 The linear regression models based on LAI and ALOS PALSAR derived vegetation indices: (a) RRVI; (b) RNDVI.

5.4 Discussion

5.4.1 Data features and performance evaluation

Due to limitations of energy supply and memory size of sensors onboard satellites, normally there is a negative correlation between swath width and spatial resolution. Furthermore, smaller swath width and higher spatial resolution will together lead to longer revisit cycle (Table 5.1). Typically data with higher spatial resolution need higher acquisition costs, thus leading to higher prices (Table 5.5).

Table 5.5 Comparison of data characteristics and accuracy of LAI retrieval among ALOS AVNIR-2, Landsat-5 TM, MODIS NBAR and ALOS PALSAR.

Data type	Spatial resolution (m)	Temporal resolution (days)	Retrieval accuracy	Data costs (/scene)
ALOS AVNIR-2	10	46	High	Standard products: 50,000 JPY
Landsat-5 TM	30	16	Medium	Partly free; Archive: 25/50; New: 450/600 USD
MODIS NBAR	500	1-2	Low	All free
ALOS PALSAR	10	46	Medium -High	Standard products: 50,000 JPY

The spatial resolution determined the accuracy of LAI retrieval in this study. The results indicated that the higher spatial resolution, the higher the accuracy. In consideration of the higher costs of remote sensing data with higher spatial resolution, the actual needs and accuracy requirements should be fully evaluated, while the funding support may also be carefully considered to achieve a most cost-efficient result with a balance between accuracy and cost.

Normally, lower spatial resolution will result in higher spatial heterogeneity within each pixel. Resampling of remote sensing images from low to high spatial resolution produces no effect on actual resolution. Thus the inconsistency between the spatial resolution (30 m, 500 m) and the size of field plots (10 m) can substantially account for the reduced accuracy. This conclusion appears to be normal, reasonable and in line with general expectation. Anyhow, this unsurprising result is a well reflection and demonstration of the influence of scale matching in studies combining remote sensing technique with field measurements.

Because of the physical mechanisms of optical and radar remote sensing systems, the optical sensors are well suitable for capturing horizontally distributed characteristics and changes represented by spectral signatures, while the SAR are reasonably advantageous for the characterization of vertical features. LAI is such a basic and crucial characterization of forest attributes, both horizontally and vertically, serves as a key input variable of a large number of ecological and physiological models and attracts much attention. This study revealed a satisfactory accuracy in LAI retrieval based on linear statistical modeling using both optical and SAR data. Nevertheless, it is believed that comparatively higher accuracy will be achieved when using biomass data to correlate with SAR derived variables for statistical modeling (Watanabe *et al.*, 2006; Mitchard *et al.*, 2009; Basuki *et al.*, 2013). It is due to the deep penetration of microwave signals into forest canopy and the subsequent interaction with not only leaves, but branches and trunks. Compared to LAI,

above-ground biomass can better characterize this complex interaction and correlate with backscatter intensity or derived indices more closely, especially for the cross-polarization (Kobayashi *et al.*, 2012; Suzuki *et al.*, 2013).

5.4.2 Future-oriented points for improvements

Although some positive results have been obtained in this scenario, there are many aspects which could be discussed and improved.

First, there were only 18 sample plots used for regression modeling because of the hot weather and hard sampling conditions in the forests in the Greater Hinggan Mountain area. There is no doubt that more sample plots should be investigated for both modeling and validation in future work.

Additionally, it should be admitted that generally the application of statistical regression models are restricted to a specific study area with certain environmental conditions (e.g. topography, climate, vegetation species), thus it is necessary to adjust the coefficients for other regions or build physical models which represent the abstract of common circumstances. In this way, the issues of the models or algorithms should be taken into account when conducting the comparison of performance between sensors with different resolutions.

Finally, the optical image used in this study is only the multispectral data with varied spectral and spatial resolution. The SAR data comes from the L-band PALSAR sensor alone. In future exploration, we need to try other types of data, including hyperspectral imagery (e.g. Hyperion), other active remote sensing data (e.g. LiDAR, X-band and C-band SAR) and explore their potential for the estimation of LAI as well as other ecological parameters. In addition, the synergic application combining optical images with LiDAR or SAR data simultaneously can be considered.

6 Synthesis

This thesis represents a typical case of the fire disturbance detection and post-fire forest recovery monitoring based on remote sensing and field survey data. In addition to the data from conventional field measurements, multi-source remote sensing data from both optical and SAR sensors were utilized and a variety of indices or models were applied. The performances of remote sensors with variable characteristics were further evaluated and compared. In this chapter, the knowledge gained throughout this work is summarized, and limitations existed within this exercise has also been identified, based on which, the orientation with regard to future studies are discussed and recommended.

6.1 Research summarization

Identification and monitoring of human-induced and natural disturbances is an important global and regional application, where updated information about where disturbances have occurred, when they occurred, and the area affected, is crucial. As many forest ecosystems are under threat of anthropogenic change, the capacity to monitor such areas on a regular basis regardless of accessibility is of key importance. Traditional ground-based measurements of forest dynamics, which are implemented mainly through plot survey or digital photograph visualization, seem relatively subjective, expensive, time consuming and labor intensive, and thus appear unrealistic for the monitoring of the whole forest ecosystems in long-term and wide-range.

As an alternative, the advanced technique of remote sensing, which are greatly developed and widely applied in a variety of fields, have been proven effective to provide systematic, repetitive and comprehensive observations at scales from local, continental to global. Multi-source and time series remote sensing data provide a simple, but effective means for disturbance detection, yielding a clear indication of both the temporal and spatial characteristics of the disturbance and recovery.

Forest disturbance and recovery have been regarded as a primary mechanism for transferring carbon between land surface and atmosphere, and thus plays a key role in the terrestrial carbon balance (Frolking *et al.*, 2009; Schroeder *et al.*, 2011). Fire is one of the common disturbance regimes, especially in boreal forests. It is a complex issue, both ecologically and socially, affecting the forest ecological process either as a positive agent of renewal or a highly destructive force (Chu and Guo, 2014).

Fire effects and post-fire forest dynamics have been widely studied in boreal forests. A wide range of such studies are based on field forest investigation alone (Schulze *et al.*, 2005; Moreira *et al.*, 2009; Hollingsworth *et al.*, 2013), while more and more researchers and managers are combining field survey data with remote sensing imagery, such as the Landsat, MODIS, SPOT, SAR records, to monitor post-fire forest patterns due to their temporal coverage, sufficient spatial and spectral resolutions which enable capturing of most forest features (Bourgeau-Chavez *et al.*, 1997; Schroeder *et al.*, 2012; Matricardi *et al.*, 2013).

The Greater Hinggan Mountain area, located in the northeast China, is rich in forest resources while suffers from a high incidence of forest fires simultaneously. Among all the fires in this area, the most noteworthy one is the “5.6 Fire” that broke out on May 6 1987 and developed to be the most serious forest fire hazard in the history of P. R. China, causing tremendous damage to the forest ecosystems. Aiming at this severe fire, this thesis proposes to detect the fire scar and burned forest area, and monitor the post-fire forest recovery using field survey records and multi-source optical and SAR data. Particular emphasis has been given to the effects of different restoration strategies on post-fire forest regeneration and vegetation recovery patterns.

First of all, the fire scar and burned forest area was extracted and mapped using Landsat TM imagery by multiple methods. During the mapping, the fire perimeter, as well as rivers, roads and building areas were first delineated and masked by visual interpretation, and then four indices of NDVI, EVI, VFC and DI were calculated. For each index, the optimal threshold for separating burned from unburned forest area was determined using their histograms. For comparison, threshold segmentation using the reflectance of original six multispectral bands was performed, in addition to a MLC-based supervised classification of all features and forest area alone; their accuracies were also evaluated and analyzed. Among all the methods compared here, mapping by EVI threshold segmentation proved to be optimal with an overall accuracy of 99.78% and a kappa coefficient of 0.9946. Finally the calculated area was compared with the values from official statistics. The comparison revealed a discrepancy between the TM extracted burned land and burned forest area, 1.298 million and 0.862 million ha, and the official statistical values, 1.70 million and 1.01 million ha, respectively. Compared to the traditional methods used to report official statistics on burned areas, the remote sensing-based extraction is less labour- and time-consuming, and more objective and efficient.

Following this fire, the local forestry bureaus have taken a series of measures for the forest recovery and ecological reconstruction. Typically three different restoration treatments, namely natural regeneration (NR), artificial regeneration (AR), and artificial promotion (AP), are adopted for the forest regeneration in the burned area. The dynamics of forest renewal varied depending on the treatment selected. In order to elucidate the effects of the three treatments, a field survey was conducted to collect the attribute data, specifically species composition, structural parameters, and LAI, which were analyzed through ANOVA and a post-hoc test. Results indicated that the broad-leaved species occupied the main component of the forest under NR while the coniferous species dominated those under the other two treatments. Tree height and DBH were significantly highest for the forests under AR, but an insignificant difference was found for crown widths. Significantly highest LAI was observed in forest under NR. The results suggest AR to be adopted in post-fire recovery if the goal is timber production, while NR should be selected when focusing on canopy vertical density and species richness. The AP showed no advantage. These findings can be used for reference in local forest management.

Taking into account the many limitations of field forest investigation, multi-source remote sensing data were also employed to monitor the forest recovery trajectories

after the “5.6 Fire”. These data include the Landsat TM/ETM+ imagery, MODIS Land Cover Type and Vegetation Indices products, and ALOS PALSAR FBD data.

Concerning Landsat TM/ETM+ imagery, totally 12 scenes covering the period of 1987-2011 were used for the monitoring of post-fire forest recovery. In addition to the commonly used vegetation indices (e.g. NDVI), a more effective index of DI was examined and evaluated. As forest area with a larger DI had a higher degree of being disturbed and the DI values in the year of 1999-2002 were significantly larger than those in other years, the forest definitely suffered a new disturbance during this period for some reasons. Furthermore, in combination with the field survey data, the recovery trajectories under the three restoration treatments were also tracked and compared. Results indicated that the forest under NR achieved a totally different recovery process with those under the other two treatments. There was a relatively slower regeneration rate for forest under NR in the early stage since fire. But after about 20 years, the recovery process had a breakthrough and the completely naturally recovered forest became more vigorous than those under artificially assisted restoration.

Due to the unique characteristics of MODIS data, in terms of low spatial resolution and high radiometric and temporal resolutions, the well-developed MODIS Land Cover Type products were exploited to monitor the temporal and spatial dynamics in post-fire forest coverage. It was centered on the hypothesis that the annual variability in coverage of different types of forests during 2001-2012 can be detected. Results suggested that the area of “Mixed forest” in the IGBP classification scheme gradually increased from 46.34% in 2001 to 80.50% in 2012, while that of “Cropland/Natural vegetation mosaic” decreased from 30.46% to 5.94% in this period. More specifically, the defined high-level class of “Forests” area increased from 50.29% to 89.35%. By examining the responses of MODIS Vegetation Indices values to the recovery activity, it was found that the four types of forests and three classes of land cover vegetation can be separated by NDVI, while EVI is not applicable for the separation of forests from other vegetation types. The difference between the burned and unburned forest area can be identified by MODIS NDVI and EVI.

In addition to the optical images, ALOS PALSAR data were also applied to detect the post-fire forest dynamics under different restoration treatments during the period 2007-2010. The backscattering intensity in HH and HV polarization and the derived radar indices of RRVI and RNDVI were examined and evaluated. Results showed that, compared to the other two treatments, the forests under NR presented a different recovery trajectory, especially for the forestry bureau of Amuer when characterized by RRVI and RNDVI. No significant difference was observed between the treatments of AR and AP. These results were consistent with those achieved by LAI and DI in former chapters which together demonstrated the reliability of the forest recovery trajectory monitoring.

As summarized, multi-source optical and SAR data have been employed to detect the forest disturbance and recovery after the “5.6 Fire”. It is evident that these data have considerably different temporal coverage and spatial resolution, and hence gave variable performances. In order to perform more direct and targeted evaluation and

comparison among the performances of different sensors, the linear statistical modeling was applied using field measured LAI and remote sensing indices from ALOS AVNIR-2, Landsat-5 TM and MODIS NBAR, ALOS PALSAR data. These data was acquired at the close dates in 2010. During the modeling, six diverse optical vegetation indices were selected for the comparison among the three optical sensors, and two radar indices were determined for the comparison between optical and SAR sensors. Results revealed the highest accuracy with AVNIR-2 while relatively lowest accuracy with MODIS NBAR. No significant difference was found between results from AVNIR-2 and PALSAR. The gap between the spatial resolution of Landsat-5 TM (30 m) and MODIS NBAR (500 m) data with the field plot size (10 m) can account for the reduced accuracy. Nonetheless, the data with higher spatial resolution and retrieval accuracy usually have lower efficiency in spatial and temporal coverage, and require higher acquisition costs. Thus in specific applications, the actual accuracy needs should be carefully considered to achieve a cost-efficient result.

6.2 Criticisms and future prospects

In spite of these positive results and knowledge obtained through the efforts in this study, there are many limitations and deficiencies, pending future improvements and enhancements. Now they will be further discussed and commented.

6.2.1 Fire frequency and severity

The research reported in this thesis only focused on the effects of one severe forest fire, “5.6 Fire”, that occurred in the boreal forest grown in the Greater Hinggan Mountain area of northeast China. Although it is a fairly serious fire and the damaged forest ecosystems comprise both coniferous and deciduous tree species as well as abundant shrubs and ground organic layer, the comparative study with the fires distributed in other forest ecosystems (e.g. tropical forests, other boreal forests in Central Siberia, Canada and Alaska) will enrich the research framework, enhance the significance of achievements, and improve the possibility for obtaining more compelling findings. Thus it should be included in future studies.

It has been demonstrated in many previous studies that there is a transition in the dominant species of naturally regenerated forests, usually from dominance of broad-leaved pioneers in the initial period to that of conifers in the late-establishment stage (Johnstone *et al.*, 2004; Schulze *et al.*, 2005; Gauthier *et al.*, 2010; Otoda *et al.*, 2013), particularly in 60–180 years after the fire. The forest regeneration rate and patterns are also affected by fire frequency (Senici *et al.*, 2013) and fire severity (Schimmel and Granstrom, 1996; Hollingsworth *et al.*, 2013).

Since there are only 27 years after the “5.6 Fire” and no apparent fires have occurred with significant influence on ecological environment in the burned area of this fire, the effect of fire frequency was not considered. As the field observations on forest recovery will be continued in future work, this factor may be examined on the basis of a sufficient length of time and number of fire activities.

Additionally, the fire severity for the sampling plots in the three forestry bureaus

was evaluated using DI as a proxy, and comparison among the plots under the three restoration treatments was made. As no significant difference was found, the influence of fire severity was not incorporated into subsequent identification of the effects of different restoration strategies based on remote sensing data. Nevertheless, from the perspective of the entire burned forest area, the fire severity is potentially in great need of consideration when performing long-term recovery monitoring.

6.2.2 Deficiencies of remote sensing data

As stated, the multi-source and time series remote sensing data from ALOS AVNIR-2, Landsat TM/ETM+, MODIS, and ALOS PALSAR have been employed to represent an affordable, cost-effective and standardized source of information on fire effect and forest recovery. However, several evident deficiencies in remote sensing data coverage existed.

First, when extracting the burned forest area, only single-phase Landsat TM images acquired after the fire was applied since no appropriate data covering the whole burn scar with an acquisition date just before the fire occurrence is available. Despite the high accuracy achieved in the extraction, the results can be better verified and new insights will be gained into the burned forest area mapping with the availability of two-phase images.

Then, it should be admitted that the time series Landsat TM/ETM+ data used for the forest recovery trajectory monitoring are not continuous annually although there are as many as 12 images spanning the period of 1987-2011. Especially the lack of data during 1988-1992 and pre-1999 presents a potentially great flaw as it may result in the loss of key features in the whole recovery process. Also the sample area used for the convenience to develop the Landsat path 122 row 23 time series seems a little pity. Besides, there are some Landsat 7 ETM+ images for 2003-present can be explored, while requiring appropriate pre-processing techniques to compensate for the Scan Line Corrector (SLC) failure.

Additionally, owing to the launch of Terra MODIS in 1999 and Aqua MODIS in 2002 as well as the ALOS satellite in 2006, there is limitation in the temporal coverage of these data for the whole post-fire period monitoring. Certainly, the detection based on MODIS Land Cover Type product within the time period of 2001-2012 and ALOS PALSAR FBD data during 2007-2010 both gave satisfactory results and thus provided the opportunity for mutual validation as with Landsat records. Consequently, the research with regard to other fire disturbances occurred within the coverage of these data would definitely be a meaningful attempt.

Furthermore, the remote sensing data with high spatial resolution (no less than 10 m) used in this thesis was the only one scene of AVNIR-2 image acquired in 2010. No IKONOS or QuickBird data have been utilized. In fact, long time series detection and monitoring of forest dynamics using such high resolution data seems not cost-effective due to the high data acquisition costs, especially in large scales. It is similar to the case of airborne LiDAR. But for local-scale studies, particularly those key scenarios needing extraordinary high accuracy, it is necessary and deserves to be tried. In addition, the hyperspectral imagery which is able to characterize forest with

extremely fine spectral features (e.g. Hyperion) can be taken as an excellent supplement to multispectral and SAR data. It has fallen into our plans for the discrimination of forest types, complementary to the endeavor throughout this thesis.

Finally, the advantages of SAR systems for all-weather and day-and-night observations have not been reflected in this study. Due to the lack of quad-polarization PALSAR data covering the study area, it is not possible to carry out polarimetric decomposition to acquire many more useful polarimetric parameters for the forest identification. On the other hand, by examination, it is found that InSAR can be implemented to provide more accurate characterization of forest structural parameters (e.g. tree height). Despite the difficulties with this technique, it is the focus of the work during next phase.

As an aside, due to the termination of ALOS mission in April 2011, the successor of ALOS-2 has been designed and successfully launched just on May 24 2014. It is equipped with only one remote sensing instrument, the PALSAR-2 for 24-hours all-weather land observation. The PALSAR-2 will succeed to the radar mission of PALSAR aboard ALOS with enhanced performances and the functions. The sensor achieves 1 m-resolution by the spotlight mode, and wide observation swath of 350 km or 490 km by the ScanSAR mode, and multiple polarimetric strip mode imaging. As an ALOS Principal Investigator (PI), I will continue to conduct my research with the support of free ALOS and ALOS-2 data from the JAXA.

6.2.3 Limitations and extensions in field survey

The field survey data of species composition, structural parameters and LAI come from the ground-based investigation conducted in July 2012, which was the 25th year after the “5.6 Fire”. Totally 27 plots with a size of 10 m × 10 m were surveyed and particular emphasis was laid on the effects of three different restoration treatments, NR, AR and AP. It was found that in all plots under AR and AP treatments, the trees are evenly distributed within the plots and their surrounding areas, making the size of the plot effectively irrelevant. But it was not such a case for the plots under NR. Thus, in future measurements, the size of plots should be increased and the number of observations in each combination of treatment and region is in need of augmentation.

Post-fire recruitment of tree species is closely related to species-specific regeneration strategies and environmental conditions. For example, trees with vegetative regeneration capabilities, such as *Populus* and *Betula* species, may be able to recover quickly after fire even though seed supply is insufficient (Uemura *et al.*, 1997; Dainou *et al.*, 2011), whereas dispersal limitation of seeds would be a primary cause of regeneration failure in non-sprouters (Lavoie and Sirois, 1998; Asselin *et al.*, 2001). Consequently, these factors including tree characteristics (e.g., seed supply, stem density and leaf water content) and environmental conditions (e.g., soil moisture, slope and aspect) should be taken into account when operating the field survey due to their potential influences on the local post-fire forest recovery (Camill *et al.*, 2010).

In addition to the field survey data used in this thesis, there is another group of field measurement data coming from the permanent plots designed for the National Forest Inventory of China. National Forest Inventory is a periodic review of permanent plots

carried out to detect the macro situation and monitor the dynamics of forest resources throughout China, with province as a unit. It is an important component of the national forest monitoring system.

The orientation and size of these permanent plots are shown in Fig. 6.1. The side length of the plot is 25.82 m and its area equals to 0.0667 hectares (1 mu- an area unit commonly used in China). In the field survey, only the trees with $DBH \geq 5.0$ cm and DBH (unit: cm) $\geq 2L$ (unit: m) are considered and measured. Here the parameter L denotes the horizontal distance between the center of plot (central pile) and sample tree (Fig. 6.2). The forest attributes of above-mentioned trees, including tree age, DBH, tree height and crown closure are measured and recorded. However, only living woods are included while snags, dead logs, felled tree and cut stumps are excluded. The restoration treatments for forests within the plots are not referred.

The plots located within the burned and unburned forest area of "5.6 Fire" were extracted and analyzed, respectively (Fig. 6.3). There are totally 131 plots located in the burned forest area and 80 plots in the unburned forest area. For some reason, these "confidential" data are not permitted to serve this thesis, while may be authorized to utilize in the future.

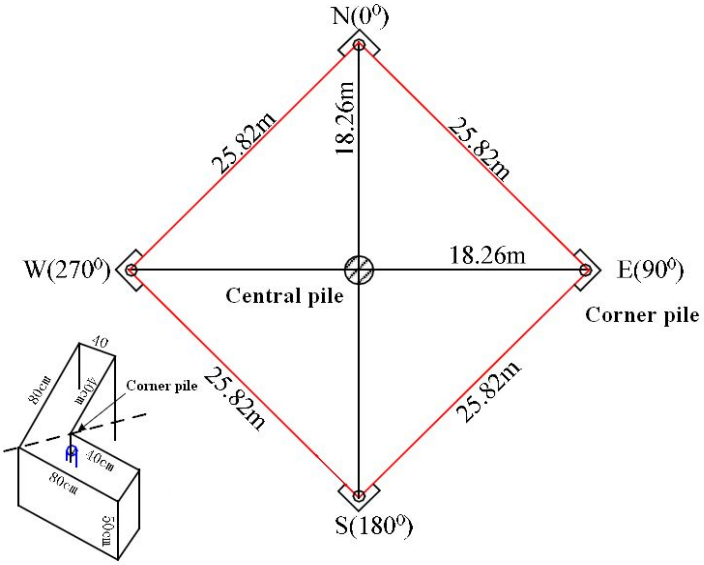

Figure 6.1 Sketch map of permanent plots for the National Forest Inventory of China.

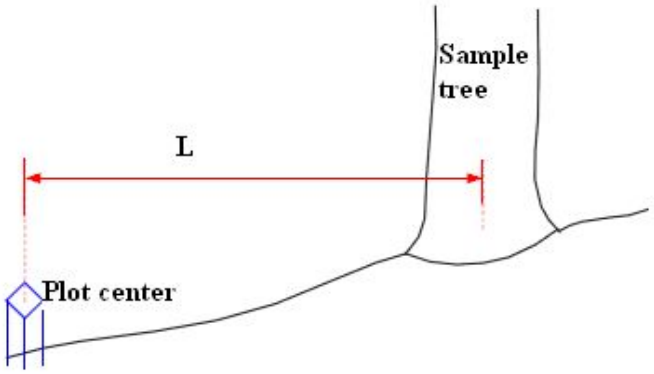

Figure 6.2 The meaning of the parameter L.

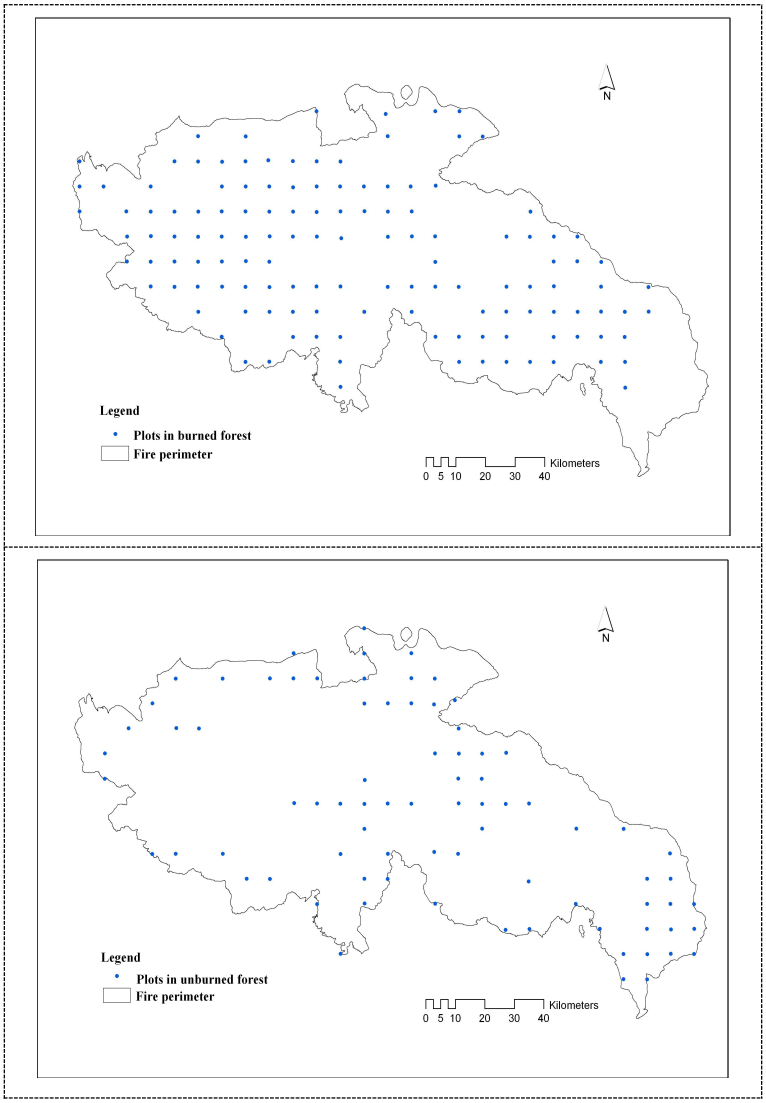

Figure 6.3 The plots located in the burned and unburned forest area of the "5.6 Fire".

6.3 Concluding remarks

Measurements and investigation from spaceborne passive (optical) and active (e.g. radar) sensors and their integration into science and management heralds new possibilities for advanced observations and monitoring of forest ecosystem, and come at a critical juncture for exploring the multidimensional relationships between forest disturbance/recovery and environmental change as well as the development of human beings. It will also be conducive to build information systems to promote coexistence between human society and the forest ecosystems.

As is known to all, forest is regarded as the "lung" of the Earth, and then remote sensing is not the medicine for the treatment of asthma that the Earth is suffering, but serves as advanced medical equipment for the health surveillance and diagnosis of the "lung". It will definitely be rapidly developed and functioning adequately.

References

Abbott, K. N., Leblon, B., Staples, G. C., Maclean, D. A. and Alexander, M. E. 2007. Fire danger monitoring using RADARSAT-1 over northern boreal forests. *International Journal of Remote Sensing*, **28**(6): 1317-1338.

Allen, J. L. and Sorbel, B. 2008. Assessing the differenced Normalized Burn Ratio's ability to map burn severity in the boreal forest and tundra ecosystems of Alaska's national parks. *International Journal of Wildland Fire*, **17**(4): 463-475.

ALOS. Available online: *http://www.eorc.jaxa.jp/ALOS/en/about/about_index.htm* (accessed on May 15, 2014).

Andersen, H. E., Strunk, J., Temesgen, H., Atwood, D. and Winterberger, K. 2011. Using multilevel remote sensing and ground data to estimate forest biomass resources in remote regions: a case study in the boreal forests of interior Alaska. *Canadian Journal of Remote Sensing*, **37**(6): 596-611.

Antropov, O., Rauste, Y. and Hame, T. 2011. Volume Scattering Modeling in PolSAR Decompositions: Study of ALOS PALSAR Data over Boreal Forest. *IEEE Transactions on Geoscience and Remote Sensing*, **49**(10): 3838-3848.

Arias, D., Calvo-Alvarado, J. and Dohrenbusch, A. 2007. Calibration of LAI-2000 to estimate leaf area index (LAI) and assessment of its relationship with stand productivity in six native and introduced tree species in Costa Rica. *Forest Ecology and Management*, **247**(1-3): 185-193.

Arino, O., Piccolini, I., Kasischke, E., Siegert, F., Chuvieco, E., Martin, P., Li, Z., Fraser, R., Eva, H., Stroppiana, D., Pereira, J., Silva, J. M. N., Roy, D. and Barbosa, P. M. 2001. Methods of mapping surfaces burned in vegetation fires. In Global and Regional Vegetation Fire Monitoring from Space: Planning a Coordinated International Effort, edited by F. J. Ahern, J. G. Goldammer, and C. O. Justice (The Hague, The Netherlands: SPB, Academic Publishing), pp. 227-255.

Arroyo, L. A., Johansen, K., Armston, J. and Phinn, S. 2010. Integration of LiDAR and QuickBird imagery for mapping riparian biophysical parameters and land cover types in Australian tropical savannas. *Forest Ecology and Management*, **259**(3): 598-606.

Ascoli, D., Castagneri, D., Valsecchi, C., Conedera, M. and Bovio, G. 2013. Post-fire restoration of beech stands in the Southern Alps by natural regeneration. *Ecological Engineering*, **54**: 210-217.

Asselin, H., Fortin, M. J. and Bergeron, Y. 2001. Spatial distribution of late-successional coniferous species regeneration following disturbance in southwestern Quebec boreal forest. *Forest Ecology and Management*, **140**(1): 29-37.

Avtar, R., Sawada, H., Takeuchi, W. and Singh, G. 2012. Characterization of forests and deforestation in Cambodia using ALOS/PALSAR observation. *Geocarto International*, **27**(2): 119-137.

Ayres, M. P. and Lombardero, M. J. 2000. Assessing the consequences of global change for forest disturbance from herbivores and pathogens. *Science of the Total*

Environment, **262**(3): 263-286.

Babintseva, R. and Titova, Y. V. 1996. Effects of Fire on the Regeneration of Larch forests in the Lake Baikal Basin. In *Fire in Ecosystems of Boreal Eurasia*; Springer: Dordrecht, The Netherlands, volume 48, pp. 358-365.

Bacles, C. F. E. 2014. Pollen, wind and fire: how to investigate genetic effects of disturbance-induced change in forest trees. *Molecular Ecology*, **23**(1): 20-22.

Bamler, R. 2000. Principles of synthetic aperture radar. *Surveys in Geophysics*, **21**(2-3): 147-157.

Bastarrika, A., Chuvieco, E. and Martin, M. P. 2011. Mapping burned areas from Landsat TM/ETM plus data with a two-phase algorithm: Balancing omission and commission errors. *Remote Sensing of Environment*, **115**(4): 1003-1012.

Basuki, T. M., Skidmore, A. K., Hussin, Y. A. and Van Duren, I. 2013. Estimating tropical forest biomass more accurately by integrating ALOS PALSAR and Landsat-7 ETM+ data. *International Journal of Remote Sensing*, **34**(13): 4871-4888.

Beghin, R., Lingua, E., Garbarino, M., Lonati, M., Bovio, G., Motta, R. and Marzano, R. 2010. Pinus sylvestris forest regeneration under different post-fire restoration practices in the northwestern Italian Alps. *Ecological Engineering*, **36**(10): 1365-1372.

Belward, A. S., Estes, J. E. and Kline, K. D. 1999. The IGBP-DIS global 1-km land-cover data set DISCover: A project overview. *Photogrammetric Engineering and Remote Sensing*, **65**(9): 1013-1020.

Bergen, K. M., Goetz, S. J., Dubayah, R. O., Henebry, G. M., Hunsaker, C. T., Imhoff, M. L., Nelson, R. F., Parker, G. G. and Radeloff, V. C. 2009. Remote sensing of vegetation 3-D structure for biodiversity and habitat: Review and implications for lidar and radar spaceborne missions. *Journal of Geophysical Research-Biogeosciences*, **114**, G00E06.

Bonan, G. B. 1989. Environmental factors and ecological processes controlling vegetation patterns in boreal forests. *Landscape Ecology*, **3**(2): 111-130.

Bonan, G. B., Oleson, K. W., Vertenstein, M., Levis, S., Zeng, X. B. and Dai, Y. 2002. The land surface climatology of the community land model coupled to the NCAR community land model. *Journal of Climate*, **15**(22): 3123-3149.

Bontemps, S., Langner, A. and Defourny, P. 2012. Monitoring forest changes in Borneo on a yearly basis by an object-based change detection algorithm using SPOT-VEGETATION time series. *International Journal of Remote Sensing*, **33**(15): 4673-4699.

Bourgeau-Chavez, L. L., Harrell, P. A., Kasischke, E. S. and French, N. H. F. 1997. The detection and mapping of Alaskan wildfires using a spaceborne imaging radar system. *International Journal of Remote Sensing*, **18**(2): 355-373.

Bourgeau-Chavez, L. L., Kasischke, E. S., Brunzell, S., Mudd, J. P. and Tukman, M. 2002. Mapping fire scars in global boreal forests using imaging radar data. *International Journal of Remote Sensing*, **23**(20): 4211-4234.

Bourgeau-Chavez, L. L., Kasischke, E. S., Riordan, K., Brunzell, S., Nolan, M., Hyer, E., Slawski, J., Medvecz, M., Walters, T. and Ames, S. 2007. Remote monitoring

of spatial and temporal surface soil moisture in fire disturbed boreal forest ecosystems with ERS SAR imagery. *International Journal of Remote Sensing*, **28**(10): 2133-2162.

Broich, M., Hansen, M. C., Potapov, P., Adusei, B., Lindquist, E. and Stehman, S. V. 2011. Time-series analysis of multi-resolution optical imagery for quantifying forest cover loss in Sumatra and Kalimantan, Indonesia. *International Journal of Applied Earth Observation and Geoinformation*, **13**(2): 277-291.

Cahoon, D. R., Levine, J. S., Cofer, W. R., Miller, J. E., Minnis, P., Tennille, G. M., Yip, T. W., Stocks, B. J. and Heck, P. W. 1991. The great Chinese fire of 1987: A view from space, *Global Biomass Burning: Atmospheric, Climatic, and Biospheric Implications*, 61–66, MIT Press, Cambridge, Mass.

Cahoon, D. R., Stocks, B. J., Levine, J. S., Cofer, W. R. and Pierson, J. M. 1994. Satellite analysis of the severe 1987 forest fires in northern China and southeastern Siberia. *Journal of Geophysical Research-Atmospheres*, **99**(D9): 18627-18638.

Cai, T. J., Zhou, X. F. and Yang, W. H. 1995. Impact of Da xing'an ling forest fires on the river runoff. *Scientia Silvae Sinicae*, **31**(5): 403-407. (In Chinese)

Cai, W. H., Yang, J., Liu, Z. H., Hu, Y. M. and Weisberg, P. J. 2013. Post-fire tree recruitment of a boreal larch forest in Northeast China. *Forest Ecology and Management*, **307**: 20-29.

Camac, J. S., Williams, R. J., Wahren, C. H., Morris, W. K. and Morgan, J. W. 2013. Post-fire regeneration in alpine heathland: Does fire severity matter? *Austral Ecology*, **38**(2): 199-207.

Camill, P., Chihara, L., Adams, B., Andreassi, C., Barry, A., Kalim, S., Limmer, J., Mandell, M. and Rafert, G. 2010. Early life history transitions and recruitment of Picea mariana in thawed boreal permafrost peatlands. *Ecology*, **91**(2): 448-459.

Canisius, F. and Fernandes, R. 2012. ALOS PALSAR L-band polarimetric SAR data and in situ measurements for leaf area index assessment. *Remote Sensing Letters*, **3**(3): 221-229.

Cansler, C. A. and McKenzie, D. 2012. How Robust Are Burn Severity Indices When Applied in a New Region? Evaluation of Alternate Field-Based and Remote-Sensing Methods. *Remote Sensing*, **4**(2): 456-483.

Canty, M. J. and Nielsen, A. A. 2008. Automatic radiometric normalization of multi-temporal satellite imagery with the iteratively re-weighted MAD transformation. *Remote Sensing of Environment*, **112**: 1025-1036.

Cao, C. X. 2013. Monograph Series in Remote Sensing based Diagnosis: Diagnosis of Environmental Health by Remote Sensing. Beijing: Science Press. (In Chinese)

Cao, C. X., Chen, W., Li, G. H., Jia, H. C., Ji, W., Xu, M., Gao, M. X., Ni, X. L., Zhao, J., Zheng, S., Tian, R., Liu, C. and Li, S. 2011. The retrieval of shrub fractional cover based on a geometric-optical model in combination with linear spectral mixture analysis. *Canadian Journal of Remote Sensing*, **37**(4): 348-358.

Carlson, T. N. and Ripley, D. A. 1997. On the relation between NDVI, fractional vegetation cover, and leaf area index. *Remote Sensing of Environment*, **62**(3): 241-252.

Castellana, L., D'Addabbo, A. and Pasquariello, G. 2007. A composed supervised/unsupervised approach to improve change detection from remote sensing. *Pattern Recognition Letters*, **28**(4): 405-413.

Chang, D. and Song, Y. 2009. Comparison of L3JRC and MODIS global burned area products from 2000 to 2007. *Journal of Geophysical Research-Atmospheres*, **114**, D16106.

Chang, Y., He, H. S., Bishop, I., Hu, Y. M., Bu, R. C., Xu, C. G. and Li, X. Z. 2007. Long-term forest landscape responses to fire exclusion in the Great Xing'an Mountains, China. *International Journal of Wildland Fire*, **16**(1): 34-44.

Chen, C. X., Tang, P. and Bian, Z. 2012. Tasseled cap transformation for HJ-1A/B charge coupled device images. *Journal of Applied Remote Sensing*, **6**, 063575.

Chen, H. W., Hu, Y. M., Chang, Y., Bu, R. C., Li, Y. H. and Liu, M. 2011. Simulating impact of larch caterpillar (Dendrolimus superans) on fire regime and forest landscape in Da Hinggan Mountains, Northeast China. *Chinese Geographical Science*, **21**(5): 575-586.

Chen, J. M. and Black, T. A. 1992. Defining leaf-area index for non-flat leaves. *Plant Cell and Environment*, **15**(4): 421-429.

Chen, J. M. and Cihlar, J. 1996. Retrieving leaf area index of boreal conifer forests using Landsat TM images. *Remote Sensing of Environment*, **55**(2): 153-162.

Chen, W. and Cao, C. X. 2012. Topographic correction-based retrieval of leaf area index in mountain areas. *Journal of Mountain Science*, **9**(2): 166-174.

Chen, W., Cao, C. X., He, Q. S., Guo, H. D., Zhang, H., Li, R. Q., Zheng, S., Xu, M., Gao, M. X., Zhao, J., Li, S., Ni, X. L., Jia, H. C., Ji, W., Tian, R., Liu, C., Zhao, Y. X. and Li, J. L. 2010. Quantitative estimation of the shrub canopy LAI from atmosphere-corrected HJ-1 CCD data in Mu Us Sandland. *Science China Earth Sciences*, **53**(Suppl.I): 26-33.

Chen, W., Sakai, T., Moriya, K., Koyama, L. and Cao, C. X. 2013. Extraction of burned forest area in the Greater Hinggan Mountain of China based on Landsat TM data. In proceedings of *2013 IEEE International Geoscience and Remote Sensing Symposium (IGARSS)*. IEEE Geoscience and Remote Sensing Society, NY, USA.

Chen, X., Vierling, L., Deering, D. and Conley, A. 2005. Monitoring boreal forest leaf area index across a Siberian burn chronosequence: a MODIS validation study. *International Journal of Remote Sensing*, **26**(24): 5433-5451.

China DXAL - Da Xing An Ling. Available online: *http://www.dxal.gov.cn/index.jsp* (accessed on May 15, 2014).

Chowdhury, T. A., Thiel, C., Schmullius, C. and Stelmaszczuk-Gorska, M. 2013. Polarimetric Parameters for Growing Stock Volume Estimation Using ALOS PALSAR L-Band Data over Siberian Forests. *Remote Sensing*, **5**(11): 5725-5756.

Chu, T. and Guo, X. 2014. Remote Sensing Techniques in Monitoring Post-Fire Effects and Patterns of Forest Recovery in Boreal Forest Regions: A Review. *Remote Sensing*, **6**: 470-520.

Chuvieco, E., Englefield, P., Trishchenko, A. P. and Luo, Y. 2008. Generation of long time series of burn area maps of the boreal forest from NOAA-AVHRR composite

data. *Remote Sensing of Environment*, **112**(5): 2381-2396.

Cloude, S. R. and Pottier, E. 1997. An entropy based classification scheme for land applications of polarimetric SAR. *IEEE Transactions on Geoscience and Remote Sensing*, **35**(1): 68-78.

Cohen, W. B. and Goward, S. N. 2004. Landsat's role in ecological applications of remote sensing. *Bioscience*, **54**: 535-545.

Comber, A., Fisher. P., Brunsdon, C. and Khmag, A. 2012. Spatial analysis of remote sensing image classification accuracy. *Remote Sensing of Environment*, **127**: 237-246.

Cornforth, W. A., Fatoyinbo, T. E., Freemantle, T. P. and Pettorelli, N. 2013. Advanced Land Observing Satellite Phased Array Type L-Band SAR (ALOS PALSAR) to Inform the Conservation of Mangroves: Sundarbans as a Case Study. *Remote Sensing*, **5**(1): 224-237.

Corona P., Cartisano R., Salvati R., Chirici G., Floris A., Di Martino P., Marchetti M., Scrinzi G., Clementel F., Travaglini D. and Torresan C. 2012. Airborne Laser Scanning to support forest resource management under alpine, temperate and Mediterranean environments in Italy. *European Journal of Remote Sensing*, **45**: 27-37.

Corona, P., Lamonaca, A. and Chirici, G. 2008. Remote sensing support for post fire forest management. *Iforest-Biogeosciences and Forestry*, **1**: 6-12.

Crist, E. P. and Cicone, R. C. 1984. A physically-based transformation of Thematic Mapper data-the TM Tasseled Cap. *IEEE Transactions on Geoscience and Remote Sensing*, **22**(3): 256-263.

Cuevas-Gonzalez, M., Gerard, F., Balzter, H. and Riano, D. 2008. Studying the change in fAPAR after forest fires in Siberia using MODIS. *International Journal of Remote Sensing*, **29**(23): 6873-6892.

Cuevas-Gonzalez, M., Gerard, F., Balzter, H. and Riano, D. 2009. Analysing forest recovery after wildfire disturbance in boreal Siberia using remotely sensed vegetation indices. *Global Change Biology*, **15**(3): 561-577.

Dainou, K., Bauduin, A., Bourland, N., Gillet, J. F., Feteke, F. and Doucet, J. L. 2011. Soil seed bank characteristics in Cameroonian rainforests and implications for post-logging forest recovery. *Ecological Engineering*, **37**(10): 1499-1506.

De Santis, A. and Chuvieco, E. 2007. Burn severity estimation from remotely sensed data: Performance of simulation versus empirical models. *Remote Sensing of Environment*, **108**(4): 422-435.

Díaz-Delgado, R. and Pons, X. 2001. Spatial patterns of forest fires in Catalonia (NE of Spain) along the period 1975-1995 analysis of vegetation recovery after fire. *Forest Ecology and Management*, **147**(1): 67-74.

Epting, J. and Verbyla, D. 2005. Landscape-level interactions of prefire vegetation, burn severity, and postfire vegetation over a 16-year period in interior Alaska. *Canadian Journal of Forest Research-Revue Canadienne De Recherche Forestiere*, **35**(6): 1367-1377.

Epting, J., Verbyla, D. and Sorbel, B. 2005. Evaluation of remotely sensed indices for assessing burn severity in interior Alaska using Landsat TM and ETM+. *Remote*

Sensing of Environment, **96**(3-4): 328-339.

Fernandez-Manso, A., Quintano, C. and Roberts, D. 2012. Evaluation of potential of multiple endmember spectral mixture analysis (MESMA) for surface coal mining affected area mapping in different world forest ecosystems. *Remote Sensing of Environment*, **127**: 181-193.

Ferreira, N. C., Ferreira, L. G. and Huete, A. R. 2010. Assessing the response of the MODIS vegetation indices to landscape disturbance in the forested areas of the legal Brazilian Amazon. *International Journal of Remote Sensing*, **31**(3): 745-759.

Flannigan, M. D., Amiro, B. D., Logan, K. A., Stocks, B. J. and Wotton, B. M. 2005. Forest fires and climate change in the 21st century. *Mitigation and Adaptation Strategies for Global Change*, **11**: 847-859.

Food and Agriculture Organization of the United Nations (FAO). 2006. Chapter 2: Extent of forest resources, In Global Forest Resources Assessment 2005, Progress towards sustainable forest management, pp. 14-17.

Food and Agriculture Organization of the United Nations (FAO). 2010. Global Forest Resources Assessment 2010—Main Report. In *Food and Agriculture Organization of the United Nations (FAO) Forestry Paper*; FAO: Rome, Italia.

Forkel, M., Thonicke, K., Beer, C., Cramer, W., Bartalev, S. and Schmullius, C. 2012. Extreme fire events are related to previous-year surface moisture conditions in permafrost-underlain larch forests of Siberia. *Environmental Research Letters*, **7**, 044021.

Fraser, R. H. and Li, Z. 2002. Estimating fire-related parameters in boreal forest using SPOT VEGETATION. *Remote Sensing of Environment*, **82**(1): 95-110.

Freeman, A. and Durden, S. 1998. A Three-Component Scattering Model for Polarimetric SAR Data. *IEEE Transactions on Geoscience and Remote Sensing*, **36**(3):963-973.

French, N. H. F., Kasischke, E. S., Bourgeauchavez, L. L. and Berry, D. 1995. Mapping the location of wildfires in Alaskan boreal forests using AVHRR imagery. *International Journal of Wildland Fire*, **5**(2): 55-62.

Friedl, M. A., McIver, D. K., Hodges, J. C. F., Zhang, X. Y., Muchoney, D., Strahler, A. H., Woodcock, C. E., Gopal, S., Schneider, A., Cooper, A., Baccini, A., Gao, F. and Schaaf, C. 2002. Global land cover mapping from MODIS: algorithms and early results. *Remote Sensing of Environment*, **83**(1-2): 287-302.

Friedl, M. A., Sulla-Menashe, D., Tan, B., Schneider, A., Ramankutty, N., Sibley, A. and Huang, X. 2010. MODIS Collection 5 global land cover: Algorithm refinements and characterization of new datasets. *Remote Sensing of Environment*, **114**(1): 168-182.

Frolking, S., Palace, M. W., Clark, D. B., Chambers, J. Q., Shugart, H. H. and Hurtt, G. C. 2009. Forest disturbance and recovery: A general review in the context of spaceborne remote sensing of impacts on aboveground biomass and canopy structure. *Journal of Geophysical Research-Biogeosciences*, **114**, G00e02.

Gartley, M., Goodenough, A., Brown, S. and Kauffman, R. P. 2010. A comparison of spatial sampling techniques enabling first principles modeling of a synthetic aperture RADAR imaging platform. In “Algorithms for Synthetic Aperture Radar

Imagery Xvii" (Eds.: by E. G. Zelnio and F. D. Garber), Book Series: Proceedings of SPIE-The International Society for Optical Engineering. Bellingham, SPIE-Int Soc Optical Engineering. 7699, 76990N: pp. 1-10.

Gauthier, S., Boucher, D., Morissette, J. and De Grandpre, L. 2010. Fifty-seven years of composition change in the eastern boreal forest of Canada. *Journal of Vegetation Science*, **21**(4): 772-785.

George, C., Rowland, C., Gerard, F. and Balzter, H. 2006. Retrospective mapping of burnt areas in Central Siberia using a modification of the normalised difference water index. *Remote Sensing of Environment*, **104**(3): 346-359.

Giglio, L., Randerson, J. T., van der Werf, G. R., Kasibhatla, P. S., Collatz, G. J., Morton, D. C. and DeFries, R. S. 2010. Assessing variability and long-term trends in burned area by merging multiple satellite fire products. *Biogeosciences*, **7**(3): 1171-1186.

Gillett, N. P., Weaver, A. J., Zwiers, F. W. and Flannigan, M. D. 2004. Detecting the effect of climate change on Canadian forest fires. *Geophysical Research Letters*, **31**(18), L18211.

Gimeno, M. and San-Miguel-Ayanz, J. 2004. Evaluation of RADARSAT-1 data for identification of burnt areas in Southern Europe. *Remote Sensing of Environment*, **92**(3): 370-375.

Gimeno, M., San-Miguel-Ayanz, J. and Schmuck, G. 2004. Identification of burnt areas in Mediterranean forest environments from ERS-2 SAR time series. *International Journal of Remote Sensing*, **25**(22): 4873-4888.

Goetz, S. J., Sun, M., Baccini, A. and Beck, P. S. A. 2010. Synergistic use of spaceborne lidar and optical imagery for assessing forest disturbance: An Alaska case study. *Journal of Geophysical Research-Biogeosciences*, **115**, G00e07.

Goodenough, D. G., Chen, H., Richardson, A., Cloude, S., Hong, W. and Li, Y. 2011. Mapping fire scars using Radarsat-2 polarimetric SAR data. *Canadian Journal of Remote Sensing*, **37**(5): 500-509.

Gromtsev, A. 2002. Natural disturbance dynamics in the boreal forests of European Russia: a review. *Silva Fennica*, **36**(1): 41-55.

Guo, N. 2003. Vegetation index and its advances. *Arid Meteorology*, **21**(4): 71-75.

Hall, R. J., Freeburn, J. T., De Groot, W. J., Pritchard, J. M., Lynham, T. J. and Landry, R. 2008. Remote sensing of burn severity: Experience from western Canada boreal fires. *International Journal of Wildland Fire*, **17**(4): 476-489.

Han, N., Du, H. Q., Zhou, G. M., Xu, X. J., Cui, R. R. and Gu, C. Y. 2013. Spatiotemporal heterogeneity of Moso bamboo aboveground carbon storage with Landsat Thematic Mapper images: a case study from Anji County, China. *International Journal of Remote Sensing*, **34**: 4917-4932.

Hansen, M. C., DeFries, R. S., Townshend, J. R. G. and Sohlberg, R. 2000. Global land cover classification at the 1km spatial resolution using a classification tree approach. *International Journal of Remote Sensing*, **21**(6-7): 1331-1364.

Harrell, P. A., BourgeauChavez, L. L., Kasischke, E. S., French, N. H. F. and Christensen, N. L. 1995. Sensitivity of ERS-1 and JERS-1 radar data to biomass and stand structure in Alaskan boreal forest. *Remote Sensing of Environment*,

54(3): 247-260.

Healey, S. P., Cohen, W. B., Yang, Z. Q. and Krankina, O. N. 2005. Comparison of Tasseled Cap-based Landsat data structures for use in forest disturbance detection. *Remote Sensing of Environment*, **97**(3): 301-310.

Hicke, J. A., Asner, G. P., Kasischke, E. S., French, N. H. F., Randerson, J. T., Collatz, G. J., Stocks, B. J., Tucker, C. J., Los, S. O. and Field, C. B. 2003. Postfire response of North American boreal forest net primary productivity analyzed with satellite observations. *Global Change Biology*, **9**(8): 1145-1157.

Hilker, T., Wulder, M. A., Coops, N. C., Linke, J., McDermid, G., Masek, J. G., Gao, F. and White, J. C. 2009. A new data fusion model for high spatial- and temporal-resolution mapping of forest disturbance based on Landsat and MODIS. *Remote Sensing of Environment*, **113**(8): 1613-1627.

Hoan, N. T., Tateishi, R., Alsaaideh, B., Ngigi, T., Alimuddin, I. and Johnson, B. 2013. Tropical forest mapping using a combination of optical and microwave data of ALOS. *International Journal of Remote Sensing*, **34**(1): 139-153.

Hollingsworth, T. N., Johnstone, J. F., Bernhardt, E. L. and Chapin, F. S. 2013. Fire Severity Filters Regeneration Traits to Shape Community Assembly in Alaska's Boreal Forest. *PLoS One*, **8**(2), e56033.

Horne, J. H. 2003. A Tasseled Cap Transformation for IKONOS Images. *ASPRS Annual Conference Proceedings*, Alaska, USA.

Hoy, E. E., French, N. H. F., Turetsky, M. R., Trigg, S. N. and Kasischke, E. S. 2008. Evaluating the potential of Landsat TM/ETM+ imagery for assessing fire severity in Alaskan black spruce forests. *International Journal of Wildland Fire*, **17**(4): 500-514.

Huang, L., Shao, Q. Q. and Liu, J. Y. 2012. Forest restoration to achieve both ecological and economic progress, Poyang Lake basin, China. *Ecological Engineering*, **44**: 53-60.

Huang, S. L. and Siegert, F. 2006. Backscatter change on fire scars in Siberian boreal forests in ENVISAT ASAR wide-swath images. *IEEE Geoscience and Remote Sensing Letters*, **3**(1): 154-158.

Huete, A. R. 1988. A soil-adjusted vegetation index (SAVI). *Remote Sensing of Environment*, **25**(3): 295-309.

Huete, A. R., Liu, H., Batchily, K. and van Leeuwen, W. 1997. A comparison of vegetation indices over a global set of TM images for EOS-MODIS. *Remote Sensing of Environment*, **59**(3): 440-451.

Isoguchi, O., Shimada, M. and Uryu, Y. 2009. A preliminary study on deforestation monitoring in Sumatra Island by PALSAR. In: Proceedings of *2009 IEEE International Geoscience and Remote Sensing Symposium (IGARSS)*. IEEE Geoscience and Remote Sensing Society, New York, USA.

Jiang, X. G., Wang, D., Tang, L. L., Hu, J. and Xi, X. H. 2008. Analyzing the vegetation cover variation of China from AVHRR-NDVI data. *International Journal of Remote Sensing*, **29**(17-18): 5301-5311.

Jin, Y. F., Randerson, J. T., Goetz, S. J., Beck, P. S. A., Loranty, M. M. and Goulden, M. L. 2012. The influence of burn severity on postfire vegetation recovery and

albedo change during early succession in North American boreal forests. *Journal of Geophysical Research-Biogeosciences*, **117**, G01036.

Johnstone, J. F., Chapin, F. S., Foote, J., Kemmett, S., Price, K. and Viereck, L. 2004. Decadal observations of tree regeneration following fire in boreal forests. *Canadian Journal of Forest Research-Revue Canadienne De Recherche Forestiere*, **34**(2): 267-273.

Jordan, C. F. 1969. Derivation of leaf area index from quality of light on the forest floor. *Ecology*, **50**(4): 663-666.

Kajii, Y., Kato, S., Streets, D. G., Tsai, N. Y., Shvidenko, A., Nilsson, S., McCallum, I., Minko, N. P., Abushenko, N., Altyntsev, D. and Khodzer, T. V. 2002. Boreal forest fires in Siberia in 1998: Estimation of area burned and emissions of pollutants by advanced very high resolution radiometer satellite data. *Journal of Geophysical Research-Atmospheres*, **107**(D24), 4745.

Kasischke, E. S. and French, N. H. F. 1995. Locating and estimating the areal extent of wildfires in Alaskan boreal forests using multiple-season AVHRR NDVI composite data. *Remote Sensing of Environment*, **51**(2): 263-275.

Kasischke, E. S., French, N. H. F., Harrell, P., Christensen, N. L., Ustin, S. L. and Barry, D. 1993. Monitoring of wildfires in boreal forests using large area AVHRR NDVI composite image data. *Remote Sensing of Environment*, **45**(1): 61-71.

Kasischke, E. S., Loboda, T., Giglio, L., French, N. H. F., Hoy, E. E., de Jong, B. and Riano, D. 2011a. Quantifying burned area for North American forests: Implications for direct reduction of carbon stocks. *Journal of Geophysical Research-Biogeosciences*, **116**, G04003.

Kasischke, E. S., Tanase, M. A., Bourgeau-Chavez, L. L. and Borr, M. 2011b. Soil moisture limitations on monitoring boreal forest regrowth using spaceborne L-band SAR data. *Remote Sensing of Environment*, **115**(1): 227-232.

Kaufman, Y. J. and Tanre, D. 1992. Atmospherically resistant vegetation index (ARVI) for EOS-MODIS. *IEEE Transactions on Geoscience and Remote Sensing*, **30**(2): 261-270.

Kavzoglu, T. and Reis, S. 2008. Performance analysis of maximum likelihood and artificial neural network classifiers for training sets with mixed pixels. *Giscience & Remote Sensing*, **45**(3): 330-342.

Keeley, J. E. 2009. Fire intensity, fire severity and burn severity: a brief review and suggested usage. *International Journal of Wildland Fire*, **18**(1): 116-126.

Kelhä, V., Rauste, Y., Häme, T., Sephton, T., Buongiorno, A., Frauenberger, O., Soini, K., Venäläinen, A., San Miguel-Ayanz, J. Vainio, T. 2003. Combining AVHRR and ATSR satellite sensor data for operational boreal forest fire detection. *International Journal of Remote Sensing*, **24**(8): 1691-1708.

Kennedy, R. E., Yang, Z. Q., Cohen, W. B., Pfaff, E., Braaten, J. and Nelson, P. 2012. Spatial and temporal patterns of forest disturbance and regrowth within the area of the Northwest Forest Plan. *Remote Sensing of Environment*, **122**(SI): 117-133.

Kobayashi, S., Widyorini, R., Kawai, S., Omura, Y., Sanga-Ngoie, K. and Supriadi, B. 2012. Backscattering characteristics of L-band polarimetric and optical satellite imagery over planted acacia forests in Sumatra, Indonesia. *Journal of Applied*

Remote Sensing, **6**, 063525.

Koutsias, N. and Karteris, M. 2000. Burned area mapping using logistic regression modeling of a single post-fire Landsat-5 Thematic Mapper image. *International Journal of Remote Sensing*, **21**(4): 673-687.

Koutsias, N., Mallinis, G. and Karteris, M. 2009. A forward/backward principal component analysis of Landsat-7 ETM+ data to enhance the spectral signal of burnt surfaces. *ISPRS Journal of Photogrammetry and Remote Sensing*, **64**(1): 37-46.

Krishnaswamy, J., Bawa, K. S., Ganeshaiah, K. N. and Kiran, M. C. 2009. Quantifying and mapping biodiversity and ecosystem services: Utility of a multi-season NDVI based Mahalanobis distance surrogate. *Remote Sensing of Environment*, **113**(4): 857-867.

Lavoie, L. and Sirois, L. 1998. Vegetation changes caused by recent fires in the northern boreal forest of eastern Canada. *Journal of Vegetation Science*, **9**(4): 483-492.

Levy, R. C., Mattoo, S., Munchak, L. A., Remer, L. A., Sayer, A. M., Patadia, F. and Hsu, N. C. 2013. The Collection 6 MODIS aerosol products over land and ocean. *Atmospheric Measurement Techniques*, **6**(11): 2989-3034.

Li, F., Wang, X. F., Zhao, J., Zhang, X. Q. and Zhao, Q. J. 2013. A method for estimating the gross primary production of alpine meadows using MODIS and climate data in China. *International Journal of Remote Sensing*, **34**(23): 8280-8300.

Li, R. R., Kaufman, Y. J., Hao, W. M., Salmon, J. M. and Gao, B. C. 2004. A technique for detecting burn scars using MODIS data. *IEEE Transactions on Geoscience and Remote Sensing*, **42**(6): 1300-1308.

Liang, S.L. 2004. Quantitative Remote Sensing of Land Surfaces. John Wiley & Sons, Inc. Hoboken, New Jersey.

Liu, H. Q. and Huete, A. R. 1995. A feedback based modification of the NDVI to minimize canopy background and atmosphere noise. *IEEE Transactions on Geoscience and Remote Sensing*, **33**(2): 457-465.

Liu, W., Song, C., Schroeder, T. A. and Cohen, W. B. 2008. Predicting forest successional stages using multitemporal Landsat imagery with forest inventory and analysis data. *International Journal of Remote Sensing*, **29**(13): 3855-3872.

Loboda, T. V. and Csiszar, I. A. 2007. Reconstruction of fire spread within wildland fire events in Northern Eurasia from the MODIS active fire product. *Global and Planetary Change*, **56**(3-4): 258-273.

Loboda, T. V., Hoy, E. E., Giglio, L. and Kasischke, E. S. 2011. Mapping burned area in Alaska using MODIS data: a data limitations-driven modification to the regional burned area algorithm. *International Journal of Wildland Fire*, **20**(4): 487-496.

Loboda, T. V., O'Neal, K. J. and Csiszar, I. 2007. Regionally adaptable dNBR-based algorithm for burned area mapping from MODIS data. *Remote Sensing of Environment*, **109**(4): 429-442.

Lobser, S. E. and Cohen, W. B. 2007. MODIS tasselled cap: land cover characteristics

expressed through transformed MODIS data. *International Journal of Remote Sensing*, **28**(22): 5079-5101.

Lucas, R., Armston, J., Fairfax, R., Fensham, R., Accad, A., Carreiras, J., Kelley, J., Bunting, P., Clewley, D., Bray, S., Metcalfe, D., Dwyer, J., Bowen, M., Eyre, T., Laidlaw, M. and Shimada, M. 2010. An Evaluation of the ALOS PALSAR L-Band Backscatter-Above Ground Biomass Relationship Queensland, Australia: Impacts of Surface Moisture Condition and Vegetation Structure. *IEEE Journal of Selected Topics in Applied Earth Observations and Remote Sensing*, **3**(4): 576-593.

Luo, J. C. 2002. The impact of Da xing'an ling forest fires on ecosystems. *The Journal of Beijing Forestry University*, **6**: 101-107. (In Chinese)

Maingi, J. K. 2005. Mapping fire scars in a mixed-oak forest in Eastern Kentucky, USA, using Landsat ETM+ data. *Geocarto International*, **20**(3): 51-63.

Margono, B. A., Turubanova, S., Zhuravleva, I., Potapov, P., Tyukavina, A., Baccini, A., Goetz, S. and Hansen, M. C. 2012. Mapping and monitoring deforestation and forest degradation in Sumatra (Indonesia) using Landsat time series data sets from 1990 to 2010. *Environmental Research Letters*, **7**(3), 034010.

Mari, N., Laneve, G., Cadau, E. and Porcasi, X. 2012. Fire Damage Assessment in Sardinia: the use of ALOS/PALSAR data for post fire effects management. *European Journal of Remote Sensing*, **45**(2): 233-241.

Marzano, R., Garbarino, M., Marcolin, E., Pividori, M. and Lingua, E. 2013. Deadwood anisotropic facilitation on seedling establishment after a stand-replacing wildfire in Aosta Valley (NW Italy). *Ecological Engineering*, **51**: 117-122.

Masek, J. G., Huang, C. Q., Wolfe, R., Cohen, W., Hall, F., Kutler, J. and Nelson, P. 2008. North American forest disturbance mapped from a decadal Landsat record. *Remote Sensing of Environment*, **112**(6): 2914-2926.

Matricardi, E. A. T., Skole, D. L., Pedlowski, M. A. and Chomentowski, W. 2013. Assessment of forest disturbances by selective logging and forest fires in the Brazilian Amazon using Landsat data. *International Journal of Remote Sensing*, **34**(4): 1057-1086.

McMichael, C. E., Hope, A. S., Roberts, D. A. and Anaya, M. R. 2004. Post-fire recovery of leaf area index in California chaparral: a remote sensing-chronosequence approach. *International Journal of Remote Sensing*, **25**(21): 4743-4760.

Menges, C. H., Bartolo, R. E., Bell, D. and Hill, G. J. E. 2004. The effect of savanna fires on SAR backscatter in northern Australia. *International Journal of Remote Sensing*, **25**(22): 4857-4871.

Michalek, J. L., French, N. H. F., Kasischke, E. S., Johnson, R. D. and Colwell, J. E. 2000. Using Landsat TM data to estimate carbon release from burned biomass in an Alaskan spruce forest complex. *International Journal of Remote Sensing*, **21**(2): 323-338.

Mildrexler, D. J., Zhao, M. S. and Running, S. W. 2009. Testing a MODIS Global Disturbance Index across North America. *Remote Sensing of Environment*, **113**(10): 2103-2117.

Miles, V. V., Bobylev, L. P., Maximov, S. V., Johannessen, O. M. and Pitulko, V. M. 2003. An approach for assessing boreal forest conditions based on combined use of satellite SAR and multi-spectral data. *International Journal of Remote Sensing*, **24**(22): 4447-4466.

Millennium Ecosystem Assessment (MA). 2005. Ecosystems and Human Well-being (A Synthesis Report).

Millin-Chalabi, G., McMorrow, J. and Agnew, C. 2014. Detecting a moorland wildfire scar in the Peak District, UK, using synthetic aperture radar from ERS-2 and Envisat ASAR. *International Journal of Remote Sensing*, **35**(1): 54-69.

Minchella, A., Del Frate, F., Capogna, F., Anselmi, S. and Manes, F. 2009. Use of multitemporal SAR data for monitoring vegetation recovery of Mediterranean burned areas. *Remote Sensing of Environment*, **113**(3): 588-597.

Mitchard, E. T. A., Saatchi, S. S., Woodhouse, I. H., Nangendo, G., Ribeiro, N. S., Williams, M., Ryan, C. M., Lewis, S. L., Feldpausch, T. R. and Meir, P. 2009. Using satellite radar backscatter to predict above-ground woody biomass: A consistent relationship across four different African landscapes. *Geophysical Research Letters*, **36**, L23401.

Mitri, G. H. and Gitas, I. Z. 2006. Fire type mapping using object-based classification of Ikonos imagery. *International Journal of Wildland Fire*, **15**(4): 457-462.

Mitri, G. H. and Gitas, I. Z. 2008. Mapping the severity of fire using object-based classification of IKONOS imagery. *International Journal of Wildland Fire*, **17**(3): 431-442.

Mitri, G. H. and Gitas, I. Z. 2013. Mapping post-fire forest regeneration and vegetation recovery using a combination of very high spatial resolution and hyperspectral satellite imagery. *International Journal of Applied Earth Observation and Geoinformation*, **20**: 60-66.

Mooney, H., Cropper, A. and Reid, W. 2005. Confronting the human dilemma. Nature, **434**(7033): 561-562.

Moreira, F., Catry, F., Lopes, T., Bugalho, M. N. and Rego, F. 2009. Comparing survival and size of resprouts and planted trees for post-fire forest restoration in central Portugal. *Ecological Engineering*, **35**(5): 870-873.

Moreira, F., Ferreira, A., Abrantes, N., Catry, F., Fernandes, P., Roxo, L., Keizer, J. J. and Silva, J. 2013. Occurrence of native and exotic invasive trees in burned pine and eucalypt plantations: Implications for post-fire forest conversion. *Ecological Engineering*, **58**: 296-302.

Morton, D. C., DeFries, R. S., Nagol, J., Souza, C. M., Kasischke, E. S., Hurtt, G. C. and Dubayah, R. 2011. Mapping canopy damage from understory fires in Amazon forests using annual time series of Landsat and MODIS data. *Remote Sensing of Environment*, **115**(7): 1706-1720.

Moskal, L. M. and Jakubauskas, M. E. 2013. Monitoring Post Disturbance Forest Regeneration with Hierarchical Object-Based Image Analysis. *Forests*, **4**(4): 808-829.

Mouillot, F., Schultz, M. G., Yue, C., Cadule, P., Tansey, K., Ciais, P. and Chuvieco, E. 2014. Ten years of global burned area products from spaceborne remote sensing-A

review: Analysis of user needs and recommendations for future developments. *International Journal of Applied Earth Observation and Geoinformation*, **26**: 64-79.

Murphy, K. A., Reynolds, J. H. and Koltun, J. M. 2008. Evaluating the ability of the differenced Normalized Burn Ratio (dNBR) to predict ecologically significant burn severity in Alaskan boreal forests. *International Journal of Wildland Fire*, **17**(4): 490-499.

Myneni, R. B., Nemani, R. R. and Running, S. W. 1997. Estimation of global leaf area index and absorbed PAR using radiative transfer model. *IEEE Transactions on Geoscience and Remote Sensing*, **35**(6): 1380-1393.

Negron-Juarez, R., Baker, D. B., Chambers, J. Q., Hurtt, G. C. and Goosem, S. 2014. Multi-scale sensitivity of Landsat and MODIS to forest disturbance associated with tropical cyclones. *Remote Sensing of Environment*, **140**: 679-689.

Otoda, T., Doi, T., Sakamoto, K., Hirobe, M., Nachin, B. and Yoshikawa, K. 2013. Frequent fires may alter the future composition of the boreal forest in northern Mongolia. *Journal of Forest Research*, **18**(3): 246-255.

Pausas, J. G., Carbó, E., Neus, C. R., Gil, J. M. and Vallejo, R. 1999. Post-fire regeneration patterns in the eastern Iberian Peninsula. *Acta Oecologica*, **20**(5): 499-508.

Pearson, R. L. and Miller, L. D. 1972. Remote Mapping of Standing Crop Biomass for Estimation of the Productivity of the Shortgrass Prairie. In: *Proceedings of the Eighth International Symposium on Remote Sensing of Environment*. Willow Run Laboratories, Environmental Research Institute of Michigan, Ann Arbor, Michigan USA, pp. 1355-1381.

Pereira, J. M. C., Chuvieco, E., Beaudoin, A. and Desbois, N. 1997. Remote sensing of burned areas: A review. In A review of remote sensing methods for the study of large wildland fires, edited by E. Chuvieco (Alcala de Henares, Spain: Universidad de Alcala), pp. 127-183.

Perry, D. A., Oren, R. and Hart, S. C., 2008. Forest Ecosystems (Second edition). The Johns Hopkins University Press, Baltimore, Maryland, USA.

Pflugmacher, D., Cohen, W. B. and Kennedy, R. E. 2012. Using Landsat-derived disturbance history (1972-2010) to predict current forest structure. *Remote Sensing of Environment*, **122**(SI): 146-165.

Pinto, N., Simard, M. and Dubayah, R. 2013. Using InSAR Coherence to Map Stand Age in a Boreal Forest. *Remote Sensing*, **5**(1): 42-56.

Pleniou, M. and Koutsias, N. 2013. Sensitivity of spectral reflectance values to different burn and vegetation ratios: A multi-scale approach applied in a fire affected area. *ISPRS Journal of Photogrammetry and Remote Sensing*, **79**: 199-210.

Polychronaki, A., Gitas, I. Z., Veraverbeke, S. and Debien, A. 2013. Evaluation of ALOS PALSAR Imagery for Burned Area Mapping in Greece Using Object-Based Classification. *Remote Sensing*, **5**(11): 5680-5701.

Potapov, P., Hansen, M. C., Stehman, S. V., Loveland, T. R. and Pittman, K. 2008. Combining MODIS and Landsat imagery to estimate and map boreal forest cover

loss. *Remote Sensing of Environment*, **112**(9): 3708-3719.

Pu, R. L., Li, Z. Q., Gong, P., Csiszar, I., Fraser, R., Hao, W. M., Kondragunta, S. and Weng, F. Z. 2007. Development and analysis of a 12-year daily 1-km forest fire dataset across North America from NOAA/AVHRR data. *Remote Sensing of Environment*, **108**(2): 198-208.

Ranson, K. J., Kovacs, K., Sun, G. and Kharuk, V. I. 2003. Disturbance recognition in the boreal forest using radar and Landsat-7. *Canadian Journal of Remote Sensing*, **29**(2): 271-285.

Rastmanesh, F., Moore, F., Kharrati-Kopaei, M. and Behrouz, M. 2010. Monitoring deterioration of vegetation cover in the vicinity of smelting industry, using statistical methods and TM and ETM+ imageries, Sarcheshmeh copper complex, Central Iran. *Environmental Monitoring and Assessment*, **163**(1-4): 397-410.

Remmel, T. K. and Perera, A. H. 2001. Fire mapping in a northern boreal forest: assessing AVHRR/NDVI methods of change detection. *Forest Ecology and Management*, **152**(1-3): 119-129.

Roder, A., Hill, J., Duguy, B., Alloza, J. A. and Vallejo, R. 2008. Using long time series of Landsat data to monitor fire events and post-fire dynamics and identify driving factors. A case study in the Ayora region (eastern Spain). *Remote Sensing of Environment*, **112**(1): 259-273.

Rouse, J. W., Haas, R. H., Schell, J. A. and Deering, D. W. 1974. Monitoring Vegetation Systems in the Great Plains with ERTS. In *Proceedings of Third Earth Resources Technology Satellite-1 Symposium*, NASA/GSFC, Greenbelt, MD, USA, pp. 309-317.

Ruiz, J. A. M., Riano, D., Arbelo, M., French, N. H. F., Ustin, S. L. and Whiting, M. L. 2012. Burned area mapping time series in Canada (1984-1999) from NOAA-AVHRR LTDR: A comparison with other remote sensing products and fire perimeters. *Remote Sensing of Environment*, **117**: 407-414.

Running, S. W., Loveland, T. R. and Pierce, L. L. 1994. A vegetation classification logic based on remote sensing for use in global scale biogeochemical models. *Ambio*, **23**: 77-81.

Rykhus, R. and Lu, Z. 2011. Monitoring a boreal wildfire using multi-temporal Radarsat-1 intensity and coherence images. *Geomatics, Natural Hazards and Risk*, **2**(1): 15-32.

Samanta, A., Ganguly, S. and Myneni, R. B. 2011. MODIS Enhanced Vegetation Index data do not show greening of Amazon forests during the 2005 drought. *New Phytologist*, **189**(1): 11-15.

Schimmel, J. and Granstrom, A. 1996. Fire severity and vegetation response in the boreal Swedish forest. *Ecology*, **77**(5): 1436-1450.

Schleppi, P., Thimonier, A. and Walthert, L. 2011. Estimating leaf area index of mature temperate forests using regressions on site and vegetation data. *Forest Ecology and Management*, **261**(3): 601-610.

Schmullius, C. C. and Evans, D. L. 1997. Synthetic aperture radar (SAR) frequency and polarization requirements for applications in ecology, geology, hydrology, and oceanography: a tabular status quo after SIR-C/X-SAR. International Journal of

Remote Sensing, **18**(13): 2713-2722.

Schroeder, T. A., Cohen, W. B., Song, C., Canty, M. J. and Yang, Z. 2006. Radiometric correction of multi-temporal Landsat data for characterization of early successional forest patterns in western Oregon. *Remote Sensing of Environment*, **103**(1): 16-26.

Schroeder, T. A., Wulder, M. A., Healey, S. P. and Moisen, G. G. 2011. Mapping wildfire and clearcut harvest disturbances in boreal forests with Landsat time series data. *Remote Sensing of Environment*, **115**(6): 1421-1433.

Schroeder, T. A., Wulder, M. A., Healey, S. P. and Moisen, G. G. 2012. Detecting post-fire salvage logging from Landsat change maps and national fire survey data. *Remote Sensing of Environment*, **122**(SI): 166-174.

Schulze, E. D., Wirth, C., Mollicone, D. and Ziegler, W. 2005. Succession after stand replacing disturbances by fire, wind throw, and insects in the dark Taiga of Central Siberia. *Oecologia*, **146**(1): 77-88.

Senici, D., Lucas, A., Chen, H. Y. H., Bergeron, Y., Larouche, A., Brossier, B., Blarquez, O. and Ali, A. A. 2013. Multi-millennial fire frequency and tree abundance differ between xeric and mesic boreal forests in central Canada. *Journal of Ecology*, **101**(2): 356-367.

Sharma, R. C., Kajiwara, K. and Honda, Y. 2013. Estimation of forest canopy structural parameters using kernel-driven bi-directional reflectance model based multi-angular vegetation indices. *ISPRS Journal of Photogrammetry and Remote Sensing*, **78**: 50-57.

Shibayama, M. and Akiyama, T. 1989. Seasonal Visible, Near-Infrared and Mid-Infrared Spectra of rice canopies in relation to LAI and above-ground dry biomass. *Remote Sensing of Environment*, **27**: 119-127.

Shorohova, E., Kuuluvainen, T., Kangur, A. and Jogiste, K. 2009. Natural stand structures, disturbance regimes and successional dynamics in the Eurasian boreal forests: a review with special reference to Russian studies. *Annals of Forest Science*, **66**(2), 201.

Shvidenko, A. Z. and Schepaschenko, D. G. 2013. Climate change and wildfires in Russia. *Contemporary Problems of Ecology*, **6**(7): 683-692.

Skinner, W. R., Shabbar, A., Flannigan, M. D., Logan, K. 2006. Large forest fires in Canada and the relationship to global sea surface temperatures. *Journal of Geophysical Research-Atmospheres*, **111**(D14), D14106.

Soja, A. J., Sukhinin, A. I., Cahoon, D. R., Shugart, H. H. and Stackhouse, P. W. 2004. AVHRR-derived fire frequency, distribution and area burned in Siberia. *International Journal of Remote Sensing*, **25**(10): 1939-1960.

Song, C., Schroeder, T. A. and Cohen, W. B. 2007. Predicting temperate conifer forest successional stage distributions with multitemporal Landsat Thematic Mapper imagery. *Remote Sensing of Environment*, **106**(2): 228-237.

Sönmez, İ., Erdi, E., Tekeli, A. E., Demir, F. and Arslan, M. 2011. Foogle: fire monitoring tool for EUMETSAT's active fire product over Turkey using Google Earth. *Geomatics, Natural Hazards and Risk*, **2**(1): 1-13.

Soverel, N. O., Coops, N. C., Perrakis, D. D. B., Daniels, L. D. and Gergel, S. E. 2011.

The transferability of a dNBR-derived model to predict burn severity across 10 wildland fires in western Canada. *International Journal of Wildland Fire*, **20**(4): 518-531.

Stocks, B. J., Mason, J. A., Todd, J. B., Bosch, E. M., Wotton, B. M., Amiro, B. D., Flannigan, M. D., Hirsch, K. G., Logan, K. A., Martell, D. L. and Skinner, W. R. 2002. Large forest fires in Canada, 1959-1997. *Journal of Geophysical Research-Atmospheres*, **108**(D1), 8149.

Stroppiana, D., Bordogna, G., Carrara, P., Boschetti, M., Boschetti, L. and Brivio, P. A. 2012. A method for extracting burned areas from Landsat TM/ETM plus images by soft aggregation of multiple Spectral Indices and a region growing algorithm. *ISPRS Journal of Photogrammetry and Remote Sensing*, **69**: 88-102.

Stueve, K. M., Cerney, D. L., Rochefort, R. M. and Kurth, L. L. 2009. Post-fire tree establishment patterns at the alpine treeline ecotone: Mount Rainier National Park, Washington, USA. *Journal of Vegetation Science*, **20**(1): 107-120.

Sun, L., Hu, H. Q., Guo, Q. X. and Lv, X. S. 2011. Estimating carbon emissions from forest fires during 1980 to 1999 in Daxing'an Mountain, China. *African Journal of Biotechnology*, **10**(41): 8046-8053.

Sunderman, S. O. and Weisberg, P. J. 2011. Remote sensing approaches for reconstructing fire perimeters and burn severity mosaics in desert spring ecosystems. *Remote Sensing of Environment*, **115**(9): 2384-2389.

Suzuki, R., Kim, Y. and Ishii, R. 2013. Sensitivity of the backscatter intensity of ALOS/PALSAR to the above-ground biomass and other biophysical parameters of boreal forest in Alaska. *Polar Science*, **7**(2): 100-112.

Tanase, M. A., de la Riva, J., Santoro, M., Perez-Cabello, F. and Kasischke, E. 2011. Sensitivity of SAR data to post-fire forest regrowth in Mediterranean and boreal forests. *Remote Sensing of Environment*, **115**(8): 2075-2085.

Tanase, M. A., Perez-Cabello, F., de la Riva, J. and Santoro, M. 2010a. TerraSAR-X Data for Burn Severity Evaluation in Mediterranean Forests on Sloped Terrain. *IEEE Transactions on Geoscience and Remote Sensing*, **48**(2): 917-929.

Tanase, M. A., Santoro, M., Aponte, C. and de la Riva, J. 2014. Polarimetric Properties of Burned Forest Areas at C- and L-Band. *IEEE Journal of Selected Topics in Applied Earth Observations and Remote Sensing*, **7**(1): 267-276.

Tanase, M. A., Santoro, M., de la Riva, J., Perez-Cabello, F. and Le Toan, T. 2010b. Sensitivity of X-, C-, and L-Band SAR Backscatter to Burn Severity in Mediterranean Pine Forests. *IEEE Transactions on Geoscience and Remote Sensing*, **48**(10): 3663-3675.

Tian, X. R., Douglas, J. M., Shu, L. F., Zhao, F. J., Wang, M. Y., Liu, Y. M., Liu, S. Q., Gao, H., Zhan, H. Y., Fu, S. Y. and Luo, X. L. 2010. Changes of forest fire danger and the evaluation of the FWI system application in the Daxing'anling region. *Scientia Silvae Sinicae*, **46**(5): 127-132. (In Chinese)

Tian, X. R., McRae, D. J., Jin, J. Z., Shu, L. F., Zhao, F. J. and Wang, M. Y. 2011. Wildfires and the Canadian Forest Fire Weather Index system for the Daxing'anling region of China. *International Journal of Wildland Fire*, **20**(8): 963-973.

Tong, A. and He, Y. H. 2013. Comparative analysis of SPOT, Landsat, MODIS, and AVHRR normalized difference vegetation index data on the estimation of leaf area index in a mixed grassland ecosystem. *Journal of Applied Remote Sensing*, **7**, 073599.

Townshend, J. R., Masek, J. G., Huang, C. Q., Vermote, E. F., Gao, F., Channan, S., Sexton, J. O., Feng, M., Narasimhan, R., Kim, D., Song, K., Song, D. X., Song, X. P., Noojipady, P., Tan, B., Hansen, M. C., Li, M. X. and Wolfe, R. E. 2012. Global characterization and monitoring of forest cover using Landsat data: opportunities and challenges. *International Journal of Digital Earth*, **5**(5): 373-397.

Tucker, C. J. 1979. Red and Photographic Infrared Linear Combinations for Monitoring Vegetation. *Remote Sensing of Environment*, **8**(2): 127-150.

Tucker, C. J., Grant, D. M. and Dykstra, J. D. 2004. NASA's global orthorectified Landsat data set. *Photogrammetric Engineering and Remote Sensing*, **70**(3): 313-322.

Uemura, S., Kanda, F., Isaev, A. P. and Tsujii, T. 1997. Forest structure and succession in southeastern Siberia. *Vegetation Science*, **14**: 119-127.

Urban, M., Hese, S., Herold, M., Pocking, S. and Schmullius, C. 2010. Pan-Arctic Land Cover Mapping and Fire Assessment for the ESA Data User Element Permafrost. *Photogrammetrie Fernerkundung Geoinformation*, **4**: 283-293.

USGS-EROS (Earth Resources Observation and Science Center). Available online: *http://earthexplorer.usgs.gov/* (accessed on May 15, 2014).

Veraverbeke, S., Gitas, I., Katagis, T., Polychronaki, A., Somers, B. and Goossens, R. 2012. Assessing post-fire vegetation recovery using red-near infrared vegetation indices: Accounting for background and vegetation variability. *ISPRS Journal of Photogrammetry and Remote Sensing*, **68**: 28-39.

Verbyla, D. and Lord, R. 2008. Estimating post-fire organic soil depth in the Alaskan boreal forest using the Normalized Burn Ratio. *International Journal of Remote Sensing*, **29**(13): 3845-3853.

Wang, M. H., Tang, J. W. and Shi, W. 2007. MODIS-derived ocean color products along the China east coastal region. *Geophysical Research Letters*, **34**(6), L06611.

Watanabe, M., Shimada, M., Rosenqvist, A., Tadono, T., Matsuoka, M., Romshoo, S. A., Ohta, K., Furuta, R., Nakamura, K. and Moriyama, T. 2006. Forest structure dependency of the relation between L-band sigma0 and biophysical parameters. *IEEE Transactions on Geoscience and Remote Sensing*, **44**(11): 3154-3165.

Weber, M. G. and Flannigan, M. D. 1997. Canadian boreal forest ecosystem structure and function in a changing climate: Impacts on fire regimes. *Environment Review*, **5**: 145-166.

White, K. 1998. Remote sensing. *Progress in Physical Geography*, **22**(1): 95-102.

Whittle, M., Quegan, S., Uryu, Y., Stuewe, M. and Yulianto, K. 2012. Detection of tropical deforestation using ALOS-PALSAR: A Sumatran case study. *Remote Sensing of Environment*, **124**: 83-98.

Wilson, E. H. and Sader, S. A. 2002. Detection of forest harvest type using multiple dates of Landsat TM imagery. *Remote Sensing of Environment*, **80**(3): 385-396.

Wotton, B. M., Nock, C. A. and Flannigan, M. D. 2010. Forest fire occurrence and

climate change in Canada. *International Journal of Wildland Fire*, **19**(3): 253-271.

Wu, J. A. and Peng, D. L. 2010. Tree-Crown Information Extraction of Farmland Returned to Forests Using QuickBird Image Based on Object-Oriented Approach. *Spectroscopy and Spectral Analysis*, **30**(9): 2533-2536.

Wu, Z. W., He, H. S., Liang, Y., Cai, L. Y. and Lewis, B. J. 2013. Determining Relative Contributions of Vegetation and Topography to Burn Severity from LANDSAT Imagery. *Environmental Management*, **52**(4): 821-836.

Wulder, M. A., White, J. C., Alvarez, F., Han, T., Rogan, J. and Hawkes, B. 2009. Characterizing boreal forest wildfire with multi-temporal Landsat and LIDAR data. *Remote Sensing of Environment*, **113**(7): 1540-1555.

Xie, F. J., Xiao, D. N., Li, X. Z., Hu, Y. M. and Wang, X. G. 2006. Change of wetland pattern and regulating capacity of forest hydrology in burned area of northern great Hingan Mountains. *Journal of Liaoning Technical University*, **25**(5): 765-768. (In Chinese)

Xin, Q. C., Olofsson, P., Zhu, Z., Tan, B. and Woodcock, C. E. 2013. Toward near real-time monitoring of forest disturbance by fusion of MODIS and Landsat data. *Remote Sensing of Environment*, **135**: 234-247.

Xu, M., Cao, C. X., Tong, Q. X., Li, Z. Y., Zhang, H., He, Q. S., Gao, M. X., Zhao, J. A., Zheng, S., Chen, W. and Zheng, L. F. 2010. Remote sensing based shrub above-ground biomass and carbon storage mapping in Mu Us desert, China. *Science China-Technological Sciences*, **53**(suppl.I): 176-183.

Yi, K. P., Tani, H., Zhang, J. Q., Guo, M., Wang, X. F. and Zhong, G. S. 2013. Long-Term Satellite Detection of Post-Fire Vegetation Trends in Boreal Forests of China. *Remote Sensing*, **5**(12): 6938-6957.

Zhang, Q. F., Pavlic, G., Chen, W. J., Latifovic, R., Fraser, R. and Cihlar, J. 2004. Deriving stand age distribution in boreal forests using SPOT VEGETATION and NOAA AVHRR imagery. *Remote Sensing of Environment*, **91**(3-4): 405-418.

Zhang, Y., Hu, H. Q. and Wang, Q. 2011. Carbon Emissions from Forest Fires in Great Xing'an Mountains from 1980 to 2005. In the book titled *2011 3rd International Conference on Environmental Science and Information Application Technology Esiat 2011, Vol 10, Pt C.* (Editor: Y. Wu.) Amsterdam, Elsevier Science Bv. **10:** 2505-2510.

Zhang, Y. H., Wooster, M. J., Tutubalina, O. and Perry, G. L. W. 2003. Monthly burned area and forest fire carbon emission estimates for the Russian Federation from SPOT VGT. *Remote Sensing of Environment*, **87**(1): 1-15.

Zhao, K. Y., Zhang, W. F., Zhou, Y. W. and Yang, Y. X. 1994. The impact of Da xing'an ling forest fires on environment and its countermeasures. Beijing: Science Press. (In Chinese)

Zhao, Y. S. 2003. Remote sensing applications and its principles. Beijing: Science Press. (In Chinese)

Acknowledgements

Time flies by and three years of doctoral life are fleeting as a flash. At this moment, I am sincerely grateful to many people for a wide variety of support.

First and foremost, I express my eternal gratefulness to Prof. Tetsuro Sakai for accepting me as his close disciple and supporting me in almost every respect, academically, financially and spiritually. It is my honor to be his student. He guided me to seek the interests and determine the theme of my doctoral thesis, as well as providing the useful ideas and necessary data. Especially, the fact that he drove to Kansai airport to pick me up personally when I came to Japan for the first time three years ago made me a strong impression and would definitely left me everlasting memories.

Then I would like to offer heartfelt gratitude to another supervisor of Prof. Kazuyuki Moriya. He is such affable in manner with great patience, enthusiasm, broad-mindedness and immense knowledge. I am deeply grateful to him for his support in research and life as well as the trust granted to me. He and Prof. Sakai have always showing rigorous scientific spirit during seminars, while seem like a kind grandfather at parties.

My greatest thanks are also due to Assoc. Prof. Lina Koyama for her detailed and useful comments upon my study, and the sincere and careful help in lots of issues. I am always benefiting from the shared information and helpful recommendations from her. Sincere thankfulness also goes to Prof. Nobuaki Arai, my advisor of Prof. Masatoshi Yoshikawa, Prof. Kiyoshi Torii, and Dr. Stanko Trifkovic for the pleasant communications and discussions about research and life. Certainly, I express my highest respect and deepest gratitude to the members of the supervisory committee. I also show my gratitude to Prof. Alfredo Huete from the University of Technology, Sydney for the significant inspiration concerning vegetation indices gained through the e-mail exchanges. I could not owe my sincere gratefulness to Dr. Hiromichi Mitamura and Ms. Fusako Kamiguchi for the many supports in academic and administrative affairs.

In my opinion, the biosphere informatics laboratory serves as a nice big-family, with friendship, freedom, equality and happiness everywhere. I have been fond of this atmosphere from the very beginning and would like to take this opportunity to express the depth of my gratitude to all the classmates and friends, whether have graduated or not. Incidentally, I warmly thank another Chinese, Ms. Yanfei Wu, for her repeated help in occasions requiring fluent Japanese language.

The acquaintances with the guys living in Misasagi international student house, especially those having deep understanding and further contact are extremely valuable memories to me which will be treasured forever. It should be particularly mentioned that the internal communications and activities within the badminton group enormously expand my scope and enrich the entertainments.

I sincerely express my greatest respect and appreciation to Prof. Chunxiang Cao, who is also my supervisor in Master Program and one of the advisors in the first year

of doctoral period. It is her who gave me the opportunity to continue my graduate studies and took me into the sacred temple of remote sensing science. I can hardly express my gratitude to her for leading me to move forward on the way of forest remote sensing in terms of providing methodological guidance and experimental instructions. I would send her everlasting feelings of gratefulness for the support and recommendation to pursue the PhD in Japan. I could not have imagined my present and future without her directions.

I am cordially grateful to Prof. Shilei Lu from the Institute of Remote Sensing and Digital Earth, Chinese Academy of Sciences, for the guidance and suggestions in designing the technical scenario of the forest sampling design. I express my gratitude to the three friends, Dr. Haibing Xiang, Dr. Zhou Fang, and Dr. Mingren Huang, also from the Institute of Remote Sensing and Digital Earth for their cooperation in the field forest survey. I send the warmest thankfulness to the forestry leaders, technicians and workers from the forestry bureaus of Xilinji, Tuqiang and Amuer, for their assistance in the field investigation, especially in the measurements of forest structural parameters.

I betoken my thankfulness to the staffs, Dr. Min Xu, Mr. Yunfei Xu, and students, Mr. Sheng Zheng, Ms. Rong Tian, and Ms. Cheng Liu, Dr. Jian Zhao as well as others from my Master laboratory in the Institute of Remote Sensing and Digital Earth for the stimulating discussions associated with the research reported in this thesis. Special thanks are expressed to Mr. Wentao Hu, Dr. Danlu Cai and some other comrades for the intimate friendship. It is a great pleasure to get along with you.

Family has always been the harbor of hearts. My parents and younger sister have my eternal loving. I wish to express my sincerest gratefulness to them for always supporting and believing me throughout my life whenever and wherever I am and whatever I choose to do.

Finally, I am particularly thankful to USGS EROS, NASA LP DAAC and JAXA EORC for providing this study with the time series Landsat, MODIS and ALOS AVNIR-2, PALSAR data. I express especial acknowledgement to JAXA for accepting my proposal for the “4th ALOS Research Announcement for ALOS-2” (PI No. 1185) and providing my research with free relevant data. Certainly, I extremely appreciate the funding of Monbukagakusho (MEXT) Fellowship from the Japanese Government (Grant No. 113378). It provides the basic financial support for both my research and life during doctoral program in Kyoto University.

As the outcome of my three years' dedicated effort and hard work with the sincere assistance and support from all of you throughout the process, I would be eager to wish that this dissertation will live up to your highest expectations.

Publications

As the first author:

Journal papers (with peer-review):

1. **W. CHEN**, K. MORIYA, T. SAKAI, L. KOYAMA and C.X. CAO. Mapping a burned forest area from Landsat TM data by multiple methods. *Geomatics, Natural Hazards and Risk*, 2014, DOI: 10.1080/19475705.2014.925982.
2. **Wei Chen**, Kazuyuki Moriya, Tetsuro Sakai, Lina Koyama, Chunxiang Cao. Post-fire forest regeneration under different restoration treatments in the Greater Hinggan Mountain area of China. *Ecological Engineering*, 2014, DOI: 10.1016/j.ecoleng.2014.06.016.
3. **Wei Chen**, Kazuyuki Moriya, Tetsuro Sakai, Lina Koyama, Chunxiang Cao. Monitoring of post-fire forest recovery under different restoration modes based on time series Landsat data. *European Journal of Remote Sensing*, 2014, **47**: 153-168. DOI: 10.5721/EuJRS20144710.
4. **W. Chen**, T. Sakai, K. Moriya, L. Koyama & C. X. Cao. Estimation of vegetation coverage in semi-arid sandy land based on multivariate statistical modeling using remote sensing data. *Environmental Modeling and Assessment*, 2013, **18**(5): 547-558. DOI: 10.1007/s10666-013-9359-1.
5. **CHEN Wei** and CAO Chunxiang. Topographic correction-based retrieval of leaf area index in mountain areas. *Journal of Mountain Science*, 2012, **9**(2): 166-174. DOI: 10.1007/s11629-012-2248-2.
6. **CHEN W.**, CAO C. X., HE Q. S., GUO H. D., ZHANG H., LI R. Q., ZHENG S., XU M., GAO M. X., ZHAO J., LI S., NI X. L., JIA H. C., JI W., TIAN R., LIU C., ZHAO Y. X. & LI J. L. Quantitative estimation of the shrub canopy LAI from atmosphere-corrected HJ-1 CCD data in Mu Us Sandland. *Science China Earth Sciences*, 2010, **53**(Suppl. I): 26-33. DOI: 10.1007/s11430-010-4127-4.

Conference proceedings (with peer-review):

1. **Wei Chen**, Kazuyuki Moriya, Tetsuro Sakai, Lina Koyama, Chunxiang Cao. Temporal and Spatial Monitoring of Post-fire Forest Dynamics Using Time-series MODIS Data. *IEEE International Geoscience and Remote Sensing Symposium (IGARSS2014)*, July 13-18, 2014, Québec, Canada. (Accepted)
2. **Wei Chen**, Tetsuro Sakai, Kazuyuki Moriya, Lina Koyama, Chunxiang Cao. Extraction of burned forest area in the Greater Hinggan Mountain of China based on Landsat TM data. *IEEE International Geoscience and Remote Sensing Symposium (IGARSS2013)*, pp. 995-998, July 21-26, 2013, Melbourne, Australia.
3. **Wei Chen**, Tetsuro Sakai, Chunxiang Cao, Kazuyuki Moriya, Lina Koyama. Detection of forest disturbance in the Greater Hinggan Mountain of China based on Landsat time-series data. *IEEE International Geoscience and Remote Sensing Symposium (IGARSS2012)*, pp. 7232-7235, July 22-27, 2012, Munich, Germany.
4. **Wei Chen**, Chunxiang Cao, Hao Zhang, Huicong Jia, Wei Ji, Min Xu, Mengxu

Gao, Xiliang Ni, Jian Zhao, Sheng Zheng, Rong Tian, Cheng Liu. Estimation of shrub canopy cover based on a geometric-optical model using HJ-1 data. *IEEE International Geoscience and Remote Sensing Symposium (IGARSS2011)*, pp. 1922-1925, July 24-29, 2011, Vancouver, Canada.

Conference proceedings (without peer-review):

1. **Chen Wei**, Cao Chunxiang, Zhang Hao, Jia Huicong, Ji Wei, Xu Min, Gao Mengxu, Ni Xiliang, Zhao Jian and Zheng Sheng. The retrieval and analysis of forest LAI based on SPOT5 image. *The 5th remote sensing meeting over the cross-strait*, August 8-12, 2011, Harbin, China. (in Chinese)

As a co-author:

Journal papers (with peer-review):

1. C. X. Cao, **W. Chen**, G. H. Li, H. C. Jia, W. Ji, M. Xu, M. X. Gao, X. L. Ni, J. Zhao, S. Zheng, R. Tian, C. Liu and S. Li. The retrieval of shrub fractional cover based on a geometric-optical model in combination with linear spectral mixture analysis. *Canadian Journal of Remote Sensing*, 2011, **37**(4): 348-358.
2. Chunxiang Cao, Yunfei Bao, **Wei Chen**, Yongfeng Dang, Lin Li, Rong Tian and Guanghe Li. Extraction of forest structural parameters based on the intensity information of high-density airborne LiDAR. *Journal of Applied Remote Sensing*, 2012, **6**(1), 063533.
3. C.X. CAO, Y.F. BAO, M. XU, **W. CHEN**, H. ZHANG, Q.S. HE, Z.Y. LI, H.D. GUO, J.H. LI, X.W. LI and G.H. LI. Retrieval of forest canopy attributes based on Geometric-Optical model using airborne LiDAR and optical remote sensing data. *International Journal of Remote Sensing*, 2012, **33**(3): 692-709.
4. CX Cao, J Zhao, P Gong, GR Ma, DM Bao, K Tian, R Tian, ZG Niu, H Zhang, M Xu, MX Gao, S Zheng, **W Chen**, QS He, XW Li. Wetland changes and droughts in southwestern China. *Geomatics, Natural Hazards and Risk*, 2012, **3**(1): 79-95.
5. TIAN Haijing, CAO Chunxiang, DAI Shengmao, ZHENG Sheng, LU Shilei, XU Min, **CHEN Wei**, ZHAO Jian, LIU Di and ZHU Hongyuan. Analysis of vegetation fractional cover in Jungar Banner based on time-series remote sensing data. *Journal of Geo-information Science*, 2014, **16**(1): 126-133. (in Chinese)

Conference proceedings (with peer-review):

1. Chunxiang Cao, Min Xu, **Wei Chen**, Rong Tian. A framework for diagnosis of environmental health based on remote sensing. *SPIE Asia-Pacific Remote Sensing*, International Society for Optics and Photonics, pp. 852414-852414-6, October 29-November 1, 2012, Kyoto, Japan.
2. Cheng Liu, Chunxiang Cao, Jianlong Zhang, Aiguo Ma, **Wei Chen**, Min Xu, Tetsuro Sakai. Predicting the adaptability of Sudden Oak Death in China using spatial information technology. 2012 *IEEE International Geoscience and Remote Sensing Symposium*, pp. 7256-7259, July 22-27, 2012, Munich, Germany.